AFRL-RY-RS-TR-2010-100

SENSORS TECHNOLOGY AND ADVANCED SIGNAL PROCESSING CONCEPTS FOR LAYERED WARFARE/LAYERED SENSING

April 2010

Interim

STINFO COPY

AIR FORCE RESEARCH LABORATORY
SENSORS DIRECTORATE

■ **AIR FORCE MATERIEL COMMAND**   ■**UNITED STATES AIR FORCE**   ■ **ROME, NY 13441**

NOTICE AND SIGNATURE PAGE

AFRL-RY-RS-TR-2010-100 HAS BEEN REVIEWED AND IS APPROVED FOR PUBLICATION IN ACCORDANCE WITH ASSIGNED DISTRIBUTION STATEMENT.

FOR THE DIRECTOR:

/s/   /s/
MICHAEL C. WICKS   RICHARD G. SHAUGHNESSY, Chief
Senior Scientist   Sensors Operations
Sensors Signal Processing   Rome Research Site

REPORT DOCUMENTATION PAGE

Form Approved
OMB No. 0704-0188

1. REPORT DATE *(DD-MM-YYYY)* APRIL 2010	2. REPORT TYPE Interim	3. DATES COVERED *(From - To)* October 2008 – September 2009

4. TITLE AND SUBTITLE SENSORS TECHNOLOGY AND ADVANCED SIGNAL PROCESSING CONCEPTS FOR LAYERED WARFARE/LAYERED SENSING	5a. CONTRACT NUMBER In-House
	5b. GRANT NUMBER N/A
	5c. PROGRAM ELEMENT NUMBER 62204F
6. AUTHOR(S) Michael C. Wicks, William Baldygo, Gerard Capraro, Lorenzo Lo Monte, Tapan Sarkar, Richard Schneible, and Walt Szczepanski	5d. PROJECT NUMBER 762F
	5e. TASK NUMBER 15
	5f. WORK UNIT NUMBER 03

7. PERFORMING ORGANIZATION NAME(S) AND ADDRESS(ES) AFRL/RY 26 Electronic Parkway Rome NY 13441-4514	8. PERFORMING ORGANIZATION REPORT NUMBER N/A
9. SPONSORING/MONITORING AGENCY NAME(S) AND ADDRESS(ES) AFRL/RY 26 Electronic Parkway Rome NY 13441-4514	10. SPONSOR/MONITOR'S ACRONYM(S) N/A
	11. SPONSORING/MONITORING AGENCY REPORT NUMBER AFRL-RY-RS-TR-2010-100

12. DISTRIBUTION AVAILABILITY STATEMENT
APPROVED FOR PUBLIC RELEASE; DISTRIBUTION UNLIMITED. PA# ABW-2010-1159
DATE CLEARED: 15-MARCH-2010

13. SUPPLEMENTARY NOTES

14. ABSTRACT
The primary goal of this research was the conceptualization of a baseline approach to transition knowledge-based signal processing and waveform/geometric diversity to Layered Warfare/Layered Sensing.

15. SUBJECT TERMS
Sensors, Algorithms, Signal Processing, Remote Sensing, Radar, Waveform Diversity, Distributed Sensing, Bistatic/Multi-static Radar, Knowledge-Based Control

16. SECURITY CLASSIFICATION OF:			17. LIMITATION OF ABSTRACT	18. NUMBER OF PAGES	19a. NAME OF RESPONSIBLE PERSON Michael C. Wicks
a. REPORT U	b. ABSTRACT U	c. THIS PAGE U	UU	185	19b. TELEPHONE NUMBER *(Include area code)* N/A

Standard Form 298 (Rev. 8-98)
Prescribed by ANSI Std. Z39.18

TABLE OF CONTENTS

LIST OF FIGURES

LIST OF TABLES

ABSTRACT

The purpose of this report is to summarize a technological approach for evolving the surveillance capability within the Department of Defense from the current slowly evolving stovepipe systems to revolutionary multi-sensor, multi-platform, multi-user layered sensing systems. Enhanced capabilities are required in order to address the evolving threats:

- *From a peer/near-peer enemy to an integrated combination of peer/near-peer/lesser nation enemies with a coordinated asymmetric threat,*

- *From open, reasonably flat terrain to mountainous, foliage-covered, and/or urban terrain.*

As has been demonstrated in Iraq and Afghanistan, the asymmetric threat can be inflicted at a very low cost to the enemy. Therefore, our response to the evolving threats must be a cost-effective upgrade of existing surveillance systems and yet have our systems embrace revolutionary disruptive technologies to enhance capabilities. This upgrade must not only build upon fielded systems, but must also continue to function as systems are upgraded or replaced with the next generation cyber, airborne and space-based intelligence, surveillance and reconnaissance (ISR) systems.

One thrust of a layered sensing approach is the development of advanced Heuristic and Algorithmic Source (signal, image, data, and cyber) Processing (HASP) and system concepts, for a transformational approach to surveillance and reconnaissance. Layered sensing development will be demonstrated via mathematical analysis, modeling and simulation, bench top testing, chamber measurements and outdoor range experimentation. Another thrust is to develop technology for new layered sensors and provide seamless integration with upgrades to legacy systems, providing a cost effective and technically superior capability. These emerging sensors and systems are computing, cyber, and signal/image/data processing centric, and should be designed to address issues associated with current systems that: 1) Are data rich but information/knowledge poor; 2) Support individual users without exploiting commonality to support multiple users at multiple levels; 3) Cannot be extrapolated without a high cost to fully address futuristic threats; 4) Address only the peer/near-peer threat but are unaffordable or even ineffective against lesser nations and/or asymmetric threats; 5) Function inadequately in difficult environments without human intervention; and 6) Are not cyber secure and net centric efficient.

The beneficial consequences of HASP technologies are made possible by the combined effects of Moore's and Metcalfe's laws making the technological equivalent to cognition and social networking applicable to heterogeneous sensing. We believe that the impact of these "laws" will cause disruptive changes in many fields (i.e. Kurzweil's singularity) that will have to be embraced and countered in order to defeat our ingenious asymmetric enemy.

1 INTRODUCTION

1.1   Threat/Problem

As the weapons, command, control, communications and computing (C4) and countermeasure capabilities of emerging threats grow exponentially, it is essential that the United States (US) capabilities permit timely, cost effective engagement of the peer/near-peer/lesser nation plus asymmetric threats in difficult environments (urban, mountain, foliage, subsurface, etc.) in all battle-space locations; including cyber components of the engagement, (see Figure 1 and Figure 2). Current US command, control, communications and computing intelligence, surveillance and reconnaissance (C4ISR) was developed to address the peer/near-peer threat and has done so successfully in reasonable environments. This is true even though there is limited integration of the individual sensors (i.e., stovepipes). In the more difficult environments mentioned above, the performance of current fielded systems is limited and thus has become an important issue as the requirements evolved to address the asymmetric threat. More importantly, tomorrow's C4ISR systems need to adequately address the integrated nation state/asymmetric threat.
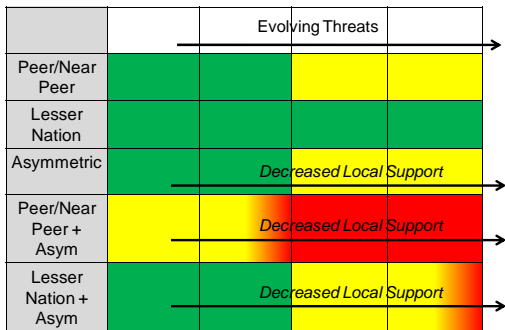
Figure 1. Capabilities Assessment – Conventional, Irregular & Disruptive Warfare
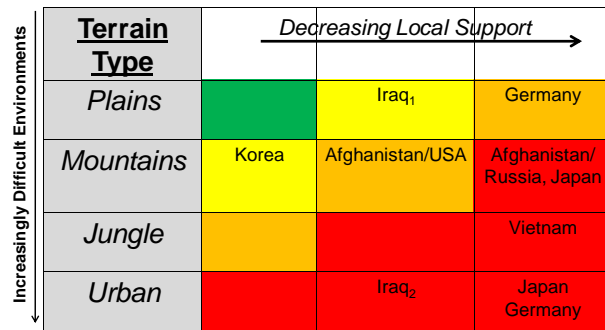
Figure 2. Significant Military Engagements

The asymmetric threat, alone or integrated with other threats, presents unique problems that have the capacity to bankrupt the US and our allies as we attempt to mitigate them, (see Figure 3). By their use and complete acceptance of human collateral damage, our current enemy is able to rapidly and inexpensively engage our soldiers, destroy our assets and counter our sensors. They are able to further complicate our solving this problem by their use of difficult environment scenarios: areas where terrain, foliage, manmade structures and/or significant background traffic are used to the advantage of the asymmetric threat to mask their activities. Extension of our existing technological sensor systems to individually address all of these issues (small localized attacks, difficult environments), or to develop a full space-based ISR capability, is technically feasible but totally unreasonable in cost.
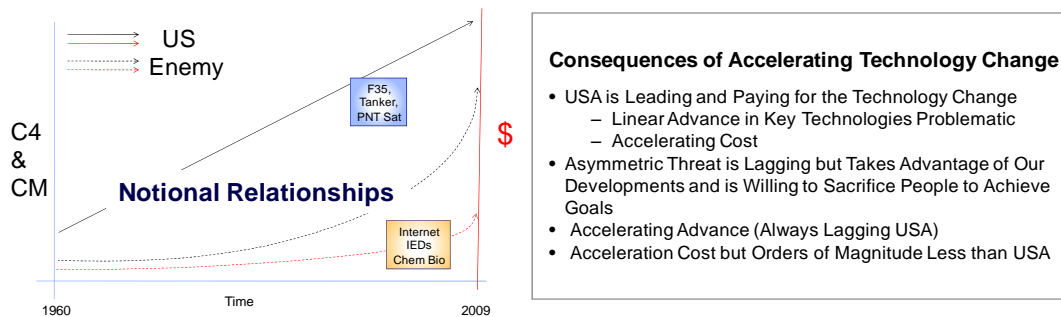
Figure 3. Capabilities and Cost Evolution

Today's threat, as well as future threats, can be addressed in a cost-effective manner if the existing ISR capabilities were effectively integrated with each other, with new small, and mobile (asymmetric-like) assets (which should include cyber). Arguably the largest issue we face today is having too much data with too little actionable information and knowledge. With our present systems, multiple levels of operators and analysts are required to transfer accurate/actionable data and information to a single user, and this process often requires days to achieve. Integrated attacks, including asymmetric actions, require that current relevant information be sent to many users at many levels simultaneously on a shortened timescale. Our goal must be: *"The right actionable information and knowledge to the right people at the right time."* As an example, this could include:

- Theater overview with predictions of future hostile activity to the theater commander
- Locations of critical targets to the appropriate commanders
- Exact coordinates of kill targets to pilots and gunners
- Improvised Explosive Device (IED), locations to convoys and patrols
- Movements, actions and intent of suicide bombers
- Providing timely information to the individual soldier in the field

This goal will not be possible without significant advances in autonomous signal/data processing, cyber surveillance, and multiple sensor control and integration.

Figure 4 presents the relationship between the topics discussed in this report:

- Future operational systems – Multi-User, Multi-Mission, Multi-Int Autonomous C4ISR (requirements discussed here in Section 1)
- Technology required to achieve future system capability – Layered Sensing (some aspects discussed in Section 2)
- The signal/data/image processing aspects of the technology along with sensor concepts with unique signal processing requirements – HASP for Integrated Air, Ground, Space, & Cyber Sensors (Section 3).
- A technology area important to this and other future systems – ISR-Human Interface (future research, Section 4).
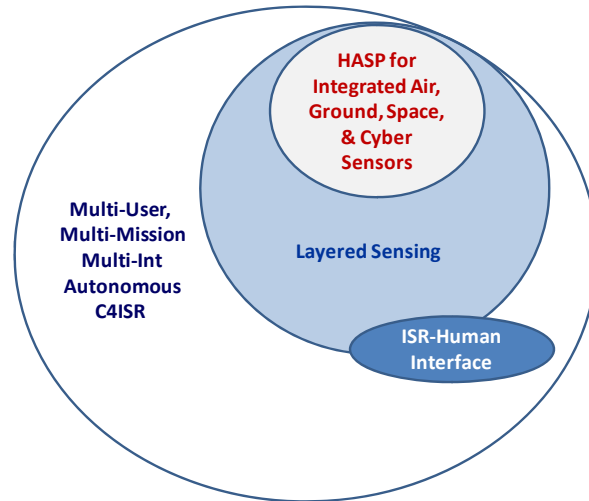
Figure 4. Program/Technology Interfaces

We envision an evolution of C4ISR:

- *From isolated, stove-piped systems (with limited post-detection integration)*
- *To integration at multiple levels (detection, track, classification) of multiple ISR assets on multiple platforms (ground, air, space, cyber)*
- *Further, to rapidly task, reconfigurable ISR architectures, and systems focusing on a specific set of threats*
- *Finally, to ubiquitous dynamic multi-theater layered warfare*

To achieve these goals, future weapon systems will require focusing on three major areas:

- *Futuristic and emerging sensor concepts addressing unique issues with the asymmetric threat in a cost-effective manner*
- *Autonomous processing capability that produces the required actionable information and knowledge for each "decision maker"*
- *Layered warfare modeling, simulations, experiments and demonstrations*

The future success of C4ISR has three key attributes that currently cannot be achieved:

- *Provide actionable information and knowledge, not just data, in timely and cost-effective manner.*
- *Achieve a C4ISR – Human interface that will both permit users at many levels to simultaneously request actionable information and knowledge, and provide timely, relevant information to all "decision makers' simultaneously.*
- *Satisfy the goals of multiple users with the correct priority.*

3

2 TECHNICAL BACKGROUND

Much of today's research in cognition focuses on sensory inputs, the interpretation of those by the brain and the integration of multiple sensor inputs to form higher level abstractions in order to turn data into information and knowledge. HASP will use a cognitive sensing approach and will require an understanding of multiple sensor types and sensor signal processing to defeat the integrated peer/near peer and asymmetric threat.

This section describes some selected AFRL enabling technologies and future sensor concepts. These and other technologies/concepts will have to be integrated to provide the required capability.

2.1 Multistatics and its Relationship to Radio Frequency (RF) Tomography

In a multistatic radar the transmit/receive aperture is divided into a number of sub-apertures that can be placed in selected locations relative to each other. These locations can be chosen to optimize the performance of the radar in terms of some specific task and/or goals.

For example, multistatic radars can potentially provide significantly improved target tracking when the apertures are appropriately configured to provide a large baseline. The resulting angular resolution can be orders of magnitude better than the resolution of a monolithic system (single large radar). However, this capability comes with a cost, either large grating lobes (multistatic with evenly spaced apertures) or high sidelobes (multistatic with randomly spaced apertures). See Appendix A.

The same angular resolution can provide improved interference rejection capability. For a single aperture radar, electromagnetic interference (EMI) sources located near a target of interest cannot be nulled without impacting the target return itself. But the multistatic system, with its large baseline and receiver gain on the target can be maintained while simultaneously placing a deep null in the direction of the EMI.

These closely-spaced multistatic systems are also called distributed aperture radars (DARs). Widely separated sub-apertures have the potential to provide improved discrimination by the formation of coherent multistatic images (see Appendix B).

Tomography extends the performance of multistatics further. It can provide high resolution in multiple dimensions and can address both fixed and moving targets (see Appendix C). This can be accomplished with a set of very narrow waveforms and thus it permits operation in many interference environments where wideband operation is not possible.

To date, multistatics and tomography have focused on a limited set of waveforms and processing approaches. For example, our distributed aperture and tomography efforts have all transmitted the same waveform bandwidth from each transmitter, simply offset in frequency. Improved performance should be possible if the widest bandwidth waveform possible were radiated at each frequency. HASP will investigate the optimum combination of frequency diversity and spatial diversity to meet various missions in various environments (see Appendix I).

2.2   Identification/Classification Processing

2.2.1   Generalized Inner Product (GIP) – Real Beam Radar (RBR)

Fixed objects on the ground can only be detected by airborne radars if target backscatter sufficiently exceeds the return from the ground (clutter). For point targets, this requires that the target's cross-section exceed the cross-section of the clutter patch established by the range and cross-range resolutions of the radar. For extended targets, both the target and clutter patch can be resolved using wide bandwidth synthetic aperture radar (SAR) processing. The result is an image, where the returns from some or all of the resolved components of the target exceed the return of their respective clutter patch. This image is interpreted (usually by an analyst) and a target detection declared. This interpretation is basically an incoherent integration process.

A technique has been developed that can achieve significantly better detection of extended targets in clutter. This GIP algorithm assumes some knowledge of the target of interest and its orientation. Analysis has been accomplished for targets whose parameters are known perfectly and for targets whose parameters are only known approximately with excellent results.

2.2.2   Declaration Algorithms for Resonant Targets (DART)

The goal of DART is to develop, validate and transition algorithms for the detection of a specific target set. These algorithms will also have the ability to estimate the parameters of those targets (i.e., declaration). This development will address the signatures of the specific targets in their environment. Signature modeling will employ an accurate and efficient method-of-moments code (**T**arget **IDE**ntification **S**oftware [TIDES]) that directly solves Maxwell's equations in an accurate and efficient fashion to deal with targets embedded in or above the ground. Thus, we will avoid the limitations of empirical models and rules-of-thumb that have been previously employed because of the lack of computational resources. The development includes a high-fidelity radar simulation that supports the analysis of radar systems on various platforms in realistic environments. This simulation will be validated through experiments using a ground vehicle as a test platform. The validated DART simulation with TIDES will permit efficient transition through development and analysis of system concepts based on the modifications to existing radars/antennas/platforms.

2.3 Multi-Intelligence Sensor Technology (MIST) - Sensor Manager Simulation (SMS)

2.3.1 Sensor Manager Simulation (SMS)

The MIST SMS is a knowledge-aided controller that utilizes situational awareness, system feedback, user-defined rules, and needs-identification to adapt its functionality to dynamically and optimally meet mission goals and objectives. Its primary objective is to map dynamic situational needs into optimally-ordered sensor tasks. The MIST SMS consists of Situational Assessment, Mission Management, and Task Scheduling, (see **Figure 5**a). The MIST SMS was designed to integrate various simulation components and sensor management algorithms to enable performance evaluation of multiple sensor resource managers under dynamically varying conditions and objectives. Currently, the sensor controller/scheduler approaches being investigated include Knowledge Based, Markov Decision Based, Fuzzy Logic Based Controllers, as well as the Online Greedy Urgency-Driven Preemptive Scheduling Algorithm (OGUPSA). Our multi-sensor simulation implements each of these approaches and provides a comparison of their performance. Each of these controller's approaches will require a list of tasks for each radar and a prioritization of these tasks. Section 2.3.2 provides a description of the mode set currently being used for sensor manager evaluation.

The simulation architecture and defined interfaces between each module allow for switching of system components for effective sensor management evaluation. A detailed overview of its operation can be seen in **Figure 5**b.
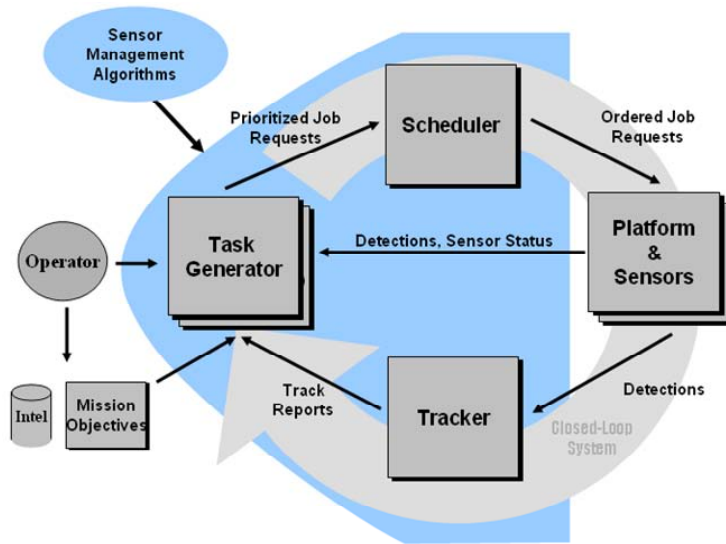
a) Sensor Manager Simulation Concept & Architecture
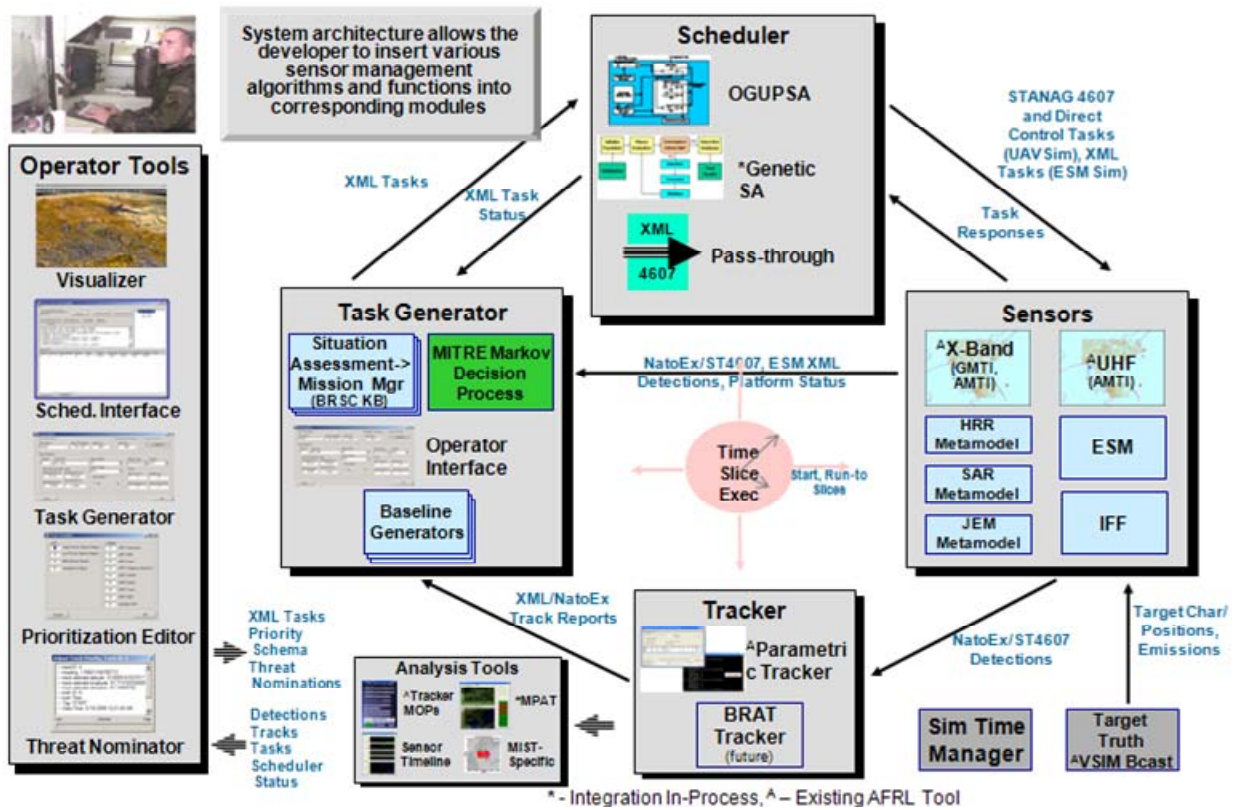
b) Sensor Management Simulation System Components

Figure 5. Sensor Manager Simulation Overview

The SMS architecture provides a closed-loop system which allows sensor manager algorithms, along with operator input, to dynamically and simultaneously task multiple sensors to meet mission goals and objectives. The SMS is tasked with dynamically scheduling the modes and submodes of the MIST Representative Operational System ultrahigh frequency (UHF) and X-band radar sensors described in Table 1, Section 2.3.2, in an optimum way. Typical SMS operation is as follows. The **Operator** can interact with the SMS when desired by optionally controlling mission objectives, submitting operator tasks, and nominating targets as threats. The **Task Generator** is responsible for creating prioritized job requests based on situational assessment, operator input, and mission goals and objectives. The **Scheduler** orders tasks in a dynamically modifiable time window and submits them to the corresponding sensor. The **Platform and Sensors** are responsible for servicing the requests from the scheduler and producing detections based on truth data. The **Tracker** produces track reports from the detections received and passes them on to the Task Generator, completing the System Loop. The SMS is currently being used for the performance evaluation of a number of scheduling algorithms using the Multi-Intelligence Sensor Technology Representative Operational System design described below in Section 2.3.2. Details of the MIST Sensor Manager Simulation can be found in Appendix D.

2.3.2   *Multi-Intelligence Sensor Technology Representative Operational System (MIST ROS)*

The MIST ROS is a notional, airborne ISR system that is being created to provide a launching point for investigating and evaluating multifunction, multi-mission, multi-sensor operations and control on a single platform using the MIST Sensor Manager Simulation.

The baseline MIST ROS consists of a UHF radar subsystem, an X-band radar subsystem, an electronic support measures (ESM) subsystem, and an Identification Friend or Foe (IFF) subsystem installed on a wide body platform. The MIST radars provide 360 degree air surveillance with ground surveillance of an assigned Ground Referenced Coverage Area (GRCA) in a complex environment.

The MIST UHF requirements include high priority surveillance, early warning and interceptor control against the airborne threats over the GRCA, as well as continuous 360 degree-air surveillance. The high priority airborne threats over the GRCA require precision tracking and weapon control data. Additional UHF radar requirements include track, handover to the X-band radar, high range resolution ground moving target indications (GMTI) and Ballistic Missile Defense.

The X-band radar requirements are also expanded from the traditional ground surveillance requirements of both GMTI and stationary ground targets (SGT). The expanded requirements include accepting hand over from the UHF radar tracks, precision tracking of high priority airborne and ballistic targets (including height measurement), as well as location of ESM ground emitters. The additional X-band radar requirements include both Quick SAR and Go-Stop-Go SAR.

A summary of the MIST ROS UHF and X-band radar modes and submodes which are dynamically scheduled using the Sensor Manager Simulation are presented in Table 1.

Table 1. MIST Radar Suite Mode/Submode Summary

UHF Radar Tasks		
AMTI	High-Priority Region Search (U1)	
	Low-Priority Region Search (U2)	
	UHF Priority Target Track (U3)	
BMD	Search (U4)	
	UHF Radar Ballistic Missile Defense Track (U5)	
X-band Radar Tasks		
AMTI	High Accuracy Track (X1)	Aircraft (X1A)
		Cruise Missiles (X1B)
	Air Target Classification (X2)	High Range Resolution (HRR)/ 1-D Imaging (X2A)
		2-D Imaging (X2B)
	Height Finding (X3)	
	Handoff to Fighter (X4)	
GMTI	GRCA Search (X5)	General Search (X5A)
		High-Priority Region Search (X5B)
		Low-Priority Region Search (X5C)
	GMTI Track (X6)	Track While Scan (X6A)
		Priority Target Track (X6B)
		Priority Target in Priority Region (X6C)
	Ground Moving Target Classification (X7)	HRR (X7A)
		Inverse Synthetic Aperture Radar (ISAR) (X7B)
	Slow Target Surveillance (X8)	
SAR	Strip-Map (X9)	Low Resolution (X9A)
		Medium Resolution (X9B)
		High Resolution (X9C)
	Quick-SAR (X10)	
	Spotlight (X11)	Low Resolution (X11A)
		Medium Resolution (X11B)
		High Resolution (X11C)
	Special SAR (X12)	
BMD	Track (X13)	Boost-Phase (X13A)
		Ballistic (X13B)
		Terminal-Phase (X13C)
Other	Go-Stop-Go (X14)	
	Mobile TEL Location (X15)	
	Emitter Location (X16)	Single Radiation (X16A)
		Triangulation (X16B)
Combined UHF and X-Band Radar Modes		
AMTI	Track Handoff (UX1)	Aircraft Sized Targets (UX1A)
		Cruise Missile Sized Targets (UX1B)
BMD	Track Handoff (UX2)	

    Xn: n'th mode of the X-band radar

    Un: n'th mode of the UHF radar

    UXn: n'th mode of the UHF to X-band radar target track handoff

2.4   Knowledge-Aided CFAR

Constant False Alarm Rate (CFAR) processors were developed to maintain a constant average false alarm rate through adaptive threshold control while maintaining adequate target detection performance. The classical Cell Averaging (CA) CFAR processor assumes a homogeneous, Gaussian, thermal noise environment. It is, in fact, optimum under these conditions. However, in a wide area surveillance radar these assumptions are routinely violated, presenting a variety of returns whose statistical characteristics are varied and unpredictable and quite unlike those of thermal noise, even after filtering. The resulting effect is such that conventional CA CFAR processing may generate excessive false alarms. A significant amount of research has resulted in new CFAR algorithms developed for target detection in non-homogeneous clutter environments.   For example, Greatest-Of CFAR is appropriate for improved performance near clutter edges, Smallest-Of CFAR was developed to detect two closely spaced targets, and Ordered Statistics CFAR was conceived as a robust processor to minimize the effects of outliers. However, any single CFAR algorithm is likely to be inadequate in a dynamic environment, such as that observed from an airborne platform.   In light of the many constraints imposed upon radar systems, improvements in detection performance are most likely to be a result of advanced processing techniques which are able to recognize the existence of these situations and apply appropriate processing while effectively maintaining a constant false alarm probability and an adequate detection probability.

The AFRL's solution was based upon the combined use of algorithms and heuristics (artificial intelligence) techniques to assess the characteristics of the environment and apply the most appropriate CFAR algorithm. The solution incorporates many relatively new methods to deal with a wide variety of non-homogeneous environments.

Under the Expert System - CFAR (ES-CFAR) program, AFRL formulated rules dictating the dynamic selection of CFAR algorithms by the ES-CFAR Processor. These rules were incorporated into a prototype and refined through extensive testing and evaluation. Results indicated that the ES-CFAR Processor maintains a more uniformly constant false alarm probability (closer to the design value) than a conventional CFAR in the same dynamic, non-Gaussian background. This is also true of the detection probability which tends to vary and fall to inadequately low levels for the conventional CFAR processor. In the ES-CFAR Processor, a satisfactorily high value of detection probability is maintained through regions of dynamically changing, non-Gaussian interference.   After the rules had been completely developed and refined using results obtained from deterministic evaluation, AFRL investigated the performance of the system with input data from an external source showing similarly promising results. In many non-homogeneous environments the ES-CFAR proved to be superior to conventional CFAR techniques resulting in higher probability of detection and significantly lower false alarm rates.   A detailed description of the ES-CFAR is presented in Appendix E.

2.5 Knowledge –Aided Signal Processing

The AFRL Sensors Directorate has been instrumental in developing knowledge-aided adaptive technologies enabling significantly improved current and future Airborne Moving Target Indications (AMTI), GMTI, and SAR sensors. When operating in complex clutter environments potentially encountered in modern military applications, current ISR AMTI, GMTI, and SAR sensor performance may fall significantly short of expectations based on typical benign test environments. These operational environs typically contain one or more of the following effects: (1) Complex heterogeneous clutter; (2) Dense target backgrounds (military and/or civilian); (3) Urban and littoral clutter plus other large clutter discretes; (4) Nonstationary clutter loci arising from bistatic, multistatic and other advanced applications and concepts. Current and planned ISR architectures characterize interference from the same data used to detect targets. While sufficient in benign environments and less-stressing applications, this circa 1950's signal processing framework is inadequate when confronted with complex surface target engagement applications being addressed by layered sensing. The instability of the statistical signal processing methodology increases with higher adaptive sensor-dimensionality and needs to be avoided to maintain the United States' combat advantage in surface target engagement.

Over the past 20+ years, the US has gathered a large quantity of information on the physical and electrical characteristics of the operational environment, but was not able to adequately apply this information in the radar front-end signal processing to address the complex clutter problem. Recent breakthroughs at AFRL and elsewhere in high performance embedded computing (HPEC) and real-time database technologies enabled many AFRL developed adaptive knowledge-aided concepts - radically altering the fundamental 'front-end' signal processing architectures through intelligent, real-time integration of environmental knowledge (Digital Terrain Elevation Data (DTED)/Digital Feature Analysis Data (DFAD), SAR Imagery, and other onboard/offboard sources), high performance embedded computing, electromagnetic codes, and real-time database query and retrieval technologies (see Appendix H), AFRL/RYRT investigated techniques to radically alter the fundamental signal processing architectures of traditional ISR radar systems. Revolutionary concepts for improved sensor signal processing performance in complex interference environments through the exploitation of environmental knowledge sources within the high-speed front-end processing environment were investigated. Specific areas of research and development included: (1) knowledge-aided adaptive signal processing techniques for interference mitigation and constant false alarm detection processing (see Appendix F). Specific examples included, but were not limited to: knowledge-aided intelligent 'training' methods for optimum space-time weight vectors (see Appendix G); and knowledge-aided pre-whitening of the space-time multichannel received signals to reduce the number of adaptive degrees-of-freedom required; and (2) real-time knowledge-aided processing architectures. Hence, compatibility of the adaptive filtering process Space-Time Adaptive Processing (STAP) with the (CFAR) detection process and the utilized knowledge sources was essential in this effort. AFRL developed the signal processing, evaluation, analysis, and research (SPEAR) signal processing testbed laboratory to evaluate and quantify the performance benefit of proposed knowledge-aided algorithms and techniques and related innovations in a systematic manner.

2.6   Sensors as Robots

AFRL's Sensor-as-Robots program is developing and validating the technologies that support an intelligent C4ISR system of systems. This system of systems will be based upon a signal processing, image processing and artificial intelligence architecture that fully orchestrate the operation, tasking, and management of multiple sensors on multiple ground, air, and space vehicles.

An individual sensor system's performance can be enhanced by changing a sensor's parameters (e.g., waveforms) and algorithms as the environment changes. It has been shown that if an airborne radar system is aware of certain features of the earth (e.g. land/sea interfaces) and its surroundings, then it can intelligently improve system performance. Sensors as Robots leverages and extends this approach beyond a single sensor onboard a single platform to multiple sensors on multiple platforms performing distributed sensing with heterogeneous sensors.

The monolithic military adversary of the twentieth century is no longer the number one threat. Single function radar systems are necessary but not sufficient for combating the integrated and coordinated threat of peer/near-peer countries and asymmetric threat. The desire to anticipate, find, fix, track, target, engage, and assess, anything, anytime, anywhere (AF2T2EA4) by the US Air Force will require changes to how we develop sensor systems.

On-going work is investigating coherent signal level fusion of homogeneous sensors (see Appendices A, B and C) and data fusion and mode/parameter control of heterogeneous sensors on a single platform (under the MIST program). Sensors-as-Robots will further integrate these radar systems with heterogeneous sensors (e.g. acoustic, IR, EO) located on the ground, in the air, in space, and underground (see Appendix K). The individual radar system of the future must be intelligent and integrated within sophisticated systems of heterogeneous sensors that operate on many hypotheses at the same time.

2.7   GEOsynchronous-orbit Moving Target Indication (GEO-MTI)

As discussed above, layered sensing considers different domains of layering. One of those domains is physical layering and the outermost physical layer is space. GEO-MTI (see **Figure 6** and **Figure 7**) is a space-based radar concept that provides multiple mission coverage of a single theater at a time. It can provide persistent all-weather coverage of airborne, ground-moving and theater ballistic targets. In our first-order analysis, the system consists of twelve space-based radars at geostationary orbit. Each of the radars has a 50-meter diameter reflector antenna and radiates 10 kilowatts peak power (therefore 10 kilowatts of average power). Each radar radiates one of a set of orthogonal waveforms and each radar receives all waveforms. Thus, the system consists of 144 radars (12 monostatic and 132 bistatic). The returns of the 144 radars are coherently and adaptively combined using distributed aperture processing technology. The range resolution is set by the bandwidth of the individual waveforms, < 30m, and the cross-range resolution is set by the baseline of the twelve radars (1 – 10 km), therefore <10 m.
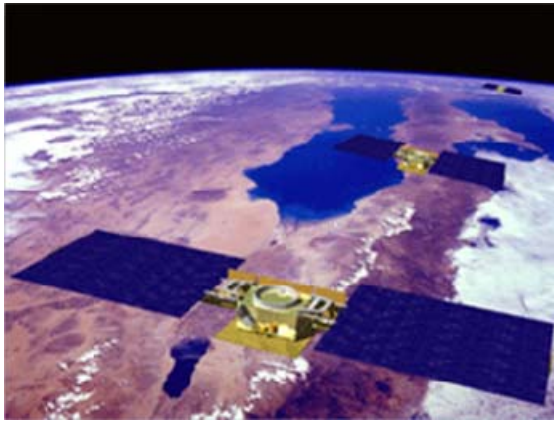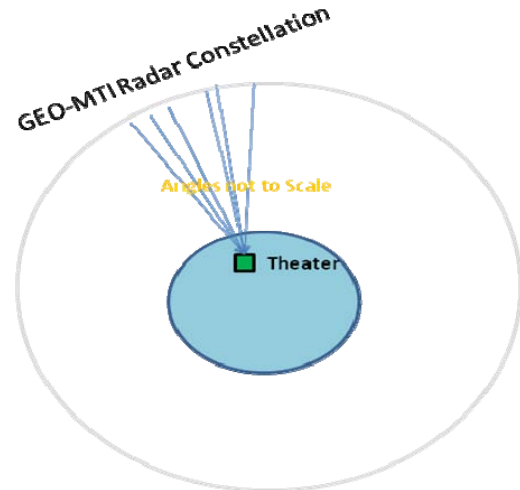
a) GEO-MTI Concept b) GEO-MTI Geometry

Figure 6 . GEO-MTI
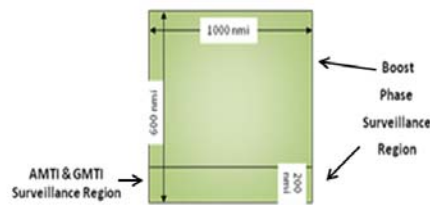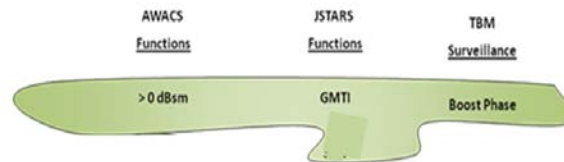
Figure 7. GEO-MTI Coverage Capability

GEO-MTI provides coverage of ground/surface-moving targets over the regions from 20° to 60° latitude (North or South) and for airborne/ballistic missile targets from 20° to 70° latitude. It is sized to continuously address a 1,000 mile by 1,000 mile theater. It will operate at either UHF or L-band. It will operate in difficult environments and must operate in conjunction with the other physical layers.

14

3 SIGNAL PROCESSING FOR LAYERED SENSING

3.1 Overview

As described in the Introduction, the threat of the future is more complex and more uncertain than that of previous situations that we have faced: including major wars (World War II), smaller wars (Vietnam, Korea), and the Cold War. In addition to these possible peer, near-peer and lesser nation conflicts, the asymmetric threat of terrorism can exist either independent of conventional wars, or even more importantly, integrated within them. As we have seen in the last twenty years, asymmetric threats can exist in the conflict region, in support locations, and also in our own country.

Since the asymmetric threat has much more flexibility in choosing when and where to attack, we must be prepared to address all terrain and environmental situations: foliage, mountains, urban, storms, snow, etc. A very critical aspect of the asymmetric threat is the overwhelming asymmetry between the terrorist cost to attack and our cost to defend. Our major surveillance assets (Airborne Early Warning and Control System (AWACS), Joint Surveillance Target Attack Radar System (JSTARS), Rivet Joint, etc.) are vital to our ability to effectively accomplish many major missions. But, to use them to counter one or a few terrorist activities would bankrupt the US in short order. On the other hand, these major assets accumulate data that can be of value to many users but their use is usually limited to a single user because of the stovepipe approach of most of our ISR systems (see Figure 8).
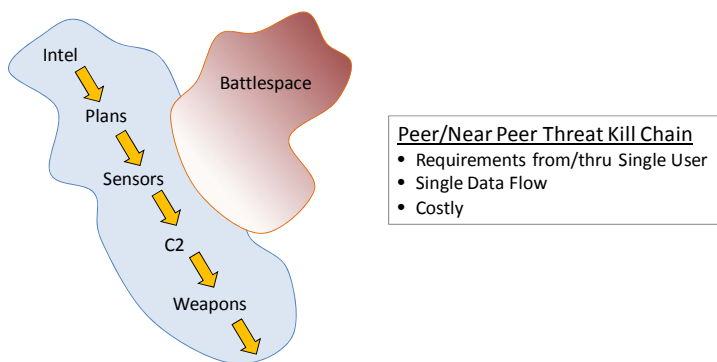
Figure 8. Classical/Legacy Stovepipe Approach

Another ever increasing issue is our reliance on the cyber world and the terrorists' ability to use this world at relatively no cost to them. How do we defend, utilize and deny the enemy the current freedom they have in the cyber world?

Layered Sensing is a technology thrust to address these issues. It includes existing ISR capabilities and many new C4ISR capabilities, some of which were presented in Section 2.

HASP is a necessary component of this initiative. HASP will support the transformation (see **Figure 9**) from isolated stovepipe ISR to:

- Multi-level integrated ISR

- Retaskable/reconfigurable ISR with the ability to quickly and cost-effectively address specific threats

- Multi-theater, multi-platform (space, air, surface, below ground, cyber) ISR
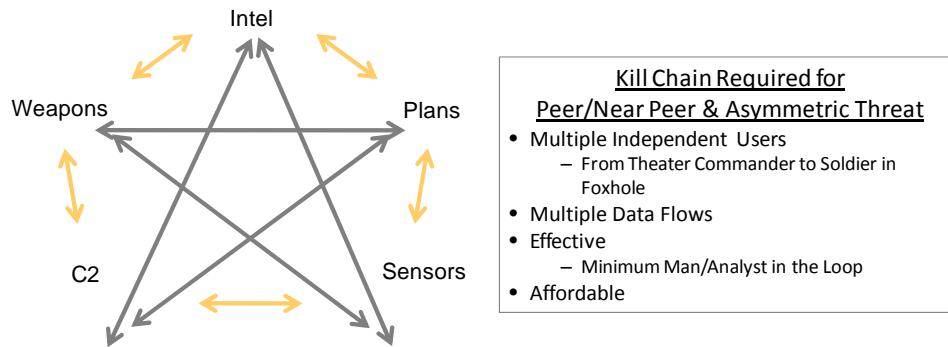
Figure 9. Layered Sensing Approach To The Kill Chain

HASP will permit the parallel and efficient addressing of multiple goal missions. Two major aspects will be a focus on information (what a user needs) not data (what a sensor provides), and on the importance of the interface between the C4ISR and the human (user). Existing ISR, planned ISR and as yet unenvisioned ISR will be supported by HASP.

3.2   Changing Threat

The cold war is over but the US continues to face a multitude of threats. Some threats are similar to threats during the Cold War, and yet some are significantly different than they were in the past twenty years. In addition, many threats continue to evolve - just when we have a solution to the problem, the enemy changes their tactics just enough to cause the solution to be ineffective. We have partitioned these threats into three categories, i.e., peer or near-peer nations, lesser nations, and the asymmetric threat. A peer or near-peer nation has approximately the same types of weaponry as the US, e.g., it has a nuclear capability and delivery system, i.e., chemical, biological, radiological, nuclear, explosives (CBRNE), a space program, an air force, army, navy, etc. They may not match the quantity of weapons the United States has in each category but they have similar technologies. These threats are marginally addressed with classical triad and C4ISR assets of today. A lesser nation may have some of the same types of weaponry, i.e., a conventional army, navy, and air force but they don't have a nuclear capability. They may have a CBRNE capability with a limited delivery system but they don't have space sensors and a communications program, and they may have a limited missile capability. We can address this enemy in offensive engagements abroad with our classical triad and C4ISR assets. An asymmetric threat has very little weaponry and no conventional armies. They have conventional weapons, i.e., explosives, fire arms, shoulder held missile launchers, and they may have some chemical and biological weapons with a crude delivery system. They have conventional communications systems and are well equipped in the cyber domain as are all our potential threats. We can address this enemy in offensive engagements abroad with our classical triad and C4ISR assets, however, with very high cost ratios. We do not have a significant institutionalized cost effective defense of the homeland. In pre-engagement scenarios, we cannot separate enemy combatants from the civilian populations. During engagements we require accurate high precision weapons in order to obtain our desired results and minimize collateral damage. Our old enemies, i.e., peer, near-peer and lesser nations, have recognized the cost effectiveness of using the asymmetric tactics against the US. The military must counter this threat abroad and the Department of Homeland Security

(DHS) must prevent asymmetric attacks at home with help from the Department of Defense (DoD) and all the relevant branches of government and law enforcement. **Figure 10** illustrates our capabilities assessment as it relates to the US obtaining local support as related to different enemies; significant engagements as it relates to terrain and local support, and the relationship of cost to the US; and our asymmetric enemies and their relationships to time, money, C4, and counter measures. The presence of the asymmetric threat and the dependence of our nation on the cyber domain have created the demand for more intelligent sensor system architectures. These sensor architectures must be engineered to be intelligent, accurate, precise, and autonomous, and be able to anticipate actions before they occur.
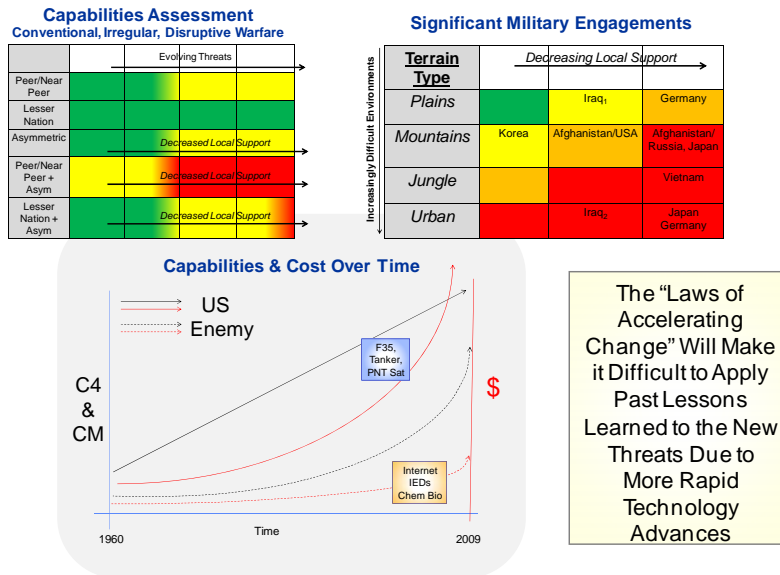
Figure 10. US Capabilities Assessment

3.3   Central Role of Net Centric

Recent research over the last 20 years in bringing artificial intelligence (AI) techniques to radar signal processing has been very successful in enhancing a radar's performance strictly through algorithm development, software advances, and higher speed computers. It is time to leverage these faster computers equipped with new signal processing and AI algorithms to assist the US Air Force in transforming how sensors are deployed and managed. Tasking sensors to gather data over a region, where each sensor is independently managed by different groups is ineffective when addressing these emerging threats. One approach is to partition the earth into regions where each region manages all the sensors operating within its region. This includes sensors in space, on an aircraft flying within the region, or on or under the ground. **Figure 11** provides an abstract diagram of a regional sensor manager (RSM). RSMs task sensors in an abstract manner such as "look for targets leaving roads" or "determine if a vehicle stops near a road or side of a road" or "perform persistent tracking of a particular target". (A specific task is not "fly a race track for 8 hours and save all data for future analysis and hope an operator identifies something out of the ordinary".) To achieve this capability we must place more intelligent software closer to the sensor. There must be intelligent software on each platform such as on an aircraft, on an Unmanned Air Vehicle (UAV),

space asset, etc. These intelligent software managers will manage all the sensors on its platform and also communicate with nearby sensor platforms and the RSM. They will obtain direction from the regional manager and provide results to their current sensor managers, if required, and to the regional manager. In so doing they will reduce the bandwidth required, for example reporting every detection of a GMTI radar can be reduced to only reporting those detections that meet the predefined tasks provided by the regional manager. All regional managers will communicate with each other and to a global sensor manager (GSM). The number of regional managers can easily expand or contract and any RSM can assume the GSM's responsibilities if it fails.
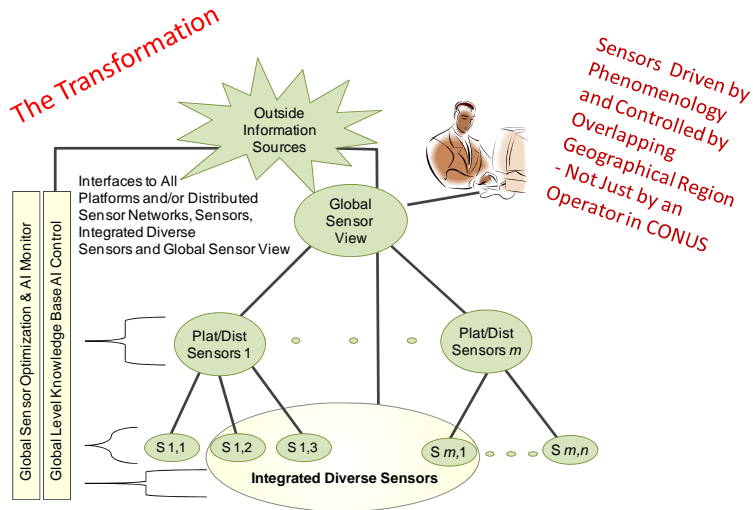
Figure 11. Regional Sensor Manager (RSM) Concept

To put this architecture in perspective consider the following two diagrams of Building Block 1 (BB1) and Building Block 2 (BB2) as shown in **Figure 12** and **Figure 13**. These types of sensors or cluster of sensors allow us to construct a more complex architecture. Consider the following diagram as our Sensors As Robots architecture (see **Figure 14**).
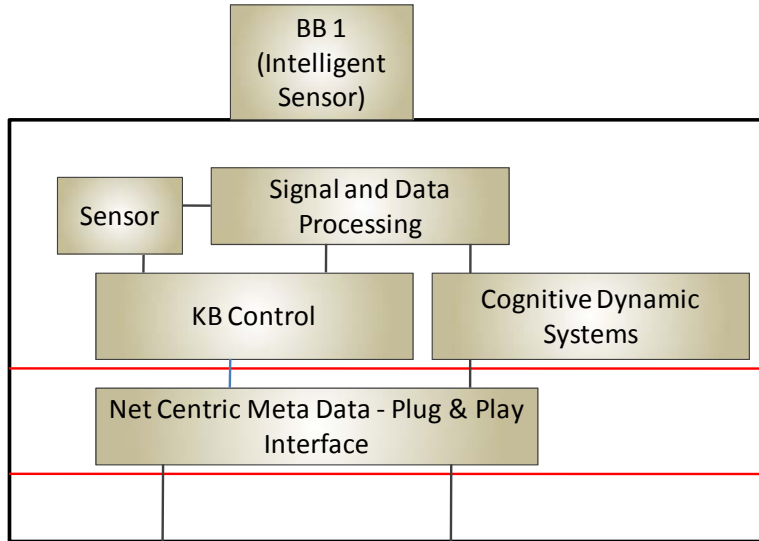
Figure 12. Plug and Play Sensor Building Block (BB) for Intelligent or Cognitive Sensors (e.g. Cognitive Radio, Airborne Intelligent Radar System (AIRS) with Waveform Diversity, etc.; Appendix J)
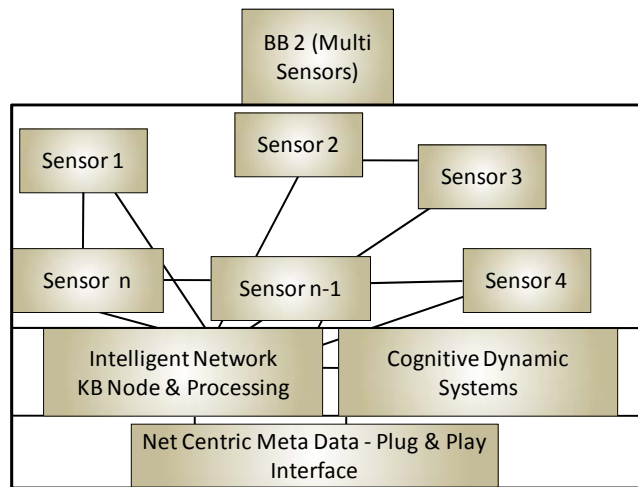
Figure 13. Plug and Play Sensor Building Block (BB) for Swarms of Intelligent Sensors or Collections of "Dumb" Sensors(Electro-Optic Cameras on Light Posts, Ground Based Seismic Sensors, Ground Based Acoustic Sensors, etc.)
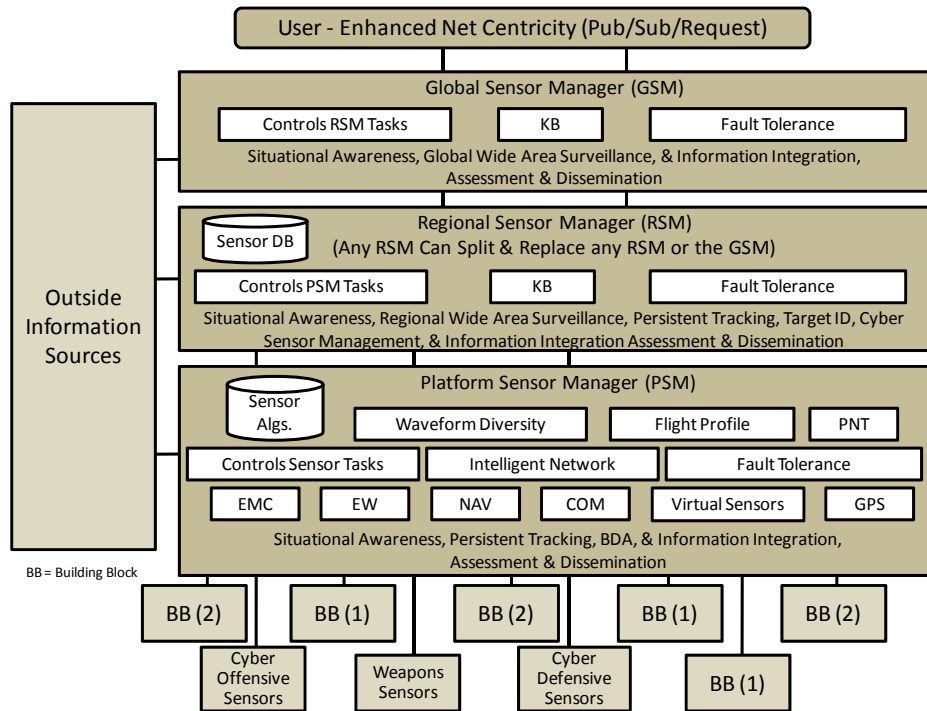
Figure 14. Sensors as Robots Architecture

A more detailed view of a RSM and one of its platforms showing a hypothesized data and control flow is shown in **Figure 15**. The RSM performs all of the tasking for its platform sensor managers (PSM), sets priorities, knows how to fuse sensor data from heterogeneous and homogeneous sensors, has knowledge of all of the sensors and what tasks they are performing, has knowledge about waveform selection, is knowledgeable of all of the sensors and their capabilities, and is knowledgeable of all of the platforms and their architecture, their capabilities and their current status. The PSMs have access to information sources related to weather, maps, Electromagnetic Interference (EMI)/Electromagnetic Compatibility (EMC) rules, flight information, etc. The platform manager manages all the sensors and communication systems on board its platform. It implements the tasks presented by the RSM given the priorities of the tasks and the capabilities of its sensors and their signal and data processing algorithms. The signal processing software is contained at each of the sensors. The Intelligent Sensor Software, in this architecture design, can assign different algorithms to each sensor depending upon the tasks they were directed to perform, e.g., persistent tracking of a specific vehicle, or look for vehicles that pull off the side of a road and stop. Because of waveform diversity, neXt Generation (XG) radios and cognitive radar systems, the platform managers must coordinate all of the emissions and waveforms on the platform to reduce the probability of electromagnetic (EM) fratricide between sensors and communications equipment onboard the platform and other nearby platforms. The RSM negotiates its tasks with the PSM based upon its sensors status, priorities, and unknown parameters that the regional manager may not be aware.

20
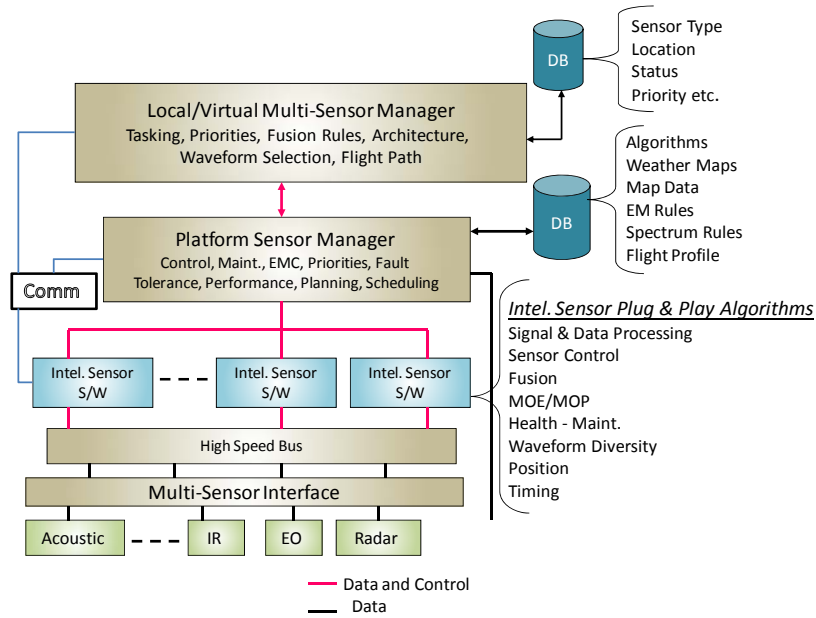
Figure 15. RSM Data and Control Flow

Information is provided and disseminated using the net centric paradigm as illustrated in **Figure 16**. We have enhanced the basic publish and subscribe paradigm to include requests. In this manner a commander or individual airman or soldier can request information based upon their requirements and justification. Developers of information publications will require the assistance of subject matter experts (SME) to automatically generate publications in a timely manner for the requesting individuals.
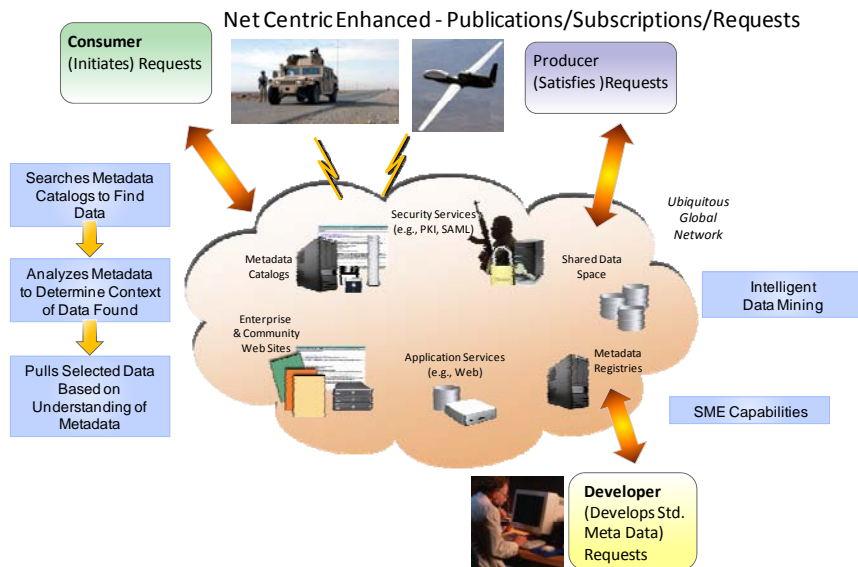
Figure 16. Illustration of the Net Centric Paradigm

The communications capability for retrieving and disseminating sensor information will require numerous technologies as shown in **Figure 17** below. The net centric paradigm will utilize classified high speed networks, low bandwidth radios, and intelligent software systems such as the Joint Communications Airborne Network (JCAN) and Intelligent Mobile Proxy (IMP) in order to produce, subscribe and request sensor information in a timely manner.
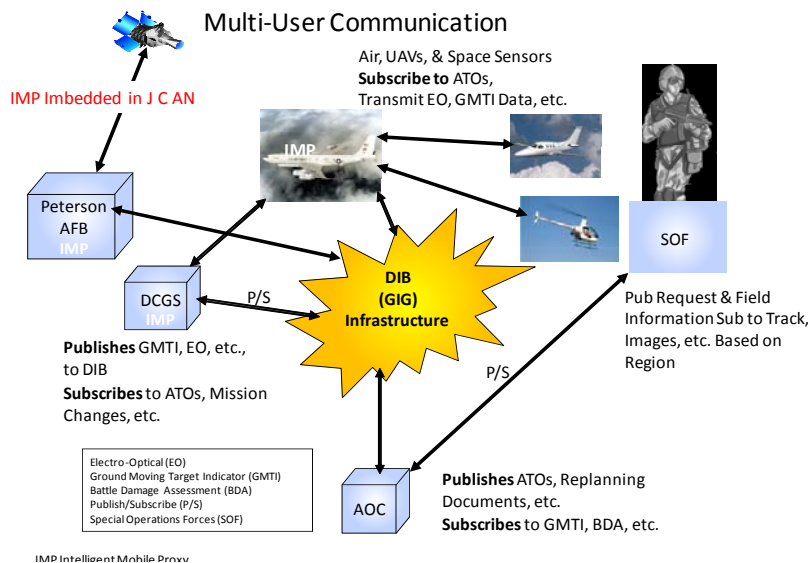
Figure 17. Notional Concept Connectivity Capability for Retrieving and Disseminating Information

3.4 Role of Cyber

Cyber plays a major role in defending our nation. As seen in **Figure 17** above, the cyber domain is used in the gathering and dissemination of sensor data and information. However, because of its low cost it is one of our current enemies' favorite domains to gather and share data, information and knowledge. It is believed by some that the cyber domain is our asymmetric enemy's main C4 Intelligence domain. It is also conjectured that our other enemies are also using this domain to spy on us and to do us harm by bringing down some of our more important server centers within our government and commercial infrastructure. It is a domain that we must monitor and protect just as we do space, air, ground and underground. We must monitor all communications of our enemies, sensing their every move, their planning, and the execution of their warfare tactics. In so doing we must try and anticipate actions before they occur and counter them with a correct and timely response.

Consider, as an example, the role of cyber in the following anticipate scenario as depicted in **Figure 18**. Imagine a Wi-Fi café within a city threatened by terrorism. A normal looking native arrives with his laptop computer and purchases a cup of coffee and accesses the freely available Wi-Fi. Intelligent software monitoring the Internet server within the café notices that someone is accessing underground web sites related to the purchasing of materials required for building a new kind of explosive. Within the immediate vicinity of the café there are hidden cameras and sensors including software that monitor all activities both wired and Wi-Fi within the café. The café's server is being managed by software that can

link the media access control (MAC) address of each computer and has a record of web sites visited. A comparison is made of the visited web sites and the corresponding MAC address is determined. Hidden RF sensors can determine in which portion of the café the laptop with the suspect MAC address is located. By increasing the bit error rate to the MAC address, cameras detect which individual is linked to the MAC address since the user will attempt to move his computer closer to the wireless access point, and/or complain to the owner about the poor quality of Wi-Fi service. At this point, the cameras have images of the suspect person, who is identified using photo identification software. Phone records, credit card transactions, and news articles are simultaneously searched to obtain all possible information concerning this person. In parallel, imagery databases obtained from strategically placed cameras throughout the city are queried to determine through timeline analysis information pertaining to where and how he arrived at the café, e.g., on foot or via a vehicle, and if so, its license plate number, etc., are obtained. Also, a simulation with multiple hypotheses will compute when and what the individual may likely do next. Messages will be sent to multiple sensors (acoustic, IR, EO, radar) throughout the city to monitor his movements and continuously update software predictions.
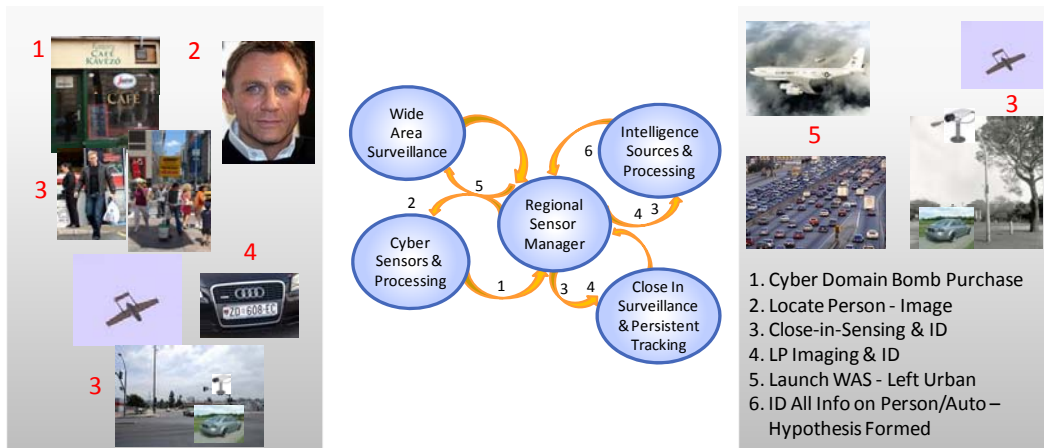
Figure 18. Role of Cyber in Anticipate Scenario (Example)

We must own the cyber domain just as we own the skies when we encounter many of our potential near and near-peer enemies. We can't win any war unless we dominate all domains. Unlike wars before, the sensing and reaction to our enemies has to be in minutes or seconds. We must tear down the restrictions that hinder our stove piped sensor systems to work together intelligently to defeat a threat that has no boundaries. Intelligent layered sensing is necessary if we are going to defeat our enemies that use asymmetric tactics.

3.5   Heuristic and Algorithmic Signal Processing (HASP)

A signal processing initiative will be the central focus of technology required to develop the Layered Sensing capability that will address the future threat addressed in Section 1. This focus will permit the integration of legacy systems, future systems and technology (some described in Section 2) and cyber for a cost-effective solution.

23

AFRL/RY has a long history of signal processing development that has always included a strong leadership role. This history has included both basic technology and specific applications:

- Algorithm Development
- Applied Statistics
- Artificial Intelligence (AI)
- Cognitive Radio and Radar
- Detection and Estimation Theory
- Detection of Concealed Targets
- Distributed sensors and Systems
- Engineering Mathematics

- Integrated ISR
- Multi-Sensor Integration
- Signal and Image Processing
- Systems Engineering
- Radar Technology
- Waveform Diversity & Design
- Ultra-Wideband Radar

Effectively addressing current and emerging critical challenges demands a willingness to look at the scientific and technical problems and innovative solutions arising across the various technical disciplines that must come together in order to provide a foundation for a more affordable, more effective and lasting technical advantage over our adversaries.

Research in knowledge based signal and data processing relies heavily upon multidisciplinary techniques being brought to bear on the detection, discrimination, and identification of difficult targets in a variety of environments. For almost two decades, AFRL/RY has been investigating the potential for significant improvements in *enterprise wide* performance by bringing all sources of data/information/knowledge into the formulation of a comprehensive signal, image and data processing solution to the sensing problems at hand. This approach addressed technology challenges in the anticipate, find, fix, track, target and assess aspects of the Air Force S&T Vision long before it was articulated as AF2T2EA4. The sources being exploited in this technology development endeavor include passive and active sensor data, real time and archival, cultural and geographical data that characterize natural formations and man-made structures, census data and dynamic population information, etc. Furthermore, we draw upon multi-intelligence sources, including cyber and communications in order to formulate the best technical solutions to the sensing problems under investigation. More often than not, cues from cyber and communications drive our sensing modalities in the current research, but sensors must also be used to drive communications and cyber signal exploitation as well.

This comprehensive approach to target detection, tracking, and identification, known as Knowledge-Based Space-Time Adaptive Processing (KB-STAP), successfully merged algorithmic and heuristic signal and data processing into a new paradigm, one in which mathematical rigor was fully compatible with intuition-based decision making popularized in game theory. AFRL/RYRT's research in KB-STAP led to the Defense Advanced Research Projects Agency (DARPA)-funded KASSPER (Knowledge-Aided Sensor Signal Processing and Expert Reasoning) program that transitioned algorithms and created an architecture that enables major weapons systems to perform multiple ISR functions simultaneously and autonomously. The efficient use of prior knowledge in applying mathematical algorithms to signal and image processing is a cornerstone of these KB-STAP algorithms and architectures. Emerging sensors now incorporate knowledge based signal processing as a result of this research.

KB-STAP was derived from the ES-CFAR processor, which was invented in 1985 under the Aircraft Defense Initiative (ADI), and was patented by the US Air Force (patent no. 5,499,030), and has impacted fielded systems. This research was integral to the formulation of advanced algorithms in KB-STAP. The early work in KB-STAP centered on extending concepts developed for detection processing in ES-CFAR to include multidimensional filtering, track processing and waveform diversity. An important invention in KB-STAP was the non-homogeneity detector (NHD), Appendix F. The fundamental tenet in the theory of the NHD is the intelligent selection of parameters and data in adaptive algorithms, specifically in training data selection and subspace architecture partitioning. An order of magnitude improvement in radar performance has been reliably and consistently demonstrated when applying the NHD and KB-STAP technology to phased array radars.

As a result of these earlier investigations into ES-CFAR and KB-STAP, a number of additional research areas were initiated. These included waveform diversity for full adaptivity on transmit and receive in radio frequency sensors and systems, with the additional benefits of embedded communications, and precision navigation and timing. Waveform diversity technology is essential to the success of the Layered Sensing vision of AFRL. In waveform diversity, a single aperture may perform active sensing, communications, navigation or electronic warfare as the engagement demands, in addition to passive sensing. However, the on-going research also explores the potential for distributed apertures to "plug and play" in a coordinated and coherent manner. The goal of this research is to create a theater-wide radio frequency "hologram", one in which sensing, electronic warfare, navigation and communications signals seen by the enemy and ally alike are of our choosing. In order to facilitate the development and deployment of waveform diversity technology, a Tri-Service consortium (AFRL, Naval Research Lab, Army Space and Missile Defense Center) was created to accelerate the rate of change and acceptance by the user community. Recently, this team was expanded to include NATO allies as well. The rapid acceptance of knowledge based signal and data processing and waveform diversity technology is a resounding endorsement of the vision AFRL articulated and evolved over the past twenty five years.

In 2002 a significant new in-house research effort, Sensors as Robots, was initiated by AFRL/RY to extend knowledge base and waveform diversity technologies to multi-sensor geographic diversity and position control. Sensors as Robots will permit "action at a distance without human intervention", even in difficult and dynamic environments. One can easily envision future military operations and emerging civilian requirements that will be both complex and stressing and will demand innovative sensors and

systems configurations. The goal of Sensors as Robots is to develop a cost effective and extendable approach for providing intelligence, surveillance and reconnaissance for a variety of applications in dynamically changing military and civilian environments. Sensors as Robots represents a new ISR sensor archetype. In this paradigm, sensor and platform position, modalities and algorithms will be autonomously altered depending upon the environment. Sensors, especially radars, will use the same returns to perform detection, discrimination and identification, to adjust the platform flight path, and change mission priorities. Active sensors will dynamically and automatically change waveform parameters to accomplish these goals. Disparate sensors will communicate and share information and instructions in real-time. Intelligent sensor systems will operate within and between sensor platforms such that the integration of multiple sensor data provides knowledge needed to achieve dynamic goals and avoid electromagnetic fratricide. Intelligent sensor platforms working in partnership will increase information flow, minimize ambiguities, and dynamically change multiple sensors' operations based upon a changing environment. Concomitant with the current emphasis on more flexible defense structures, Sensors as Robots will allow the appropriate incremental application of remote sensing assets by matching resources to the situation at hand. This research pursues the development of futuristic ISR concepts utilizing the innovative integration of cutting edge technologies such as: knowledge-based signal processing, cyber defense, robotics, wireless networking, waveform diversity, the Semantic Web, advanced computing architectures, and supporting software languages. This concept is projected as an autonomous constellation of air, space, cyber, and ground systems that would offer a robust paradigm to build toward future deployments. To paraphrase Lt. Gen David Deptula, Deputy Chief of Staff for Intelligence, Surveillance, and Reconnaissance, we are drowning in sensor data. With the maturing of the technology base, we will be able to take the human out of the loop to the greatest extent possible, and thus permit airmen to perform their essential functions without distraction or a lack of actionable information.

The future of ISR relies upon a fully adaptive and autonomous capability connected through net centricity and high performance computing. This capability will rely not just upon transforming stove-piped intelligence community assets, but also upon the entire surveillance and reconnaissance apparatus, both real-time and archival. Especially important will be the conversion of data and information from all sources into actionable knowledge or intelligence automatically, without the need for human intervention. Rapid advances in intelligence and information exploitation will exceed the capability of human operators, will rely upon emerging information concepts such as semantic web and web-based computing, and will require cyber security, sensing and offensive tactics. Previous innovations in the areas of adaptive processing, knowledge-based control, and space-time diverse waveforms will be crucial to the development of this new exploitation capability. In particular, the work in pre-detection fusion of multi-band sensor data is a fundamental predecessor to the required information fusion. The current challenge is the fusion of heterogeneous sensors and information sources.

4 TECHNOLOGY PROGRAM

Based on the technology base described in Section 2, a program plan for HASP was developed (see **Figure 19**.). The components of this program plan can be divided into two major thrusts:

- *Technology*

- *Verification and validation (See Section 4.2.1).*

The technology thrust has the following major components, objectives and approaches. Technology specific experiments are required in some cases in order to transition the technology to integrated Layered Sensing demonstrations which in turn will be transitioned to the users through integrated demonstrations.
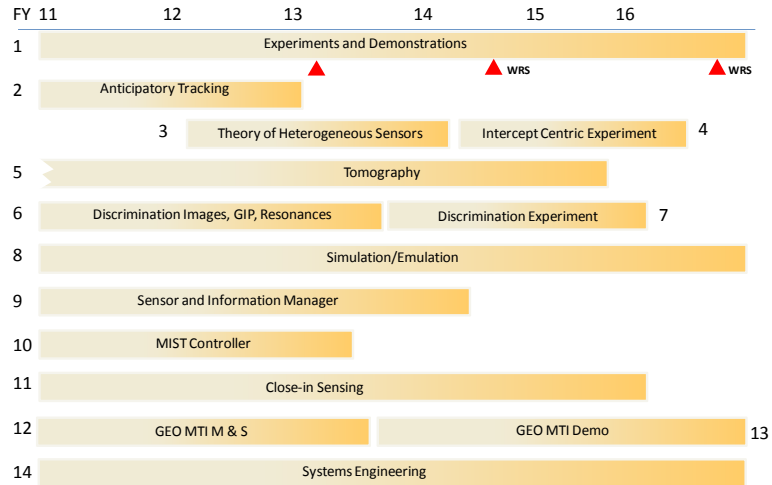
Figure 19. HASP Program Schedule

4.1 Anticipatory Tracking [1]

Most tracking algorithms in use today are memoryless i.e. if a track is dropped their history is also dropped from memory. This thrust is to develop and demonstrate the value garnered by maintaining track information throughout a sensor's mission. This is necessary for performing persistent tracking of vehicles and personnel within our ever changing war on terrorism.

4.2 Theory of Heterogeneous Sensing [2]

Most sensors in use today work independently and some share their findings after establishing tracks. It has been shown that the use of heterogeneous sensors (e.g. radar and an EO sensor) can aid in persistent tracking of targets with similar characteristics such as radar cross section and kinematics. This thrust will extend preliminary efforts and develop the basic knowledge and algorithms for intelligently utilizing heterogeneous sensors for the detection, tracking, and identifying of small targets in high clutter environments.

4.3   Intercept Centric Experiment [3]

This experiment will bring together many of the results of the previous efforts to demonstrate the integration of their findings to detect, track, identify and intercept enemy targets in complex environments. The concept of operations and the use of multiple heterogeneous sensors within a net centric approach rely on supporting technologies in order to be successfully deployed. This thrust will develop realistic scenarios, apply the necessary supporting technologies, and demonstrate how they can be integrated to outperform current sensors and their deployment tactics.

4.4   Tomography [4]

This set of tomography experiments leverages the spatial and geometric diversity of a multistatic radar to deliver high resolution MTI and will demonstrate the resolution of conventional wideband radar, while using narrowband signals. These narrowband signals are particularly attractive with consideration to the ongoing erosion of spectrum. In the RF tomography demonstration, some sites will have transmitters and receivers, while other sites are receive only. By locating transmitters and receivers in a uniform manner, beneficial effects of geometric diversity will be enhanced.

4.5   Discrimination: Images, Generalized Inner Product (GIP), Resonances [5]

Autonomous declaration of target type will be a key component in the successful implementation of Layered Sensing. Imaging (1D – HRR, 2D – SAR) has been used for almost 50 years to provide data on the parameters of targets of interest. But imaging has always required the image analyst. GIP and measurement of target resonances are two technologies with the potential of removing the man-in-the-loop in the parameter estimation process. The ongoing program focuses on single radar application of these technologies, HASP will extend each technology and integrated imaging/GIP/resonance analysis to multiple radars and to multiple sensors of disparate types.

4.6   Discrimination Experiment [6]

Experiments will be used to quantify the performance of the various discrimination approaches under various scenarios. These scenarios will include different sensor combinations and target types.

4.7   Sensor and Information Manager [7]

Layered Sensing will be 'layered' in a number of aspects: physical layers (high Earth orbit, low Earth orbit, airborne, surface-based, below ground), component layers (different sensor and command, control and communications (C3) types), user layers (national, theater, multiple component types). Each sensor and each C3 node can provide information to multiple users, so it is necessary to manage the sensors/C3 in a way to best meet those multiple information needs. HASP will develop an Information Manager that controls sensor/C3 location, pointing direction and system parameters in order to optimize the information for all users.

4.8   MIST Controller [8]

The ongoing MIST program is investigating the control of multiple sensors (low-frequency radar, high-frequency radar, Electro-Optic/Infrared (EO/IR), ESM, IFF) on a single airborne platform. The MIST system must address various AMTI, GMTI and imaging missions. HASP will extend the MIST controller to include the impact of new technologies on target detection, tracking and discrimination.

4.9   Close-in Sensing [9]

This area is dedicated to the issues related to developing and deploying heterogeneous sensors (e.g. RF, audio, video, chemical) in order to anticipate actions before they occur. In so doing we must detect, track, discriminate, and engage various targets in high clutter urban and mountainous environments. The deployment, communications, signal and data processing, and management of these heterogeneous sensors will be the major objective of this thrust along with electronic protection and EM fratricide avoidance.

4.10   GEO-MTI Modeling and Simulation [10]

GEO-MTI was designed to provide significant initial coverage in a new theater of interest. It would be located in one area but could be redeployed within hours to provide coverage of any theater worldwide (+/- 70 degrees latitude). It was sized to see any moving vehicle (airborne, surface) at any velocity and even has the potential to monitor dismounts. HASP will develop a detailed GEO-MTI system model and quantify its performance.

4.11   GEO-MTI Demonstration [11]

Multi-aperture experiments will be implemented to validate GEO-MTI performance. Issues associated with this demonstration include:

- Detection of all moving targets in the theater
- High accuracy positioning on all targets
- Continuous tracking in dense target environments.

5 VALIDATION THROUGH MODELING & SIMULATION / VERIFICATION THROUGH EXPERIMENTS & EXERCISES

Development and validation of the regional controller requires the capability to generate the outputs (1) after signal processing, (2) after tracking, and (3) after classification from each of the sensor systems in the region. These outputs will be integrated into a scenario-level simulation. Meta-models will be developed for each sensor type. These meta-models will provide a reasonable fidelity representation of the sensors and communications, including cyber, for the region. It is envisioned that the scenario must run in real-time and up to ten times faster than real-time.

Interim verification must be accomplished through multi-sensor experiments with some real-time control and significant post analysis. Final verification will be accomplished through multi-sensor/multi-user real-time exercises where the various decision makers in the region are emulated by the users of the future (e.g., AFIT professors and students).

5.1 Scenario Simulation/Emulation [12]

An example scenario to be used for performance evaluation is illustrated in **Figure 20** which represents a generic test scenario where surveillance of a small country is required including continuous monitoring of its borders. The example scenario can be characterized by:

- One of its bordering nations is a peer nation. The terrain near the border is very mountainous – enemy combatants are known to cross the boarders in vehicles, on foot, horse, donkey, etc., and sometimes disappear possibly into caves.

- There are multiple medium size cities south of the mountains with many roadways connecting them – many of these roads are periodically populated with explosives.

- Inside the cities there are enemy combatants living in buildings with the civilian population. Communications between combatants are via email, web sites, cell phones, land line phones, RF radios, couriers, etc. Combatants launch weapons from civilian populated areas, churches, schools, etc., and combatants use civilian vehicles for transportation.

Figure 20. Example Scenario for Performance Evaluation

5.2   Experiments and Demonstrations [13]

Experiments and exercises should be conducted to demonstrate the layered sensing concept incremental readiness.   In Fiscal Year (FY) 13, it is envisioned that planned experiments with representative targets and sensors be performed at Wright Patterson Air Force Base, (see **Figure 21**.). As an illustration consider five sensor types used in the experiments and a final exercise consisting of an: S-band radar, C-band radars (five small existing dish radars), bistatic/ESM system, tomographic radar system, and video cameras (five). A combination of controls by the experimentalists and autonomous control will be limited to a small number of expert system rules, e.g., approximately 10 expert system rules. Multiple ground targets of interest immersed in background traffic will be employed. Ground vehicles will be used to emulate the actions of a suicide bomber, while dismounts will be utilized to emulate the deployment of IEDs along roadsides. A variety of airborne targets will simultaneously overfly the area of interest. In addition, cyber will play a key role in our demonstrations. A number of cyber monitoring techniques will be employed throughout each experiment and exercise.
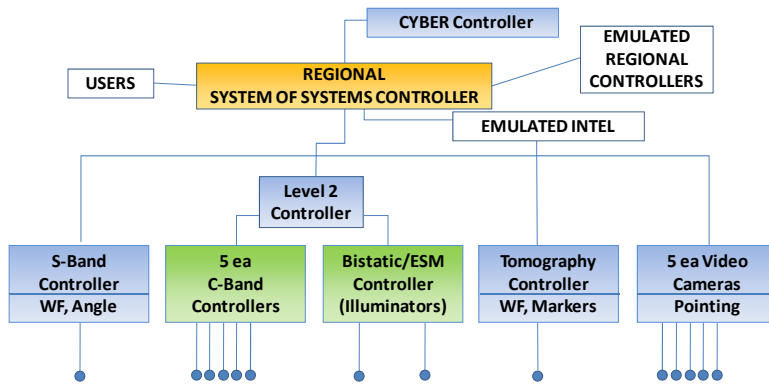
Figure 21. FY11 Control Architecture

A second, and more comprehensive experiment in FY 14 can be performed at Wright Patterson Air Force Base. The FY13 and FY14 experiments will incrementally demonstrate the level of readiness of our layered sensing research and development. Final verification will be accomplished through a multi-sensor/multi-user real-time exercise scheduled for FY16 at Wright Patterson Air Force Base. Full performance capability simultaneously addressing all major aspects of the layered sensing concept can be demonstrated. The exercise will include all of the components shown in **Figure 22**. The FY14 experiment should include as large a subset of those components as possible. A number of different operational conditions should be emulated: Normal operation, Severe counter-measures, Day without space/Global positioning system (GPS), and Day without cyber.
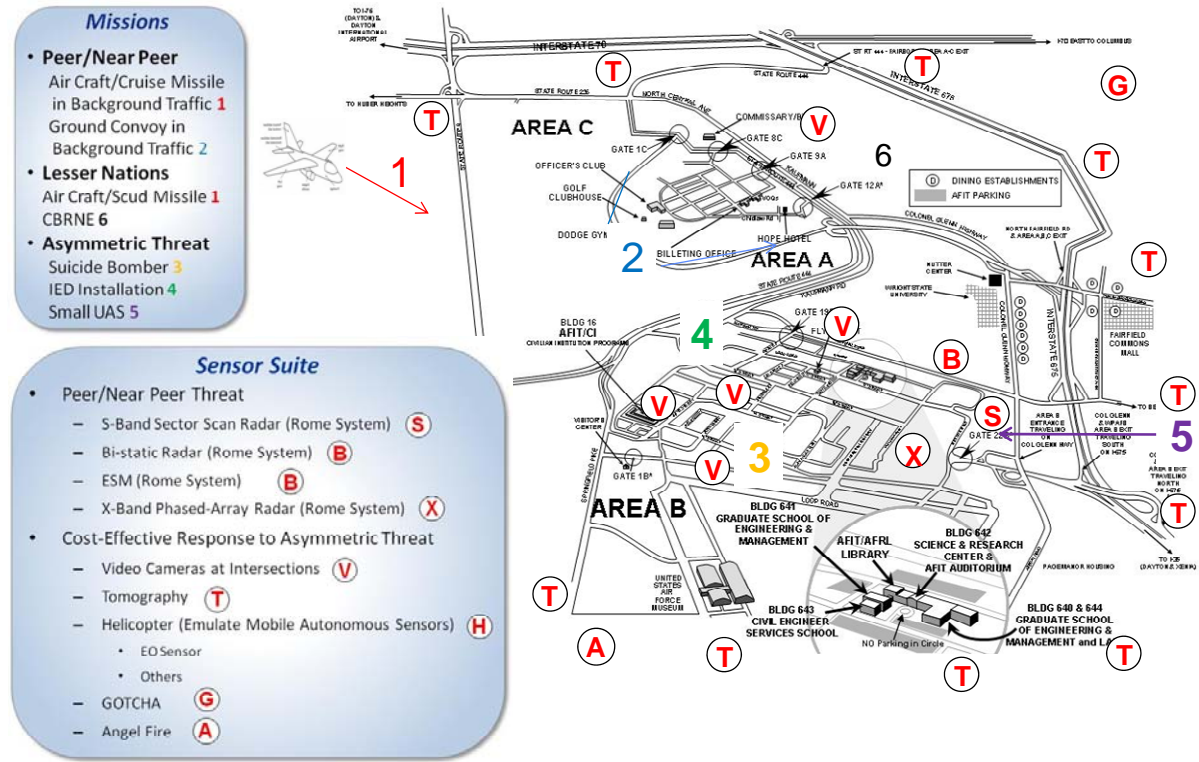
Figure 22. Layered Sensing / Outdoor Range Exercise (Geometry, Missions, and Senor Suite)

5.3   Systems Engineering & Integration [14]

The systems engineering & integration effort will focus on the complex technical design and management tasks required for realization of the layered sensing approach to surveillance and reconnaissance in challenged environments within the Air Force. Previous efforts have shown that a strong systems engineering approach has led to significant performance improvements, risk reduction and reduction of costs, as well as many other far reaching benefits. As illustrated in **Figure 23**, layered sensing is an immensely complex undertaking which will require that a disciplined design approach be employed at all levels of mathematical analysis, modeling & simulation, bench top testing, chamber measurements and outdoor range experimentation. In addition, a disciplined approach will be necessary to transform the current Air Force battlefield command and control structure to that required by a flexible, rapidly deployable layered sensing approach to surveillance and reconnaissance in challenged space, surface, sub-surface and cyber-space environments. Thus, both technical and human-centered disciplines will be needed to realize the paradigm shifts required by the layered sensing vision.
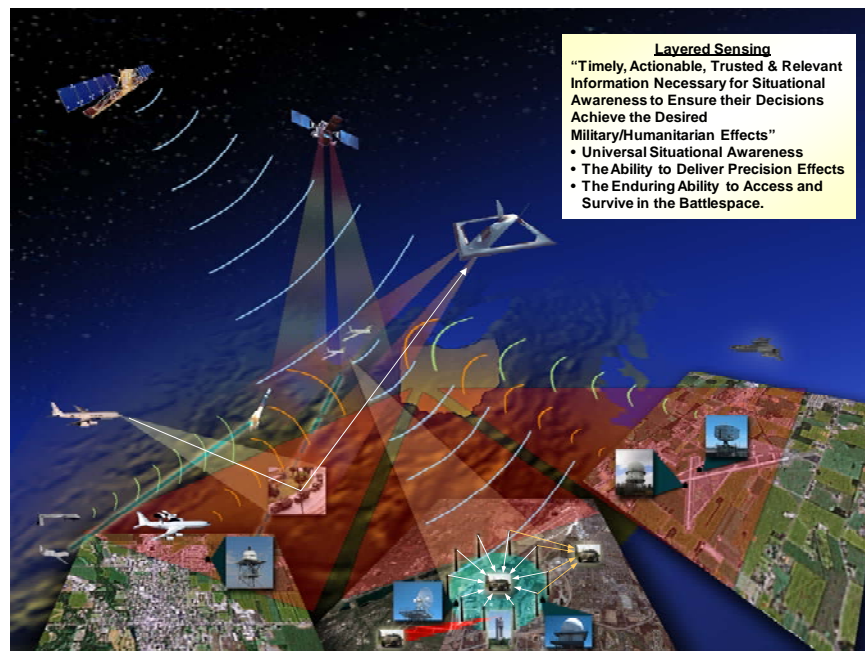
Figure 23. Systems Engineering Approach – Surveillance for Layered Sensing

In its broadest sense, the system engineering & integration approach to realizing layered sensing surveillance and reconnaissance will consist of: the identification and quantification of layered sensing goals and objectives: creation of alternative layered sensing surveillance and reconnaissance design trades; risk assessments; selection and implementation of the "best" design alternatives; verification that the designs are properly built and integrated in a cost effective manner; and post-implementation assessment of how well the designs meet the layered sensing surveillance risks and reconnaissance goals (see Figure 24). The identification of new methods and fundamental research opportunities to support long-term layered sensing needs is expected to be a natural outcome of this systems engineering focus. As such, the systems engineering & integration effort must deal with work-processes and tools to handle

layered sensing surveillance and reconnaissance implementation and the transition away from conventional warfare apparatus and techniques. The systems engineering approach to realizing the layered sensing surveillance and reconnaissance vision will heavily rely on the use of analysis, modeling & simulation, and demonstrations to validate assumptions and theories on systems and subsystems and interactions within them as previously identified. Experiments and demonstrations will be designed to generate evidence of the benefits and risks of layered sensing at all "decision maker' levels in a well defined manner for challenged space, surface, sub-surface, and cyber-space environments. Feedback at all stages of development and test will be an integral part of the design and development process.
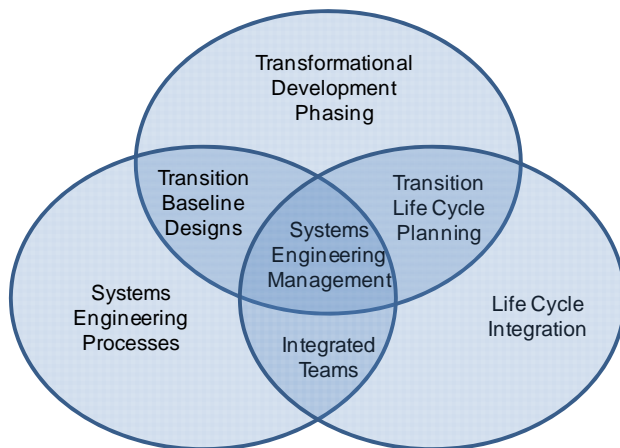
Figure 24. The Scope of Systems Engineering

The implementation of a systems approach will allow AFRL to institute a "Vision-to-Strategy-to-Task" planning process to develop a balanced S&T project portfolio for AFRL/RY. This will allow "flow-down" from vision through assessment of alternative solutions to a prioritized technology portfolio. The power of layered sensing will be demonstrated by defining and executing a set of integrated analyses and experiments to demonstrate progress towards appropriate Focused Long term Challenges (FLTCs). A natural outcome of this effort will be the development of Core Technical Competencies (CTC)-specific S&T plans to support the analyses and experiments. This systems engineering approach will then aid in the development and implementation of a process that improves the alignment of internal and external funding (DARPA, Missile Defense Agency (MDA), …) with the layered sensing vision. Adjustments of funding priorities to emphasize the exploratory investigations that may lead to "game changers" (e.g., identify new sensing phenomenologies or concepts) will naturally result with the holistic approach being pursued.

5.4   Holistic Approach

The systems engineering & integration approach which AFRL should pursue is both a holistic and interdisciplinary engineering effort that focuses on the very complex problems posed by the notion of layered sensing in challenged environments. A systems engineering & integration effort should focus on defining the "decision maker's" needs and required functionality as it relates to the entire kill chain. The process should include all levels starting early in the development cycle, documenting all requirements,

and then proceeding with the system-of-systems, system and subsystem design synthesis and system-of-systems validation while considering the complete problem, the entire system-of-systems life cycle. This holistic approach will leverage expertise in each sensing modality to provide a balanced solution to these very complex problems. The systems engineering process, then, can be decomposed into a systems engineering technical process and a systems engineering management process, i.e., to be effective the systems engineering & integration must overlap with both technical and human-centered disciplines.

5.5 Interdisciplinary Approach

Development of a layered sensing surveillance and reconnaissance capability for challenged environments will require contributions from many diverse technical disciplines across AFRL, the Air Force and beyond. By providing a systems (holistic) perspective of the development effort, systems engineers will meld all of the technical and management contributors into a unified team effort, forming a structured development process that will proceed from concept to development & test, to production to operation, and to sustainment for long periods. The interdisciplinary development team will participate on the sensor Integrated Product Teams (IPTs) as part of an ISR Task Force, work with designers across CTCs to generate roadmaps of future technical needs, engage operators (e.g., onsite with 480th Information Warfare (IW), Combatant Commands (COCOMs), NGA-P) in the refinement of the layered sensing requirements vision, and engage Air Force senior leadership to gain advocacy for the layered sensing vision. This team will work to gain advocacy for the Sensors Directorate (RY) vision within AFRL, e.g., with the Information Directorate (RI), and beyond the AFRL community. Extensive collaborations and user community engagements will be required (universities, labs, industry, Systems Program Offices (SPOs), Major Commands (MAJCOMs), other services…). By these actions the interdisciplinary team can develop and communicate the quantitative benefits of layered sensing for specific Air Force missions. This process is expected to provide a balanced approach to meeting layered sensing goals while addressing risk, vulnerabilities and anti-tamper needs, concurrently with the design process. In some cases it will be necessary to terminate and dispose of nonproductive or cost ineffective solutions as part of this process.

5.6 Technical Process

The technical process (mathematical analysis, modeling and simulation, bench top testing, chamber measurements and outdoor range experimentation) includes assessing all available information, assessing risks at all levels, defining effectiveness measures, creating behavior models, performing trade-off analyses & simulations and creating sequential build & test plans. It is important to ensure that the integration of heterogeneous sensing modalities within layers of stand-off/close-in sensing, networking and communications are appropriately considered in the over-all design process. An external, independent, comprehensive end-to-end systems analysis that includes options, limitations, need for margin, and Concept of Operations (CONOPS) to ensure successful demonstrations must be conducted. All experiments, demonstrations and exercises should be designed to provide evidence of the benefits for "decision makers" of layered sensing at all levels in challenged space, air, surface, sub-surface and cyber-space environments. Once fielded, the technical process will also include evaluation and quantification of the performance benefits and cost effectiveness of the layered sensing surveillance and reconnaissance

designs. Long term strategy, plans and roadmaps will be guided by the developed systems concepts, capability gaps which can be met, concept of operations, focused mission analyses, cost benefit analyses, and key program decision points. Implementation plans, derived from the strategy plans and roadmaps will be utilized to establish the context for technology team execution. Relationships between the various stages will be identified and will incorporate numerous opportunities for feedback.

5.7   Management Process

The complexity encountered by transition to and realization of the layered sensing surveillance and reconnaissance vision includes not only technical engineering systems and subsystems and their complex interactions, but also the logical human organization of data, information, knowledge, and communications.   Thus the goal of the technical management process is to organize the technical effort in the life cycle expectancy, as well as manage risk. The sheer size of the effort, amount of data involved, number of disparate variables and number of sensors involved in the design of a layered sensing surveillance and reconnaissance capability will require a carefully thought out and executed plan. Thus the systems engineering process will encourage the use of structured tools and methods to better comprehend and manage this complexity in realizing the benefits of layered sensing. Utilization of systematic work-processes and tools to efficiently handle the transition from   stove-piped   development   to   layered   sensing   will   include   (but   is   not   limited   to):

- Systems analysis
- Statistical analysis
- Performance optimization
- Modeling & simulation
- Measures of performance and effectiveness
- System dynamics
- Risk analysis
- Reliability & life cycle analysis
- Decision making processes

Taking an interdisciplinary approach is inherently complex since the behavior of and interaction among the system and subsystem components is not always immediately well defined or understood. Defining and characterizing the layered sensing surveillance and reconnaissance systems and subsystems and their interactions is one of the primary goals of the planned systems engineering & integration effort. The gap that exists between informal requirements from users, the "decision makers," and technical specifications must be successfully bridged.

5.8   The Systems Engineering Process for Layered Sensing

The systems engineering tools include strategies, procedures, and techniques that aid in performing systems engineering to achieve the layered sensing surveillance and reconnaissance vision. The purpose of these tools can vary significantly from sensor to sensor and subsystem to subsystem. And depending upon their application, these tools will be used for various stages of the systems engineering process.

Models play a very important and diverse role in our systems engineering process. A model can be defined in many ways such as an abstraction of reality, an imitation, analogue, or representation of a real world process or structure, or a conceptual, mathematical representation. Together, these are defined broadly enough to encompass physical models used in the verification of the layered sensing surveillance and reconnaissance system design, as well as functional flow diagrams and mathematical (e.g., quantitative) models used in the trade study process. It will be necessary to establish and apply disciplined validation approaches that improve the credibility of the models used. The model fidelity across each of the elements of the modeling and simulation (M&S) hierarchy should be linked. The layered sensing development team should ensure that the appropriate level of modeling be used is consistent with the requirements of that model, i.e., define and track appropriate fidelity metrics necessary to capture the required system dynamics. Multi-scale modeling technologies derived from distributed mission M&S, advanced signal processing, and data compression must be evaluated. Hardware in the loop should be inserted into simulation environments only when necessary to satisfy technical needs.

Mathematical models and diagrams should be used in the trade studies to provide estimates of the layered sensing surveillance and reconnaissance system-of-systems performance and effectiveness, technical attributes, and cost from the known and estimable quantities. Meaningful quantitative causal relationships relating inputs and outputs should be developed for all systems and subsystems.

Once the requirements are understood, the systems engineering function should refine them and make an assessment of the best, most cost effective technology for the job and assess the existence of feasible solutions. Constraints will be traded to find one or more feasible solutions. "Decision maker" requirements and desires are typically the most valuable input to such trade studies and cannot be assumed. Usually, several feasible solutions are found and a sufficient set of constraints defined to produce an optimum solution. Various modeling methods can and should be used to solve the problem including constraints along with cost functions. **Figure 25** summarizes the general systems engineering approach that can be employed during the development and test of the layered sensing surveillance and reconnaissance implementations.

Process Input

- "Decision Maker" Needs, Objectives & Requirements
  - Missions
  - Measures of Effectiveness
  - Environments
  - Constraints
- Technology Base
- Output Requirements from Prior Development Efforts
- Program Decision Requirements
- Requirements Applied Through Specifications and Standards
  - •
  - •
  - •

Legacy Control Protocol

Legacy Weapons Systems

Requirements Analysis

- Analyze Missions and Environments
- Identify Functional Requirements
- Define/Refine Performance and Design Constraint Requirements
- Legacy Systems Transition Constraints

System Analysis and Control

Requirements Loop

Functional Analysis / Allocation

- Decompose to Lower Level Functions
- Allocate Performance and Other Limiting Requirements to all Functional Levels
- Define/Refine Functional Interfaces (Internal/External)
- Define/Refine/Integrate Functional Architectures
- Define Exploitation of Legacy Functional Capabilities

- Trade-off Studies
- Effectiveness Analysis
- Risk Management
- Configuration Management
- Interface Management
- Data/Knowledge Management
- Performance Measures
  - Sys. Eng. Mgmt
  - Cost Mgmt
  - Technical Reviews

Design Loop

Synthesis

- Transform Architectures (Functional to Physical)
- Define Alternate System Concepts, Configuration Items and Systems Elements
- Select Preferred Product and Process Solutions
- Emerging technologies
- Cost / Open Architectures / COTS
- Define/Refine Physical Interfaces (Internal/External)

Process Output

- Development level Dependent
  - Decision Databases
  - System Configuration Item Architectures
  - Specifications and Baselines

Field Effectiveness Evaluations

Figure 25. The Layered Sensing Systems Engineering Process

38

6   BEYOND HASP

Heuristic and Algorithmic Source (signal, image, data, and cyber) Processing (HASP) will develop and demonstrate the capability to take data from multiple sources in order to provide autonomously the most relevant information to each user at all levels of the kill chain. In addition to the processing specific to each source, HASP will integrate the ongoing developments in artificial intelligence and man-machine interface. These two technical areas are outside of HASP but will continue to impact its development, as will new source concepts as they are developed.

HASP continues AFRL/RY's development of intelligent processing to achieve improved sensor performance without man-in-the-loop.   Expert System CFAR used data processing with multiple algorithms in parallel to provide better detection processing. KB STAP used understanding of the environment to more effectively reject interference. HASP efforts are generating new sensor processing outputs that can be more easily integrated autonomously in order to classify and identify targets (GIP, DART).   For individual sensor processing, HASP extends the expert-system and knowledge-aided approaches of AFRL/RY's previous work (see Figure 26).   Increased performance requirements and the need for autonomy greatly increase the complexity of the intelligent processing, even for an individual sensor (see Figure 27). This complexity will be beyond the capability of individual sensor experts and the integration of this processing will require advances in cognitive processing.
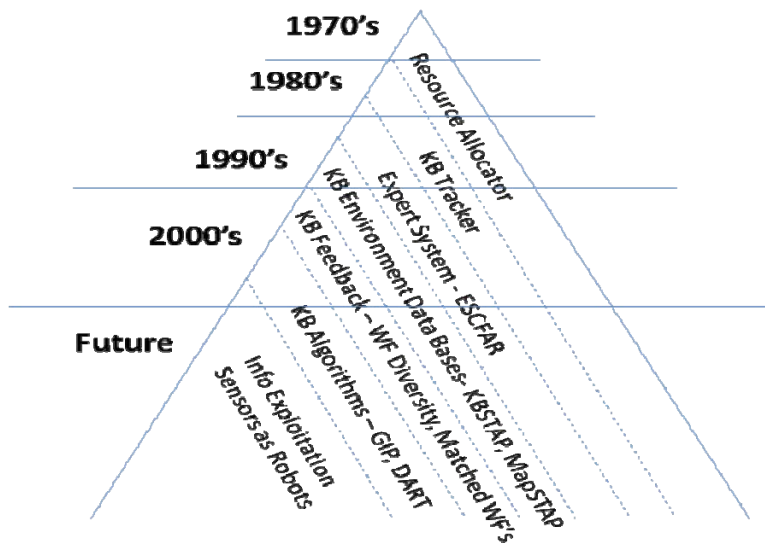
Figure 26. Intelligent Processing Evolution
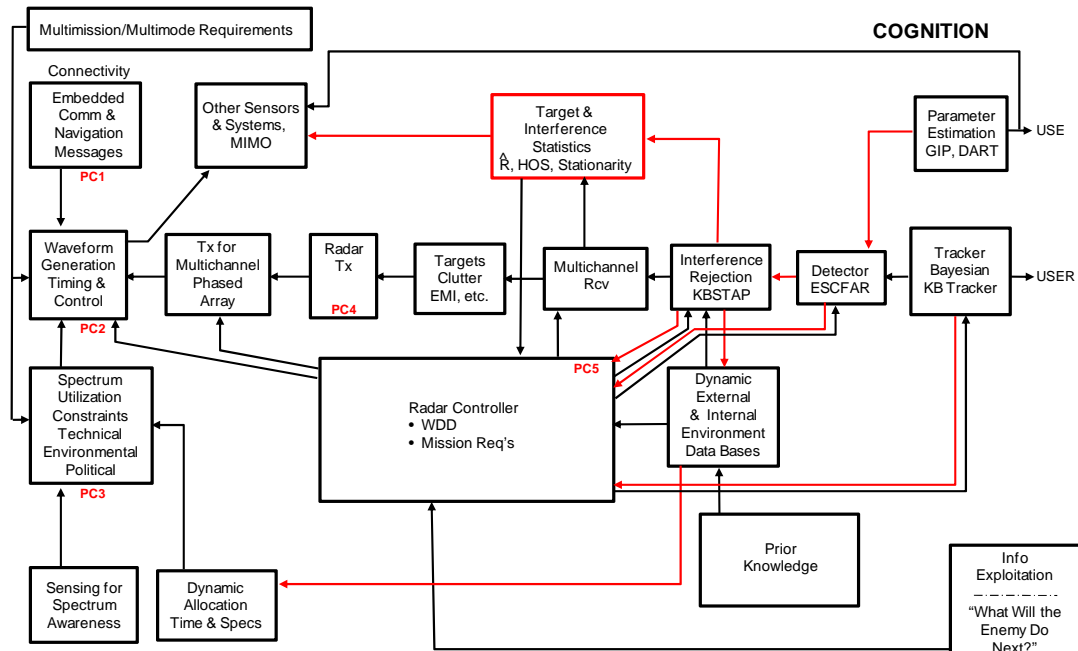
Figure 27. Cognitive Radar

Extension from sensors to sensors plus cyber will provide the potential for more data and better information. HASP will develop the processing technology for a broad spectrum of sources and will demonstrate these technologies for a limited set of sources and users.

Development of new source types (sensor, cyber, etc.), and C4 capabilities will continue. New users and user requirements will expand. Response to these changes will require an extension of HASP that includes the expertise of other directorates and other services. HASP technology and demonstrations will provide an excellent opportunity to initiate an effective outreach.

7   REFERENCES

[1] Wicks, M. C., and Zhang, Y, "Optimized Detection of Spatially Extended Fixed Objects in Clutter", *2009 IEEE Radar Conference*, Pasadena, CA, 4-8 May 2009.

[2] Capraro, G. T., Bradaric, I., Wicks, M. C., and Ratazzi, E. P., "Intelligent Sensor – Wi-Fi", *Proceedings of the 2007 International Conference on Artificial Intelligence*, Las Vegas, Nevada, USA, 25-28 June 2007.

[3] Bradaric, I., Capraro, G.T., and Wicks, M.C., "Sensor Placement for Improved Target Resolution in Distributed Radar Systems", *IEEE Radar Conference*, Rome, Italy, May 2008.

[4] Weiner, D.D., Wicks, M.C., and Capraro, G.T., "Waveform Diversity and Sensors as Robots in Advanced Military Systems", *1st International Waveform Diversity and Design Conference,* Edinburgh, UK, November 2004.

[5] Capraro, G.T., Bradaric, I., Weiner, D.D., Day, R., Perretta, J., and Wicks, M.C., "Waveform Diversity in Multistatic Radar", *2nd International Waveform Diversity and Design Conference*, Lihue, HI, January 2006.

[6] Bradaric, I., Capraro, G.T., Weiner, D.D., and Wicks, M.C., "Multistatic Radar Systems Signal Processing", *IEEE Conference on Radar*, Verona, New York, USA, April 2006.

[7] Bradaric, I., Capraro, G.T., and Wicks, M.C., "Waveform Diversity for Different Multistatic Radar Configurations", *Asilomar Conference on Signals, Systems, and Computers*, November 2007.

[8] Capraro, C. T., Bradaric, I., Capraro, G.T., and Lue, T.K. "Using Genetic Algorithms for Radar Waveform Selection", *IEEE Radar Conference*, Rome, Italy, May 2008.

[9] Bradaric, I., Capraro, G.T., Weiner, D.D., and Wicks, M.C., "A Framework for the Analysis of Multistatic Radar Systems with Multiple Transmitters", *International Conference on Electromagnetics in Advanced Applications*, Torino, Italy, September 2007.

[10] Giompapa S., Farina A., Gini F., Graziano A., Croci R., and Di Stefano R., "Study of the Classification Task into an Integrated Multisensor System for Maritime Border Control", *IEEE Radar Conference 2008*, Rome, Italy, 26-30 May 2008.

[11] "Knowledge-Based Systems For Adaptive Radar: Detection, Tracking, and Classification", *IEEE Signal Processing Magazine*, Volume 23, Number 1, January 2006.

[12] Bradaric, I., Capraro, G.T., and Zulch, P., "Signal Processing and Waveform Selection Strategies in Multistatic Radar Systems", *3rd International Waveform Diversity and Design Conference*, Pisa, Italy, June 2007, invited paper.

[13] Bryant, M., Johnson, P., Kent, B. M., Nowak, M, and Rogers, S., "Layered Sensing: Its Definition, Attributes, and Guiding Principles for AFRL Strategic Technology Development", http://www.wpafb.af.mil/shared/media/document/AFD-080820-005.pdf , 1 May 2008.

8   LIST OF ACRONYMS

ADI - Aircraft Defense Initiative

AF2TE4A - Anticipate, find, fix, track, target, engage, and assess, anything, anytime, anywhere

AFIT – Air Force Institute of Technology

AFRL - Air Force Research Laboratory

AFRL/RRS – Air Force Research Laboratory/Rome Research Site

AI - Artificial Intelligence

AIRS - Airborne Intelligent Radar System

AM – Amplitude Modulation

AMTI – Airborne Moving Target Indicators

AOA – Angle of Arrival

AOC – Area Of Concern

AOI – Area of Interest

ATOs – Air Traffic Operations, Authority to Operate,

AWACS - Airborne Early Warning and Control System

BB - Building Block

BB1 - Building Block 1

BB1 - Building Block 2

BDA – Battle Damage Assessment

C2 – Command and control

C3 – Command, Control and Communications

C4 - Command, Control, Communications and Computing

C4ISR - Command, Control, Communications and Computing Intelligence, Surveillance and Reconnaissance

CA - Cell Averaging

CA-CFAR – Cell Averaging-Constant False Alarm Rate

CBRNE - Chemical, Biological, Radiological, Nuclear, Explosives

CEP - Complex Event Processing

CFAR - Constant False Alarm Rate

CNR – Clutter-to-Noise Ratio

COCOMs – Combatant Command

COM - Communication

CONOPS - Concept of Operations

CONUS – CONtinental United States

CPI – Coherent Processing Interval

CTC- Core Technical Competencies

DARPA - Defense Advanced Research Projects Agency

DAML – DARPA Markup Language

DARs - Distributed Aperture Radar

DART - Declaration Algorithms for Resonant Targets

DB - Database

dB - decibel

DCGS - Distributed Common Ground/Surface System

DEP – Detection Environment Processor

DFAD - Digital Feature Analysis Data

DHS - Department of Homeland Security

DIB – Directory Information Base

DLG – Digital Line Graph

DoD - Department of Defense

DoF – Degree of Freedom

DTED - Digital Terrain Elevation Data

ECCM – Electronic Counter-Countermeasures

ECEF – Earth Centered Earth-Fixed

EM - Electromagnetic

EMC - Electromagnetic Compatibility

EMI - Electromagnetic Interference

EO - Electro-Optic

EO/IR – Electro-Optic/Infrared

EP - Electronic Protection

EPD – Excess Path Delay

ES-CFAR - Expert System - CFAR

ESM - Electronic Support Measures

FEBA – Forward Edge of the Battle Area

FEP – Filter Environmental Processor

FFT – Fast Fourier Transform

FLTCs - Focused Long Term Challenges

FM – Frequency Modulation

FP – fingerprint

FTC – Factored Time Space

FY – Fiscal Year

GEO-MTI – GEOsynchronous-orbit Moving Target Indication

GHz - GigaHertz

GIG – Global Information Grid

GIP – Generalized Inner Product

GMTI – Ground Moving Target Indicators

GO-CFAR – Greatest Of Constant False Alarm Rate

GOTCHA – Doesn't stand-for anything but refers to the AFRL Circular-SAR Development Project

GPS - Global Positioning System

GRCA - Ground Referenced Coverage Area

GSM - Global Sensor Manager

HASP - Heuristic and Algorithmic Source (signal, image, data, and cyber) Processing

HOS - High Order Statistics

HPEC - High Performance Embedded Computing

HRR – High Range Resolution

ICM – Internal Clutter Motion

ID – Identification

IED - Improvised Explosive Device

IFC2P2 – Intelligent Fusion Communications Control, Plug & Play

IFF – Identification, Friend or Foe

IID – Independent and Identically Distributed

IMP - Intelligent Mobile Proxy

IPT – Integrated Product Team

IPN – Intelligent Platform Network

IR - Infrared

ISAR - Inverse Synthetic Aperture Radar

ISR - Intelligence, Surveillance and Reconnaissance

IW – Information Warfare

JCAN – Joint Communications Airborne Networking

JEM – Jet Engine Modulation

JSTARS - Joint Surveillance Target Attack Radar System

KA – Knowledge Aided

KASSPER - Knowledge-Aided Sensor Signal Processing and Expert Reasoning

KB – Knowledge-Based

KBC – Knowledge Based Controller

KBSADP – Knowledge-Based Signal and Data Processing

KB-STAP - Knowledge-Based Space-Time Adaptive Processing

km - Kilometer

LULC – Land Use and Land Cover

m – Meter

M&S - Modeling and Simulation

MAC - Media Access Control

MAJCOMs - Major Commands

MCARM – Multichannel Airborne Radar Measurements

MDA – Missile Defense Agency

MFP – Matched Filter Processing

MHz - MegaHertz

MIMO - Multiple Input, Multiple Output

MIST - Multi-Intelligence Sensor Technology

MIST ROS - Multi-Intelligence Sensor Technology Representative Operational System

MMSE – Minimum Mean Squared Error

MNS – MIST National Systems

MOE – Margin of Error

MOPS – Measures of Performance

MSMI - Modified Sample Matrix Inversion

MSR - Multistatic Radar

MTI – Moving Target Indicator

MTS – Moving Target Simulator

NAGS – Narrow Area GRCA Surveillance

NATO - North Atlantic Treaty Organization

NAV – Navigation

NED – National Elevation Data

NGA – National Geospatial-Intelligence Agency

NGA-P - National Geospatial-Intelligence Agency Program

NHD - Non-Homogeneity Detector

NLCD – National Land Cover Data

OGUPSA - Online Greedy Urgency-Driven Preemptive Scheduling Algorithm

P/S - Publish/Subscribe

PDF – Probability Density Function

PDU – Protocol Distribution Unit

Pfa – Probability of False Alarm

PKI – Public Key Infrastructure

PNT - Positioning, Navigation and Timing

PPM – Preferred Performance Measure

PRF – Pulse Repetition Frequency

PSM - Platform Sensor Manager

PSP – Pattern Synthesis Processor

RBR - Real Beam Radar

RCS – Radar Cross Section

RF - Radio Frequency

RI - AFRL Information Directorate

ROC – Receiver Operator Characteristics

RSM - Regional Sensor Manager

Rx – Receiver

RY - AFRL Sensors Directorate

SAR – Synthetic Aperture Radar

S&T - Science & Technology

SSR - System Strategy Reasoner

S/W - Software

SW – Symmetric Window

SAML - Security Assertions Markup Language

SAR - Synthetic Aperture Radar

SCNR – Signal-to-Clutter-plus-Noise Ratio

SDGC – secondary data guard cells

SGT - Stationary Ground Targets

SINR – Signal-to-Interference plus Noise Ratio

SJR - Signal-to-Jammer-Ratio

SME - Subject Matter Experts

SMI – Sample Matrix Inversion

SMS - Sensor Manager Simulation

SNR – Signal-to-Noise Ratio

SOF – Special Operations Forces

SPEAR – Signal Processing, Evaluation, Analysis and Research

SPO - Systems Program Office

STAP - Space-Time Adaptive Processing

SSRP – Space/Space Range Processor

TBM - Tactical Ballistic Missile

TEP – Tracker Environmental Processor

TM-CFAR – Trim Mean-Constant False Alarm Rate

TRD - Transportable Discriminating Radar

Tx – Transmitter

UAS – Unmanned Aircraft System

UAV – Unmanned Air Vehicle

UAV Sim – Unmanned Air Vehicle Simulator

UHF - Ultrahigh Frequency

UI – Urgency Index

UIP – User Interface Processor

US - United States

USA - United states of America

USAF – United States Air Force

USGS – US Geological Survey

VTA - Virtual Tomographic Array

W3C – World Wide Web Consortium

WAGS – Wide Area Ground Surveillance

WAS – Wide Area Surveillance

WDD - Waveform Diversity & Design

WF – Waveform

WGS84 - 1984 World Geodetic System

Wi-Fi – Wireless Fidelity

XG - neXt Generation

APPENDIX A
ANALYSIS OF THE ANTI-JAM PERFORMANCE OF MULTILATERATION SYSTEMS

DISTRIBUTED CONCEPT FOR TRANSPORTABLE DISCRIMINATING RADAR (TRD)

A concept for a new fire control radar is being investigated for regional missile defense. This system will be transportable and will support target discrimination and track for mid-course and endo-atmospheric engagements (see Figure A- 1). To make such a concept a reality one might employ some of a number of enabling technologies to achieve the desired performance against expected missile threats. Such a system will have attributes that support multiple firing doctrines including shoot-look-shoot engagements and be interoperable with existing missile defense systems. An elevated EO/IR sensor may support target acquisition and possibly first intercept.
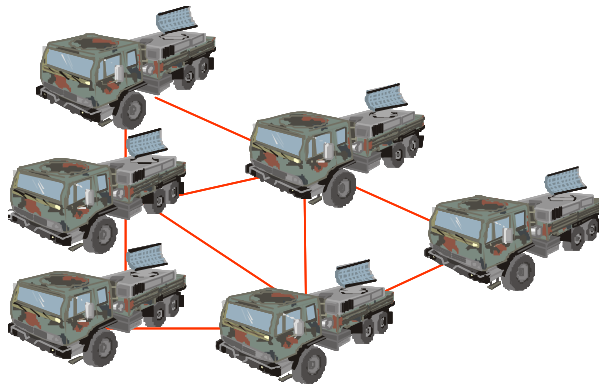
Figure A- 1. Distributed Sub Apertures

An IPT was formed to perform a feasibility analysis of developing a new TDR to meet the requirements of the regional defense concept. The first concept was a distributed aperture approach because it was believed that a single aperture system would not be transportable (the portability issue once again). Further systems analysis determined that the distributed aperture approach was not necessary for transportability but still had payoff in terms of performance against jamming and chaff and multilateration imaging.

In this distributed aperture concept for Electronic Counter-Countermeasures (ECCM) and improved discrimination there is a main radar that transmits a wideband waveform, and a number of auxiliary radars each receive the wideband waveform. There is coherent integration across all these receive apertures. For this X-band system, with the receive apertures distributed across a few kilometers, it would be possible to separate targets from chaff only 100 meters apart. Rejection of jammers that are located close in angle to the target is also possible.

In another version of this concept the TDR systems located in different countries would operate bistatically with each other. Wideband multistatic imaging could also be used with this concept (see **Figure A- 2**).
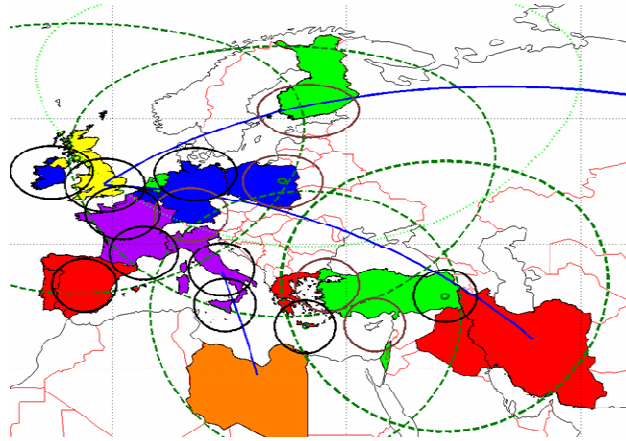
Figure A- 2. Regional Defense Layout

Jammer Rejection

An important application of the distributed aperture concept is the rejection of jammers very close to the desired target. The resolution, i.e. the angular distance between the target and a jammer that can be rejected, is determined exclusively by the baseline (in terms of wavelength) of the distributed aperture. In this regard, increasing the baseline improves resolution. However, if all sub-apertures use the same waveform, e.g. operate at the same frequency, a large baseline results in grating lobes, wasting transmit energy in unwanted directions or receiving interfering signals from unwanted directions. Similarly, if we were to use multiple frequencies, but equally spaced sub-apertures, the grating lobes are reduced, but not eliminated. In analyzing the use of distributed apertures for jammer rejection, there are, therefore, two dimensions to be investigated: the waveform dimension (choosing a different waveform for each element) and the spatial dimension (choosing an optimal spacing between elements).

In the scenarios under investigation, the overall aperture baseline was of the order of hundreds of meters. At the frequencies of operation and range to targets considered in this effort, the targets are within the near field of the overall antenna. This implies that the received signals from the target and jammer are range dependent, in contrast to the standard model for target signals that are assumed to depend on the relative angles only.

In Phase I of this effort we investigated the ability of a distributed aperture to suppress jammers using adaptive processing. The investigation covers the use of distributed apertures in four different scenarios:

- equal spacing between elements, same signals
- equal spacing between elements, orthogonal signals (different frequencies)
- unequal spacing, same signals
- unequal spacing, orthogonal signals

The analysis undertaken here is an initial effort to document the ability of the distributed aperture to suppress interference. We use the traditional fully adaptive algorithm, based on the covariance matrix of the jamming interference and noise [A-1]. One extension of this research effort is to understand the performance of the several available STAP algorithms in distributed aperture scenarios. Similarly, range dependent target and jamming signals are not addressed here and can be considered an extension of this effort.

BACKGROUND

Consider a distributed aperture with N subapertures with each subaperture possibly transmitting a different waveform. Since each subaperture receives target returns from all transmitted waveforms, there are $N \times N$ returned signals for each radar range. A space-time-waveform-range data hypercube therefore replaces the usual space-time-range data cube. In this effort, the orthogonal waveforms are chosen to be relatively narrowband signals offset in center frequency. In such a system, there are a few unique concepts:

Adaptive space/time/waveform processing: Traditionally, adaptive processing has focused on the spatial and temporal dimensions leading to STAP. The spatial steering vector is related to the look direction while the temporal steering vector is determined by the look Doppler frequency. In our case, the time dimension is augmented by the *waveform* dimension. The space/waveform steering vector is determined by the look angle uniquely with a different spatial steering vector for each transmit frequency.

Spacing of subapertures/waveforms (frequencies): Distributing the apertures and separating the transmit frequencies introduces two new degrees of freedom available to the radar designer: the spacing between the antenna elements and the frequencies. Equally spaced elements with equally spaced frequencies can lead to grating lobes that can reduce the effectiveness of the adaptive process. Here we investigate various configurations, comparing them in terms of grating lobes, mainbeam width, etc.

Targets/interference are not necessarily in the far field: By common definition, the far field region is determined by three conditions: $R > \lambda$, $R > D$ and $R > D^2/\lambda$ where R is the radial distance, D is the *total* aperture baseline and λ is the frequency of operation. From a physical point of view, the far field is the region where the spatial steering vector is effectively independent of the radial distance. In our example, we choose $D = 200$m with a center frequency 10GHz, i.e., the far field begins at approximately 1500km. The target and interference are therefore not necessarily in the far field. This impacts on the type of adaptive processing scheme chosen. Similar to STAP for bistatic radar, this range dependent steering vector reduces the secondary data available to estimate the covariance matrix [A-2]. Another concept possibly borrowed from bistatic radar is the use of spatial warping to maintain a fixed patch size, necessitating a proper choice of secondary data [A-3][A-4].

In addition to the above, another important consideration is position errors in the array. Due to the large baseline, a relatively small error in position may be comparable to the wavelength of operation. This is especially true for radars operating at X-band.

SIGNAL MODELING AND PROCESSING

The elements of the linear array are not equally spaced and each element in the array may transmit at a different frequency. Let $\{x_n, n = 0,1,2...N-1\}$ denote the positions of the N elements, each with corresponding frequency $\{f_n, n = 0,1,2...N-1\}$. Each element receives and processes the signals from all N transmissions. Consider a scenario where each element transmits M pulses within a single coherent pulse interval (CPI) at a pulse repetition frequency (PRF) of f_r. Due to these N transmissions, the return signal from a unit target at the nth element, k^{th} frequency and m^{th} pulse, for a target at relative velocity v and relative angle φ is given by

$$s(n,k,m) = \exp\left(j2\pi m \frac{f_{dk}}{f_r} \right) \exp\left(j \frac{2\pi x_n f_k \sin\varphi}{c} \right) \tag{A-1}$$

where f_{dk} is the Doppler frequency associated with transmit frequency f_k, i.e.

$$f_{dk} = \frac{2v f_k}{c} \tag{A-2}$$

$$s(n,k,m) = \exp\left(j2\pi m \frac{2v f_k}{c f_r} \right) \exp\left(j \frac{2\pi x_n f_k \sin\varphi}{c} \right) \tag{A-3}$$

This signal can be written as a length $N^2 M$ *space-waveform-time* steering vector

$$\mathbf{s}(v,\varphi) = \begin{bmatrix} \mathbf{s}_0^T & \mathbf{s}_1^T & \mathbf{s}_2^T & ...\mathbf{s}_k^T & ... & \mathbf{s}_{N-1}^T \end{bmatrix}^T \tag{A-4}$$

where each length NM vector, $\mathbf{s}_k$ is the traditional space-time steering vector for center frequency f_k

$$\mathbf{s}_k = \mathbf{b}_k(v) \otimes \mathbf{a}_k(\varphi), \tag{A-5}$$

$$\mathbf{b}_k(v) = \begin{bmatrix} 1, & \exp\left(j2\pi \frac{2v f_k}{c f_r} \right), & \exp\left(j2\pi 2\frac{2v f_k}{c f_r} \right), ... \exp\left(j2\pi (M-1)\frac{2v f_k}{c f_r} \right) \end{bmatrix}^T, \tag{A-6}$$

$$\mathbf{a}_k(\varphi) = \begin{bmatrix} 1, & \exp\left(j\frac{2\pi x_1 f_k \sin\varphi}{c} \right), & \exp\left(j\frac{2\pi x_2 f_k \sin\varphi}{c} \right), ...\exp\left(j\frac{2\pi x_{N-1} f_k \sin\varphi}{c} \right) \end{bmatrix}. \tag{A-7}$$

Note that both the spatial and temporal steering vectors are defined in terms of the N frequencies of operation f_k. Also, unlike the traditional spatial steering vector for a linear equi-spaced array, the spatial steering vector here is defined in terms of the position of the elements x_k.

The jammer signal has a structure similar to the target signal. Here we model Gaussian barrage noise jammers. Hence, the only difference between the target and jammer models is that the temporal steering vector is replaced by a vector of independent, complex, Gaussian random variables. The jammer signal, for frequency index k is modeled as

$$\mathbf{s}_{Jk} = \xi_{Jk}\, \mathbf{b}_{Jk} \otimes \mathbf{a}_k\!\left(\varphi_J\right),$$ (A-8)

where ξ_J is the amplitude of the jammer and the temporal vector $\mathbf{b}_J$ is the white, complex, Gaussian random vector of independent random variables with zero mean and unit variance. The length N^2M vector of jammer signal is therefore

$$\mathbf{s}_J = \begin{bmatrix} \mathbf{s}_{J0}^T & \mathbf{s}_{J1}^T & \mathbf{s}_{J2}^T & \ldots \mathbf{s}_{Jk}^T & \ldots & \mathbf{s}_{J(N-1)}^T \end{bmatrix}^T ,$$ (A-9)

Noise is modeled as a white complex Gaussian random variable for all frequencies, pulses and elements.

The overall received signal, is therefore given by,

$$\mathbf{x} = \xi_t \mathbf{s}(v, \varphi) + \mathbf{s}_J + \mathbf{n},$$ (A-10)

where $\mathbf{n}$ is complex Gaussian noise vector.

Using the signal in Eqn.(A-10), we can now implement a space-time-waveform adaptive processing algorithm. The algorithm chosen here is the traditional optimal approach where the N^2M elements of the received signal $\mathbf{x}$ are combined using a weight vector $\mathbf{w}$. The weight vector is determined using the relation

$$w = R^{-1}s,$$ (A-11)

where $\mathbf{s}$ is the space-time-waveform steering vector of Eqn. (A-4) and $\mathbf{R}$ is the interference plus noise covariance matrix. Note that in practice, this matrix must be estimated.

NUMERICAL EXAMPLES

Data Generation and Implementation of Adaptive Process

Using Eqn. (A-10) above, we can generate data corresponding to our chosen scenario. Repeating this several times, e.g. (P+1) times, yields a space-time-waveform-range hypercube, organized as a $N^2M \times (P+1)$ matrix. Each column of this matrix corresponds to one physical range. To evaluate the performance of the adaptive process, this data cube is processed in two ways: first, we implement the adaptive process using a sliding window to estimate a space-time-waveform interference covariance matrix.

In our implementation, the data for the (P + 1) ranges are generated without a target, i.e. $\xi_t = 0$. Then a target with chosen power is injected into the middle range, $p = (P/2+1)$. For the qth range, an interference covariance matrix is estimated by using a sliding window

$$\hat{\mathbf{R}} = \sum_{\substack{p=1 \\ p \neq q}}^{P+1} \mathbf{x}_p \mathbf{x}_p^H \tag{A-12}$$

where the superscript ^{H} represents the Hermitian of a complex matrix and $\mathbf{x}_p$ represents one of (P+1) snapshots of data. In general, for a reasonably accurate estimate of $\mathbf{R}$, we need $P > 2N^2M$. The adaptive weights are obtained using Eqn. (A-11). Using these weights we define the modified sample matrix inversion (MSMI) statistic, which as the property of having CFAR in Gaussian interference,

$$\rho_p = \frac{\left|\mathbf{w}^H \mathbf{x}_p\right|^2}{\left|\mathbf{w}^H \mathbf{s}(v,\varphi)\right|^2} . \tag{A-13}$$

This statistic is plotted as a function of range. Clearly, if the range corresponds to the one with the target, the output statistic should be as large as possible, while if the range does not contain a target, the output MSMI statistic should be close to zero.

The second approach is to estimate an interference covariance matrix using all available data, however without injecting any targets, i.e. all the data is target-free

$$\hat{\mathbf{R}} = \sum_{p=1}^{P+1} \mathbf{x}_p \mathbf{x}_p^H \tag{A-14}$$

Averaging over these data samples yields an estimate of the interference covariance matrix. The weights are the obtained using Eqn. (A-11). These weights are then used to obtain the output signal-to-jammer-ratio (SJR), assuming a unit target, as

$$SJR = \frac{\mathbf{w}^H \mathbf{s}(v, \varphi)}{\mathbf{w}^H \mathbf{s}_J} .$$ (A-15)

Note that the jammer signal $\mathbf{s}_J$ includes the jammer amplitude. In this analysis, to illustrate jammer suppression, this SJR is plotted as a function of jammer angle φ.

RESULTS

Unless stated otherwise, the parameters chosen in the test scenarios are given in Table A - 1.

Table A - 1. Parameters for Test Scenario

Number of elements (N)	6	Pulse Repetition Frequency (PRF)	2kHz
Center Frequency	10GHz	Jammer-to-Noise Ratio	50dB
Frequency Offset (if applicable)	100MHz	Target Signal to Noise Ratio (SNR)	0dB
Radar Baseline	200m	Target velocity (v)	10m/s
Pulses in CPI (M)	12	Number of range bins ($P + 1$)	1728

The frequency offset given in Table A - 1 is used in the case where different elements transmit on different frequencies. When using the frequency offset, each transmission is separated by 100MHz. The first null beam width of such an array is 0.014°.

The first example uses equally spaced elements. The target is at broadside with a 50dB jammer at 0.04297°. This jammer location is approximately three first-null beam widths. **Figure A- 3** and **Figure A- 4** plot the MSMI statistic versus range for two cases considered here: in **Figure A- 3**, all six elements transmit at the same frequency whereas, in **Figure A- 4**, each element transmits orthogonal waveforms (waveforms separated in center frequency by 100 MHz). Both figures plot the MSMI test statistic versus range close to the range cell where the target was injected. As is clear from the figures, when all elements transmit at the same frequency, the target cannot be distinguished from the interference. Whereas, when each element transmits an orthogonal waveforms (different frequencies), the target is clearly visible, with approximately a 6dB separation between target and interference.
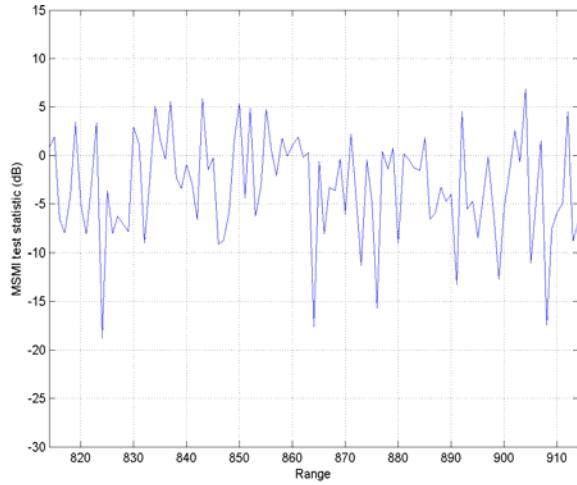
Figure A- 3.   MSMI statistic versus range. No frequency offsets.
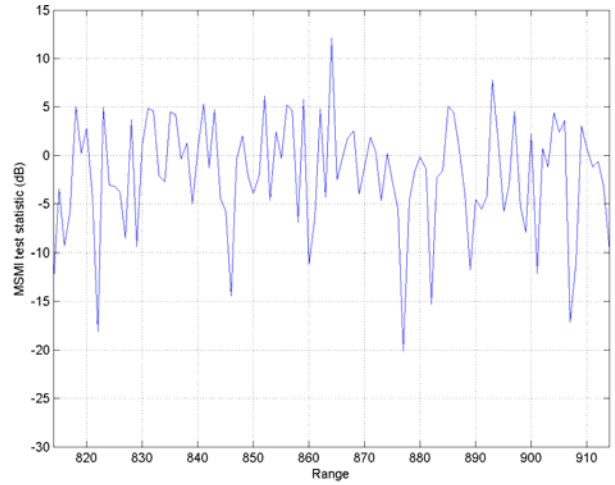
Figure A- 4. MSMI statistic versus range. Using frequency offsets (orthogonal waveforms).

The rest of the examples present the output SJR as a function of jammer angle. In these examples, the target look direction is kept fixed while the jammer direction of arrival is stepped over several angles. For each jammer angle, data for several range cells is generated and used to estimate an interference covariance matrix. Using Eqn. (A-11) the adaptive weights are generated and the SJR is estimated using Eqn. (A-15). The SJR is plotted as a function of jammer angle. Note that the interference covariance matrix includes the noise covariance matrix; however, the output SJR only uses the jamming component. This approach is chosen to focus on the interference suppression capabilities. Clearly, the ideal output would be as high as possible.

The second example, again, compares the use of the same frequency from each element with using multiple frequencies (orthogonal waveforms). The elements of the array are equally spaced. The jammers are stepped over angles spaced by 1.4×10^{-3} degrees. This example uses only one pulse, i.e. $M = 1$.
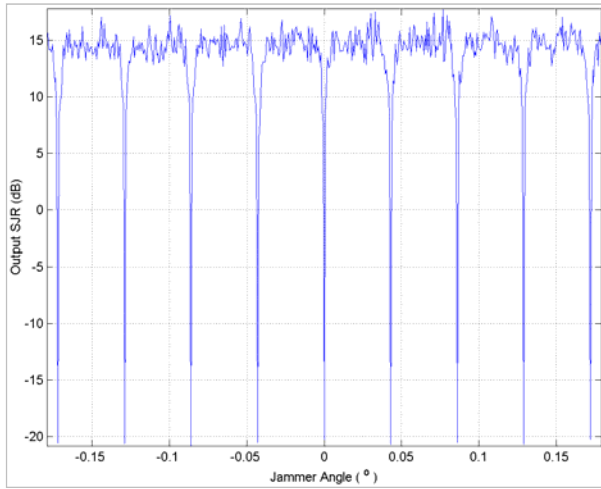
Figure A- 5. SJR. Equal frequencies and element spacing.
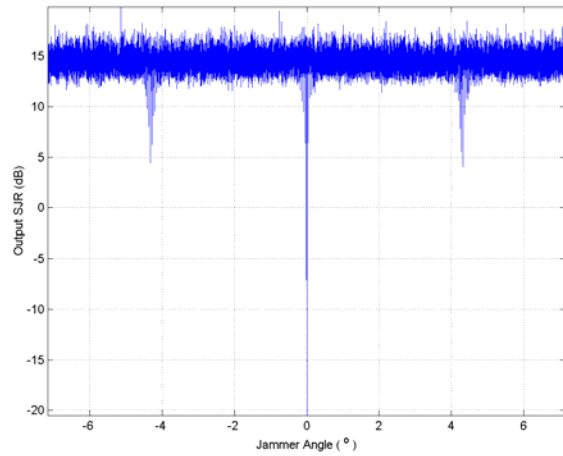
Figure A- 6. SJR versus jammer angle.

Figure A- 5 plots the output SJR versus angle for the case where all elements transmit at the same frequency. The output SJR is rather high for most angles. However, at certain angles for the jammer, the SJR shows deep nulls as the null in direction of target. The large null at the target look direction is expected as the jammer and target cannot be at the same location. The deep nulls in the other directions are due to the grating lobes associated with equal spacing and all elements transmitting at the same frequency. **Figure A-6** plots the SJR for the case where each element transmits at a different frequency. The deep null at the target is visible however clearly there is a huge improvement in grating lobes. Off-target nulls still occur the nulls are much shallower and much further away from the target location. To confirm the fact that grating lobes are reduced in this case, in **Figure A-6**, the analysis is conducted over a much larger angular extent than in **Figure A- 5**. The resolution, however, is the same. Note that the off-target nulls in **Figure A-6** are broader than the off-target nulls in **Figure A- 5**, i.e., while using multiple frequencies helps the off-target nulls broaden. This is true due to the equal spacing between array elements.
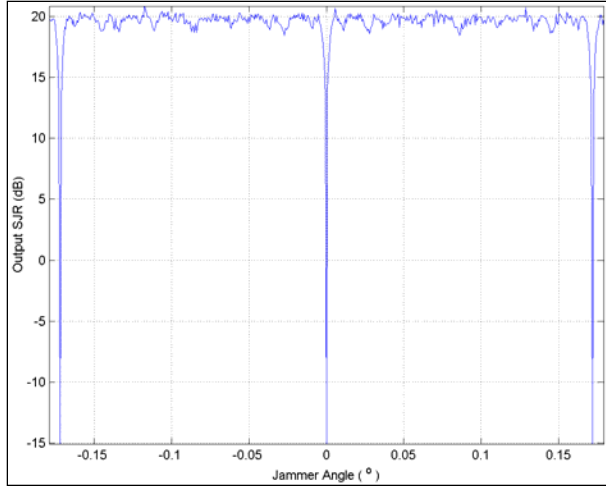
Figure A- 7. SJR. Log spacing and the same frequency.
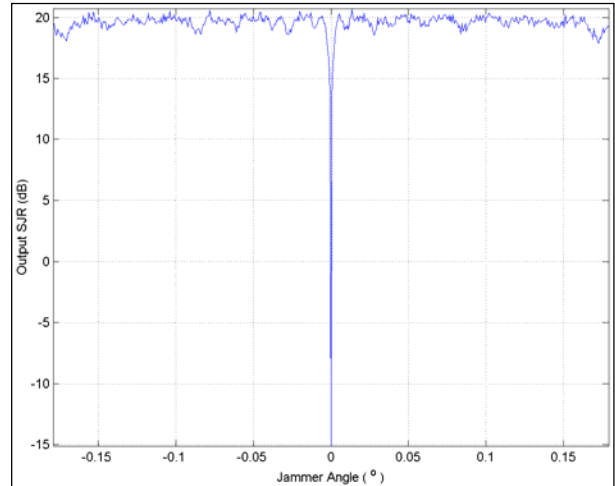
Figure A- 8. SJR. Log spacing and orthogonal waveforms.

The next example illustrates the use of unequal spacing, here close to log-spacing. The six elements are located at *0m, 20m, 60m, 140m, 190m and 200m*. **Figure A- 7** plots the output SJR versus jammer angle for the case where all elements transmit at the same frequency. In comparing with **Figure A- 5**, clearly the grating lobes are significantly reduced in number. However, note that there still exist grating lobes that are spaced further away. Figure A-8 plots the SJR for the case of using orthogonal waveforms (unequal frequencies). Here the grating lobes are totally eliminated and the output SJR is high, except at extremely close to the target look direction. We estimate the null in less than 1.4×10^{-3} degrees.

EXTENSIONS

The discussion in this section the effort, conducted in Phase I, in investigating the ability to suppress jamming. There are two main ways in which this effort can be extended: (i) the inclusion of range dependent target and jamming and (ii) the investigation into extensions of the several STAP algorithms for the range dependent space-time-waveform case. Another extension based on the two issues described here is the use of spatial warping to maintain the radar patch size, thereby retaining the homogeneity of the secondary data.

REFERENCES

[A-1]   Ward, J., Space-time adaptive processing for airborne radar. Technical Report. 1994, MIT Lincoln Laboratory: Cambridge, MA.

[A-2]   Himed, B., J.H. Michels, Y. Zhang. Bistatic STAP performance analysis in radar applications. in Proceedings of the 2001 IEEE Radar Conference. pp. 198-203, 2001. Atlanta, GA.

[A-3]   Sanyal, P.K., R.D. Brown, M.O. Little, R.A. Schneible, M.C. Wicks,. Space-time adaptive processing bistatic airborne radar. in Proceedings of the 1999 IEEE Radar Conference. pp. 1999. Waltham, MA.

[A-4]   Adve, R.s., Schneible, R., McMillan, R., "Adaptive Space/Frequency/Processing for Distributed Aperture Radars", September, 2002.

[A-5]   Balanis, C., Antenna Theory, Analysis and Design: John Wiley, 1997.

APPENDIX B

MULTISTATIC RADAR SIGNAL PROCESSING— IMPROVED INTERFERENCE REJECTION, TRACKING, AND DISCRIMINATION

By: Russ Brown, Yuhong Zhang, Richard Schneible – Stiefvater Consultants
Michael Wicks – US Air Force AFRL/RY, Robert McMillan – US Army, SMDC-RDTC-TDT

INTRODUCTION

In a multistatic radar (MSR) the transmit/receive aperture is divided into a number of sub-apertures that can be placed in various locations relative to each other. These locations can be chosen to optimize the performance of the radar in terms of some specific task. Two multistatic approaches have been investigated:

- Closely spaced apertures – distributed aperture radar (DAR)

- Widely spaced apertures

Realizing the greater capability of MSR's requires unique waveform and signal processing approaches. A computer simulation has been developed that permits the analysis of MSR signal processing. This paper presents the results of a series of experiments to validate the results of that simulation.

DAR–Interference Rejection and Tracking

Multistatic radars, in a distributed aperture mode, can potentially provide significantly improved target tracking because of the large baseline between the various apertures. The resulting angular resolution can be orders of magnitude better than the resolution of a monolithic system (single large radar). This capability comes with a cost because of the resulting grating lobes (multistatics with evenly spaced apertures) or high sidelobes (multistatics with randomly spaced apertures).

The same angular resolution can provide improved electronic protection (EP) capability. For a single aperture radar, jammers located near to targets of interest cannot be nulled without impacting the antenna mainbeam and therefore the target returns. But the multistatic system, with its very long baseline, receive aperture gain on the target can be maintained while a deep null is placed in the direction of the jammer.

Imaging and Discrimination

Two dimensional images of moving targets can be obtained through ISAR processing. The range and cross-range dimensions of radars viewing the target from widely separated angles will achieve target-centered resolution in different dimensions. For example, two radars independently viewing an object in its plane of motion (linear, rotating) with ninety degrees of separation will provide complementary information: the range resolution of one radar will be the cross-range resolution of the other and vice versa. Coherent fusion processing of the data from these two radars can provide improved resolution. Fusion of the data from the bistatic path can further improve the resolution. Also, two or more radars viewing an object from different angles not in its plane of motion can provide three-dimension images. The overall 3-D resolution of the object will be a function of the range and cross-range resolution of the individual radars and their angle separation as viewed from the target location.

MULTISTATIC INTERFERENCE REJECTION

Interference can be rejected, if and only if, the target and interference are resolvable in the dimensions/domains in which the processing is being performed.

Continuously radiating point sources (jamming) can be rejected in the spatial dimension if the target and EMI are separated in angle and cannot be rejected when that separation is sufficiently small. In general, spatially continuous interference (i.e., exo-atmospheric volume clutter) cannot be adequately suppressed by conventional non-adaptive means, i.e. by processing separately in either the spatial or Doppler domains. These techniques fail because they do not handle the space-time coupling inherent in the clutter signal return. Consequently leakage from one domain to the other limits the amount of suppression that can be achieved by operating in these domains separately.

For conventional single aperture radars the cross-range resolution may be so large that the target effectively falls within the main beam antenna spatial response. In this case, conventional STAP will not be able to adequately reject the interference. However, assuming a distributed aperture radar with high range and cross range resolution, improvements in target-clutter separation is achievable along with improvements in interference suppression. Such architectures generally lead to space-time grating lobes that can degrade performance. Using simultaneous orthogonal waveforms, however, to form narrow spatial main beams, it is possible to develop space/time/waveform adaptive processing to suppress grating lobes, reject the clutter, and detect the target in jamming, clutter and joint jamming/clutter environments.

We have demonstrated the potential for orthogonal waveforms in DAR architectures in achieving improved resolution, interference suppression, and target detection and tracking performance while simultaneously controlling space-frequency grating lobes. System operation involves radiating orthogonal waveforms from multiple sub-apertures of the DAR and then receiving and processing these waveforms at each sub-aperture. The use of orthogonal waveforms provides an additional dimension (waveform) beyond the standard space-time dimensions typically used in conventional STAP for adaptive suppression of the interference background.

Adaptive processing using frequency diversity was simulated and demonstrated. The interference was first modeled as a single point EMI source. The signal theory was then generalized to handle the more difficult problem involving distributed volumetric clutter.

EMI Rejection – Simulation and Analysis

Several key considerations for systems employing advanced adaptive processing techniques using waveform diversity were considered. A distributed aperture system with N sub-apertures was assumed. Each sub-aperture is assumed to transmit a different (orthogonal) waveform. Each sub-aperture then receives target returns from each of the transmitted waveforms, resulting in a total of N × N returned samples for each radar range gate. In this situation, the classical space-time data cube is replaced by a data hypercube where the additional dimension is 'waveform'. In this effort, the orthogonal waveforms were chosen to be relatively narrowband signals offset in center frequency. For such a system, we note:

- Adaptive space-time-waveform processing: Traditionally, adaptive processing has focused on the spatial and temporal dimensions leading to space-time adaptive processing. The spatial steering vector is related to the spatial look direction while the temporal steering vector is determined by the temporal look or Doppler frequency. In this case, the space dimension is augmented by the addition of the waveform domain. The space/waveform steering vector is determined uniquely by the look angle with a different spatial steering vector for each transmit frequency.

- Sub-aperture waveform (frequency) separation: Distribution of the sub-apertures and separation of the transmit frequencies introduces two new degrees of freedom to the radar designer: namely the spacing between the antenna sub-apertures and spacing between frequencies. Generally sub-apertures and/or sub-bands are separated by multiple wavelengths. Consequently, equally spaced elements/sub-apertures with equally spaced frequencies can lead to grating lobes that can reduce the effectiveness of the adaptive process. Analysis has shown that appropriate distribution of the elements in the spatial and temporal (frequency) domains along with weighting can eliminate, or at least mitigate grating lobes in their respective dimensions and reduce the amount of adaptive processing required to suppress interference.

- Targets/interference are not necessarily in the far field: By standard definition, the far field region is determined by three conditions: $R > \lambda$, $R > D$ and $R > \frac{}{}$ where R is the radial distance, D is the total aperture baseline and λ is the wavelength of the frequency of operation. From a physical point of view, the far field is the region where the spatial steering vector is effectively independent of the radial distance. To illustrate, we assume the distance to the target, D = 200m and center frequency is 10GHz, i.e., the far field begins at approximately 1500km. The target and any competing interference are therefore not necessarily in the far field. This may impact the adaptive processing approach. As in bistatic STAP operation, a range dependent interference ridge results, and, if no additional processing is assumed, the size of the secondary data available to estimate the covariance matrix is reduced. This in turn may limit STAP performance. Another concept borrowed from bistatic radar applies a spatial un-warping to the data to remove the range dependency and allow a larger secondary data set size to be used.

Based on these considerations a high-fidelity multistatic radar simulation was developed and the performance of various geometries predicted.

Jammer Rejection - Experiment

A rooftop experiment was accomplished at the AFRL/Rome Research Site (AFRL/RRS) to verify the multistatic radar simulation. Five sub-apertures were located in roughly linear orientation (see **Figure B - 1**). The total separation was about 200 feet. A moving target and a jammer were located about 6000 feet away (see **Figure B - 2**). The target was driven through the mainbeams of the five radars.

Target

Jammer Rejection Experiment

- 5 Transmitters (Orthogonal WF's)
- 5 Receivers (All WF's)
- 76.2m separation
- Making 25 radars
  - (5 monostatic & 20 bistatic)
- Rejected jammer near (<9m) target
- Test range ~ 1830m
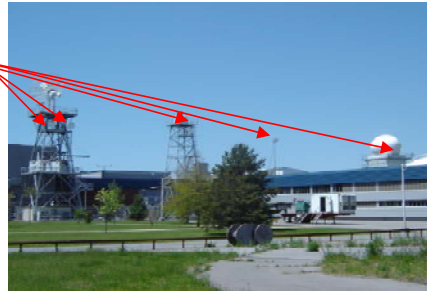
Figure B - 1. Distributed Aperture Radar (DAR)

The suite of 5 transmitters collectively radiated 5 diverse frequencies that were recorded on each receiver channel. Activation of the jammers produced a 30dB jammer/noise ratio and completely masked out the target vehicle return. After multi-channel, multi-waveform processing, jammer cancellation occurred along with target detection.
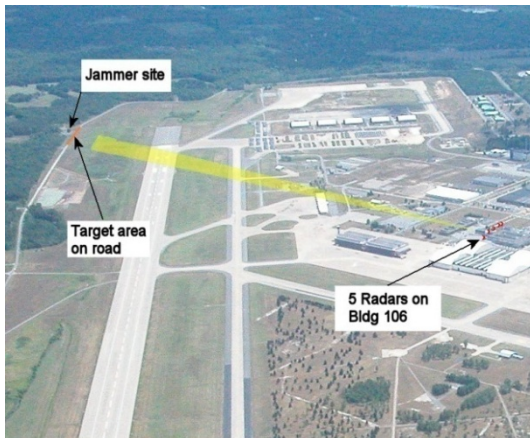
Figure B - 2. DAR Test Geometry

Figure B - 3 presents a flick run of the jammer scene (left side) alongside the cancelled jammer scene (right side). The frame rate is 2 seconds with each of the range Doppler frame plots recorded over a 256 millisecond interval at a 1kilohertz rate. Note the appearance and fading of the target as it moves through the lobe structure of the sub-aperture antenna. The target is quite visible when it is located at the 10 through 16 second positions.
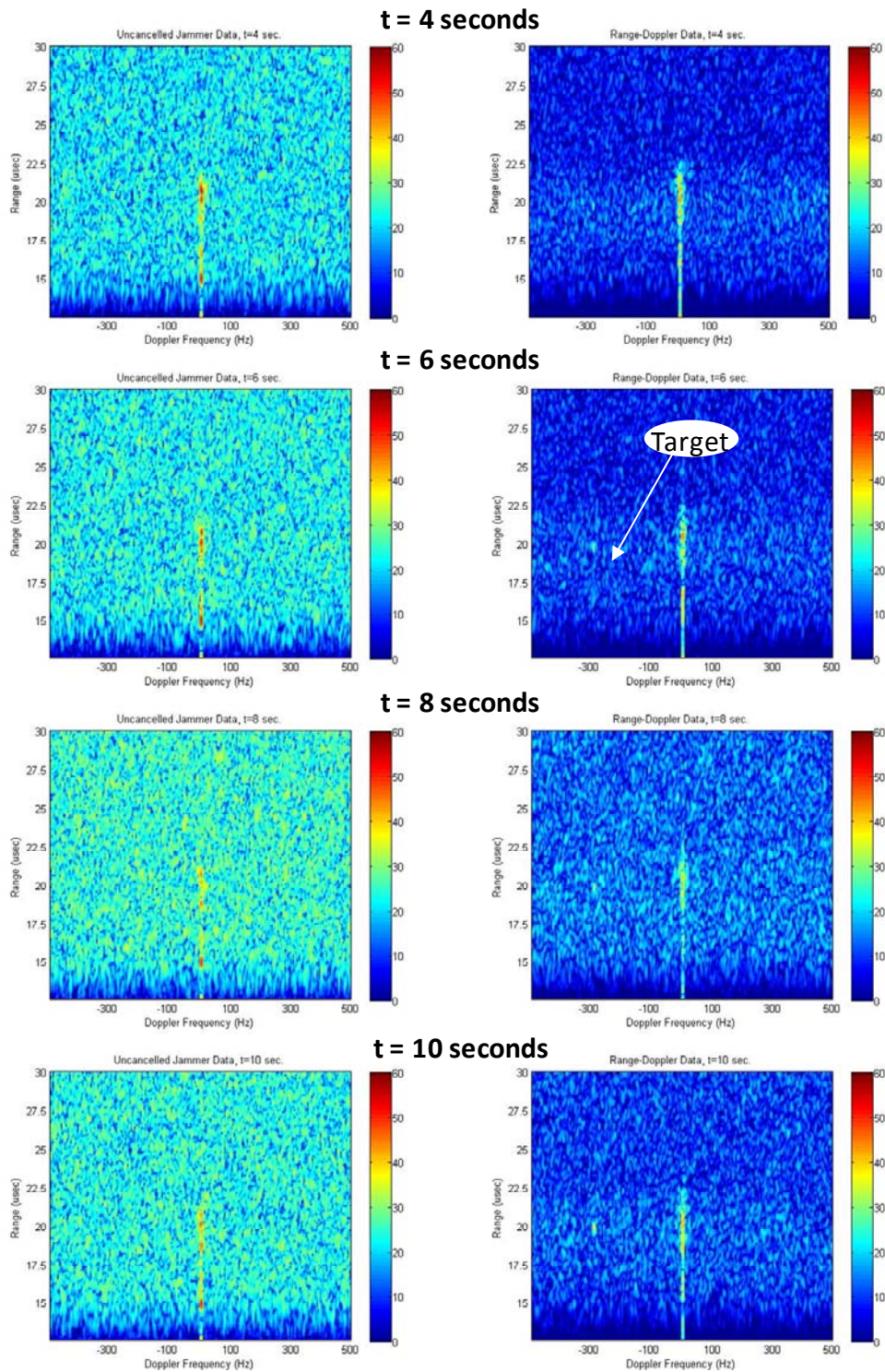
t = 4 seconds

t = 6 seconds

t = 8 seconds

t = 10 seconds

Figure B - 3. Flick Run of Jammer (left) and Cancelled Jammer Range/Doppler Scene

65

t = 12 seconds

t = 14 seconds

t = 16 seconds

t = 18 seconds

Figure B - 3. Flick Run of Jammer (left) and Cancelled Jammer Range/Doppler Scene.

Data was collected and adaptively processed as the target vehicle traveled along a course that brought it past the jammer. **Figure B - 4** shows the post processing signal-to-noise ratio (SNR) as the target traversed from -10 to +10 milliradians with respect to the jammer direction. Note that the SNR decreases significantly when the target and jammer are in the same direction. Had the sampling interval been smaller than 0.3 milliradians, the null may have been deeper.

Exo-Atmospheric Volume Clutter – Simulation

Our simulation was extended to model exo-atmospheric clutter in addition to jamming. The

Figure B - 4. Post Cancellation SNR of Target Direction with respect to Jammer

simulation generates an individual scatterer model that keeps track of particle position and velocity as a function of time. These scatterers are range gated and parse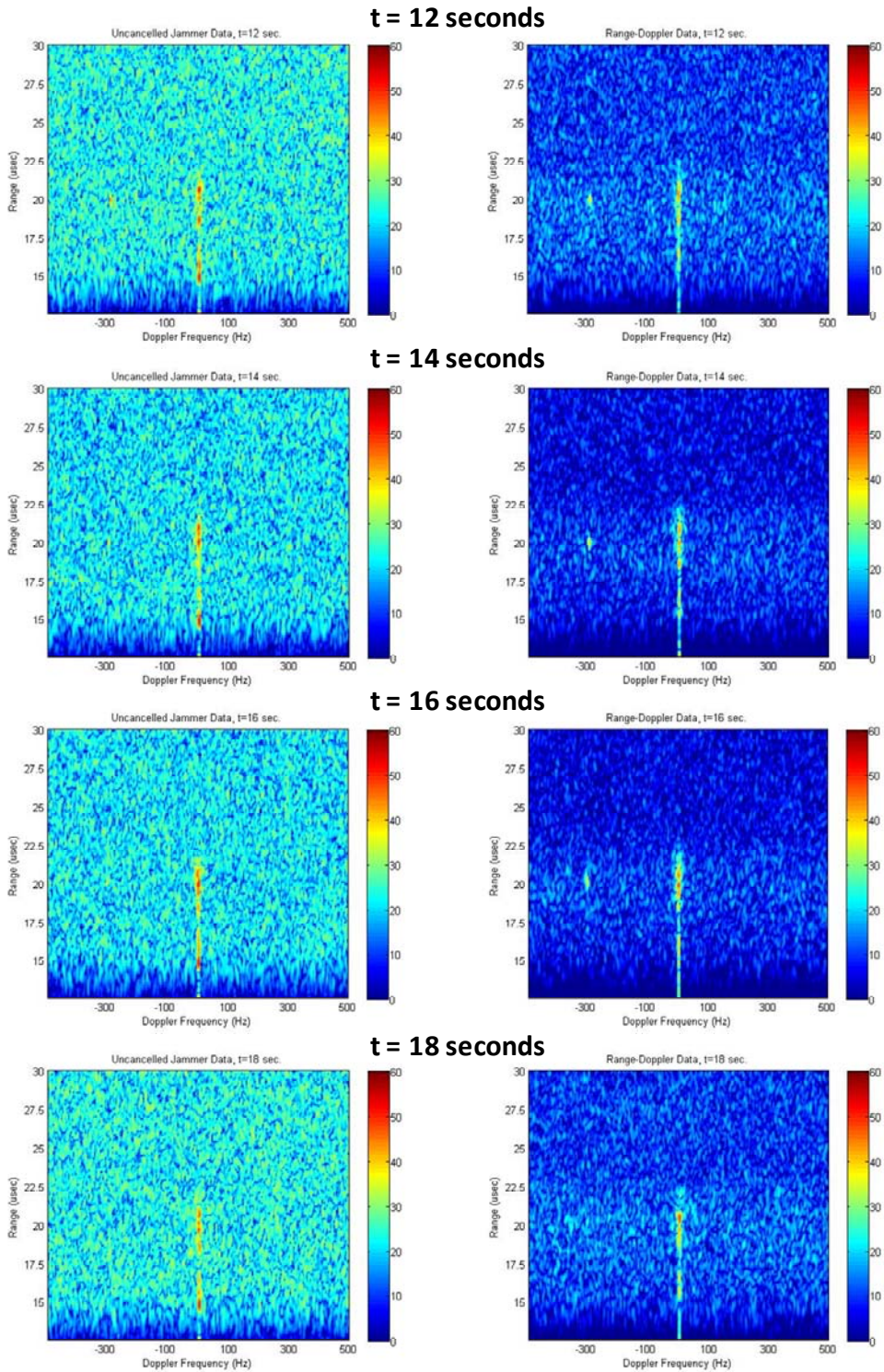d out of the scatterer cloud. Ranges are then calculated for a set of spatially diverse sub-apertures each transmitting an orthogonal waveform relative to each other. Each sub-aperture however receives each transmitted waveform. Therefore assuming N_a sub-apertures there are N_a^2 different monostatic and bistatic radar combinations (N_a monostatic radars and N_a^2–N_a bistatic radars). The range and frequency information are then used to calculate phase difference values for each of the N_a^2 radars.

Figure B - 5. Individual Scatterer Positions Starting from Initial Velocities that Are Normally Distributed

Figure B - 5 and **Figure B - 6** represent initial scatterer velocities that are normally distributed. The result of this scenario is a spherical cloud of dipole radiators.
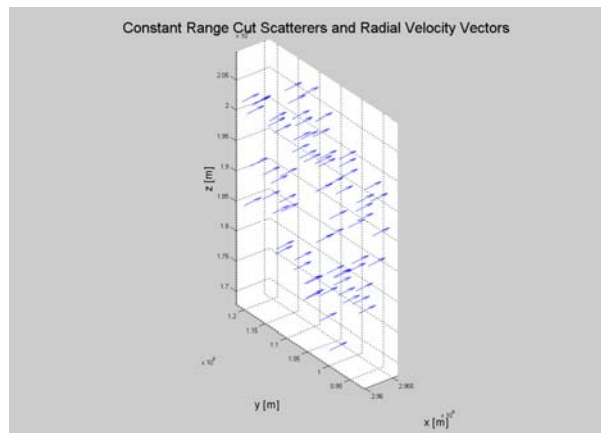
Figure B - 6. Quiver Plot of Range Gated Scatterers and their Velocities

67

The next plot, **Figure B - 7**, represents the range gated scatterers that were parsed out from a cloud of scatters that contains over 4 million individual scatterers (that is, those scatterers in the same range bin as the target of interest). There are approximately 25 hundred individuals in the parsed set. The parsed data is then used to calculate the phase differences between the scatterer returns at each aperture relative to each other aperture. The result is represented by a $N_a \times N_a$ matrix.

MULTISTATIC IMAGING

Analysis and Simulation

The resolution of a SAR or ISAR image is a function of how much of the Fourier space the measurements sample. The bandwidth of the ISAR measurement transforms to the radius in two-dimensional Fourier space. Bistatic measurements are more complex with the transform of the frequency being a function of that bandwidth and of the bistatic angle. **Figure B - 8** shows the Fourier sampling for three sensors (two radars operating both monostatically and bistatically). The aqua and blue sectors are the Fourier sampling for the

Figure B - 7. Range Gated Scatterers Parsed out of a Cloud of 4 Million Individual Scatterers.

monostatic operation of these two radars. The green sector represents the bistatic sampling. For this geometry (ISAR images as the target flies through the field of view of two radars separated by 90°, with 50% bandwidth) the combined multistatic image would have a resolution 2.5 times better than a single monostatic image.
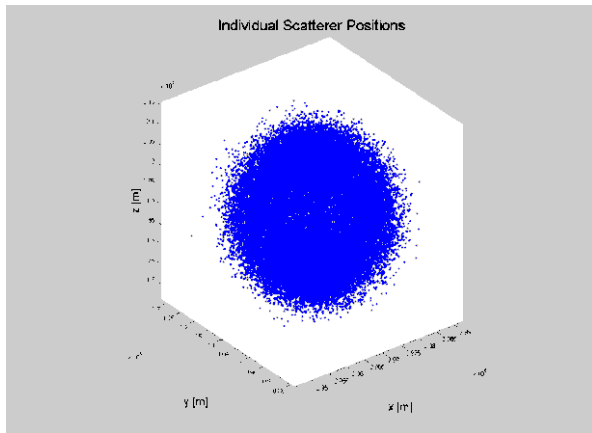
Rooftop Experiment

This experiment was also performed at the AFRL/RRS in Rome NY. The site layout is shown in Figure B-9, with the radars shown on the right and the target area (Jammer site) shown on the left of the figure. The radar path shown in yellow indicates the target aspect from the first sub-aperture, and the path shown in violet indicates the target aspect from second sub-aperture.

Figure B - 8. Multistatic Imaging

Each radar was equipped with programmable waveform generators, frequency conversion equipment, timing and coherent local oscillators based on GPS receivers, as well as data recording servers with storage, processing, and display capability. A vehicle with two dominant scatterers was driven along the road in the target area. The objective of the experiment was to demonstrate an improvement in radar imaging capability by using data from both radars compared to monostatic data from a single radar. Imaging results are also presented in Figure B-9.
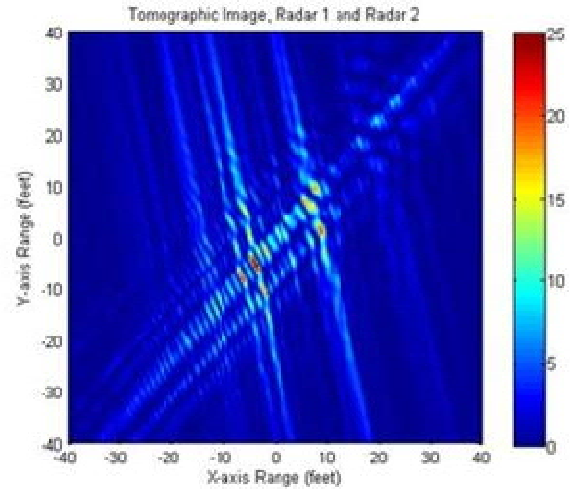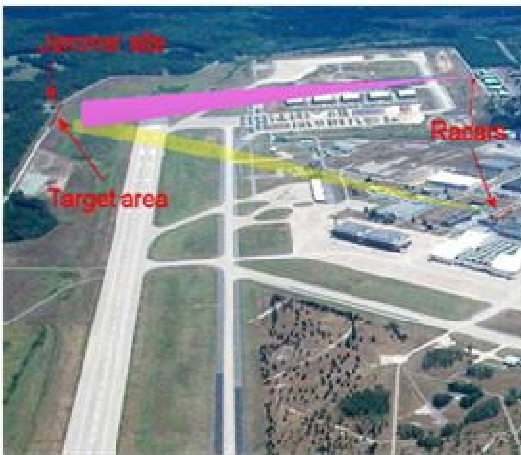
Coherent image for the test target consisted of two large scatters on a vehicle that was driven through the radars field-of-view

Figure B - 9. Coherent Fusion Imaging Experiment

Ongoing Space Object Imaging Experiment

An experiment is underway to further validate the multistatic imaging simulation (**Figure B - 10**). Two widely separated radars will track and image a space object (RadarSat or similar).
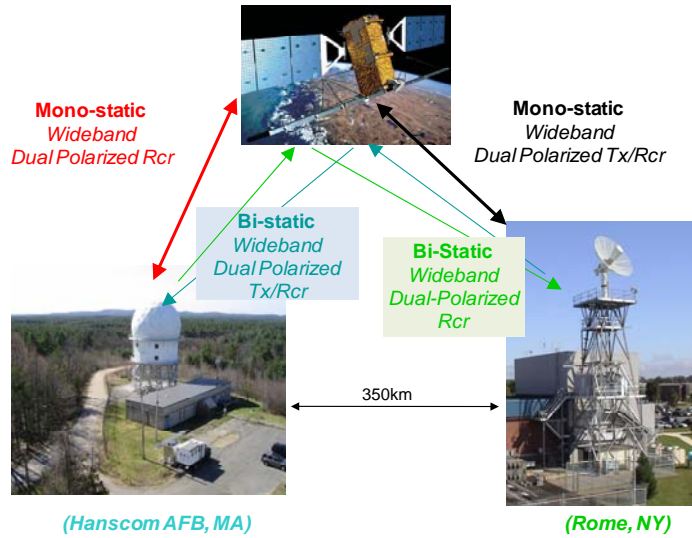
Figure B - 10.   Planned Phase II: Fusion Experiment, Multistatic Space Object Imaging

SUMMARY

Compared to conventional radars, multistatic radars have the potential to provide significantly improved interference-rejection, tracking and discrimination performance in severe EMI and clutter environments.

They can potentially provide significantly improved target tracking accuracy because of the large baseline between the various apertures. The resulting angular resolution can be orders of magnitude better than the resolution of a monolithic system (single large radar). The same angular resolution can provide improved interference rejection. For example, a DAR system with apertures distributed over a couple of kilometers can detect a target at 2000 kilometers in the presence of an interfering source that is just 100 meters away.

Two dimensional images of moving targets can be obtained through ISAR processing. Coherent fusion processing of the data from multiple radars can provide improved resolution. Also, two or more radars viewing an object from different angles not in its plane of motion can provide three-dimension images.

70

APPENDIX C
TOMOGRAPHY

TOMOGRAPHY

Typically, information concerning ground and air targets is obtained via monostatic radar. Increased information is often equated with increased bandwidth and dwell time. However, geometric diversity obtained through multistatic radar operation also affords the user the opportunity to obtain additional information concerning targets. With the appropriate signal processing, this translates directly into increased probability of detection and reduced probability of false alarm. In the extreme case, only narrow frequency bands of operation may be available. With narrowband, the need for geometric diversity becomes imperative. In addition, geometric diversity further improves target position accuracy and image resolution, which may otherwise remain unavailable.

In classical radar, frequency diversity offers one method to obtain additional information about threat targets. With the most basic form of frequency diversity, namely increased bandwidth, high range resolution is afforded to the user. With high range resolution comes increased target-to-clutter ratio (assuming the target is not over-resolved), while target-to-noise is unavoidably reduced. Geometric diversity also offers the potential for increased resolution, and is a dual to frequency diversity (increased bandwidth) in classical monostatic radar. The extreme case of 360° of geometric diversity offers high resolution, even under the narrowband assumption. Operating with narrowband radar signals permits a substantial reduction in thermal noise power as well, further improving overall detection performance.

RF tomography leverages the spatial or geometric diversity of a multistatic radar to deliver high resolution MTI. RF tomography provides the resolution of conventional wideband radar, while using narrowband signals. These narrowband signals are particularly attractive with consideration to the ongoing erosion of spectrum. In RF tomography, some sites may have collocated transmitters and receivers, while other sites are receive only. By locating transmitters and receivers in a uniform manner, beneficial effects of geometric diversity are enhanced. Radar data is easily mapped onto a polar grid in the spatial Fourier domain. The location of the transmitter(s), receiver(s), and frequency span of the signal (bandwidth), determines the mapping to Fourier space via the vector.

$$\underline{V} = 4 \cdot \pi \cdot f / c \cdot cos(B/2) \cdot \qquad \text{(C-1)}$$

where f is the frequency, c, is the speed of light, B is the bistatic angle, and $\underline{u}_B$ is the bistatic bisector unit vector [C-1].

Image formation is easily accomplished via Matched Filter Processing (MFP) in the Fourier domain, which has its origin in SAR image reconstruction, and is considered a spatial frequency domain image reconstruction technique. This matched filter replicates the signal's expected delay and Doppler, via a generalized 'steering' vector used for correlation processing. The extension to moving target detection is not complicated. For each pixel, matched filters are applied for a wide range of hypothesized target velocities. In classical adaptive processing, a Doppler steering vector is used. In MFP, the Doppler steering vector is generalized to a velocity steering vector. The receive signal is the superposition of time delayed and Doppler shifted target signals plus noise. Each target has a velocity vector (speed and heading) that presents a unique Doppler shift in each transmit/receive pair.

For MFP, a filter is computed for each scene pixel, as a function of time delay, and target velocity. To cover all pixels and target velocities, a bank of filters are employed. The MFP output is computed as a conjugate inner product of the received signals and the matched filter over all transmit and receiver pairs, in frequency and space. The received signal forms a data cube. The matched filter, for a particular scene pixel and target velocity, is also three dimensional. For multiple operating frequencies, additional cubes would be formed. A single MFP output (pixel, velocity) is the inner product of these cubes. The process is repeated for all pixels and hypothesized target velocities. Threshold processing is then performed on each pixel.

RF tomography shows promise for providing high resolution surveillance of moving targets using geometrically diverse narrowband transmitters and receivers. Building penetration is also feasible. The narrowband signals provide relief when faced with the consequence of ongoing spectrum erosion. We have begun to probe fundamental issues of imaging quality with diversity in frequency and space.
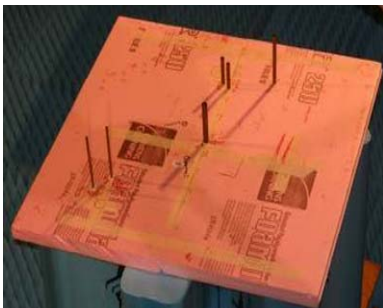
**Figure C - 1. Six Non-Specular
Tomographic Test Targets**
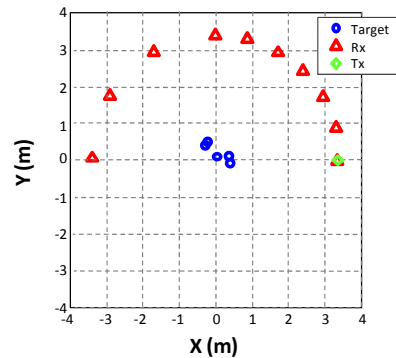
**Figure C - 2. Geometry Of The Tomography
Experiment**

EXPERIMENTAL RESULTS

Both wideband (1GHz of signal bandwidth) and narrowband (<1kHz of signal bandwidth) experimental measurements at X-Band were conducted in an indoor test facility in AFRL in Rome NY [C-2]. Six cylindrical copper test targets were arranged within a 1 m^2 test zone as illustrated in Figure C-1 above. The geometry of the tomography experiments is presented in Figure C-2. The test targets are located in a central region surrounded by the measurement apparatus. Due to the static nature of the tests, sequential

Figure C - 3. Wideband Image of Six Test Targets

measurements using one movable receiver were conducted. All six test targets are clearly visible in the wideband image presented in Figure C-3. Here, an X-Band signal with 1 GHz bandwidth was employed. In Figure C-4, the signal bandwidth is reduced to 1 KHz. Three of the test targets are clearly visible, while three low SNR test targets remain barely detectable. The green circles indicate scene calibration data. These measurements, collected sequentially using 60 transmitter locations and 480 receiver locations, clearly illustrate the imaging potential of narrowband tomographic radar using a single tone. In **Figure C - 5**, adaptive processing via the sample

Figure C - 4. Ultra Narrowband Image Of Six Test Targets

matrix inversion algorithm permits weak targets to be extracted from clutter and noise. Qualitative analysis indicates an improvement factor of 11 dB is achieved. In the next section, a multi-tone technique is used to reduce the number of transmitter and receiver sites to just three.
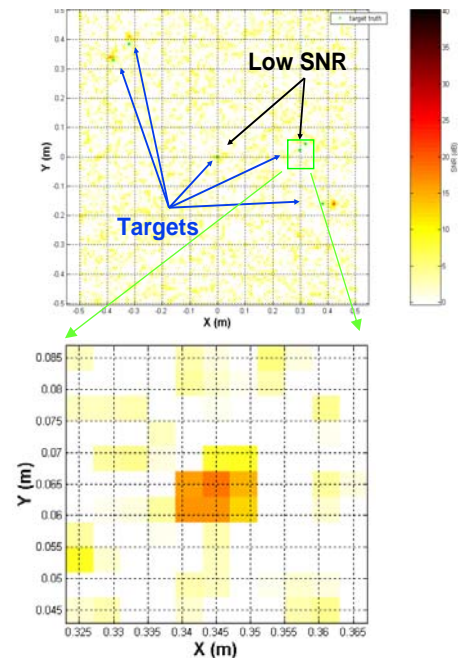
Figure C - 5. Adaptive Processing Of Ultra Narrow Band Image

73

A NEW CONCEPT: THE VIRTUAL TOMOGRAPHIC ARRAY

A tomographic system can be modeled as a spatial filter, and the factors that affect the spatial response of the system are the RF frequency and the position of the transmitters and receivers. Each RF measurement has a 1-to-1 mapping from the spatial domain to the spatial frequency domain, and the geometry of the tomographic system determines the shape of the spatial frequency response. SNR is influenced by the number of measurements used to form an image. The system designer of a distributed sensor for RF tomography is faced with the competing need of desiring a large number of transmit/receive nodes to provide favorable spatial frequency response and SNR and the practicality of using fewer numbers of nodes. SNR may also be improved through higher radiated power. Additionally, if the nodes are fixed in position the only method of altering the spatial sampling, and therefore the impulse response, is the constraining limitation of varying the RF frequency. The concept of a Virtual Tomographic Array (VTA) provides a solution to these issues.

Figure C - 6. Virtual Array Formed From Three Radiators Using Nine Discrete Frequencies

Consider an equilateral triangle with active sources located at the three vertices as illustrated in Figure C-2. If one radiates identical tones of equal amplitude from each of the vertices, then the effective phase center is located at the centroid of the equilateral triangle. If one of the elements is amplitude weighted by zero, then the phase center of the array is located along the chord connecting the remaining two vertices. This phase center is located at the bisector of the chord if the two elements radiate equal amplitude signals. If the amplitudes are unequal, the phase shifts along the chord towards the stronger amplitude source away from the weaker amplitude source (see **Figure C - 6**).
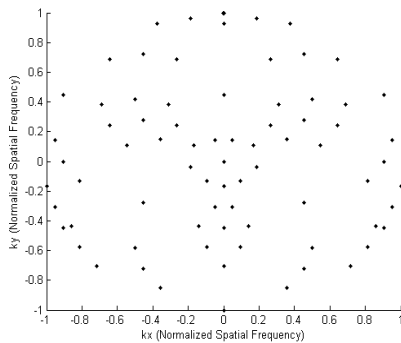
Figure C - 7. Fourier Sampling Associated With Figure C - 6 And
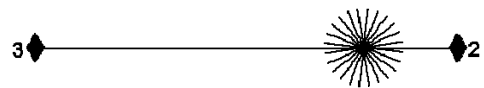
Figure C - 8. Effective Phase Center Formed From Two Elements Operating At The Same Frequency, With The Amplitude Of 2 Greater Than 3.

If the two radiating elements are spaced many wavelengths apart, then the array forms an interferometric pattern with the number of grating lobes equal to the electrical distance between the elements measured in half wavelengths. Modulating the phase of one element relative to the other causes a shift in the interferometric pattern. The use of multiple tones, each uniquely associated with a phase center, allows the existence of potentially large numbers of phase center. **Figure C – 8** shows a virtual array comprised of three transmit/receive elements and nine effective phase centers. The three elements transmit nine discrete frequencies with the weights shown in Table C - 1. Three additional frequencies are required to incorporate the vertices of the equilateral triangle into the active sensor geometry. The support in the spatial Fourier domain, based on (C-1) is shown in **Figure C - 7**.

Table C - 1 . Frequency weights for the radiators in Figure C - 6

	f_1	f_2	f_3	f_4	f_5	f_6	f_7	f_8	f_9
1	.75	.5	.25	.75	.5	.25	0	0	0
2	.25	.5	.75	0	0	0	.25	.5	.75
3	0	0	0	.25	.5	.75	.75	.5	.25

As the number of phase centers (and frequencies) are increased, the support in the Fourier domain dramatically increases. The array shown in **Figure C - 9** has a similar geometry with three radiators, however the number of frequencies used is increased such that there are 52 effective phase centers per side. The coverage in thespatial Fourier domain is apparent in **Figure C – 10** and the number of sample points is approximately equal to the square of the number of effective phase centers. This has a very favorable impact on the system impulse response and SNR.
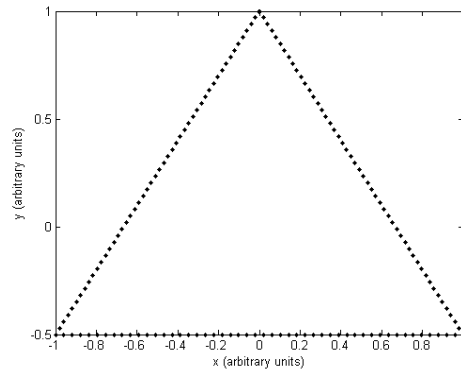
Figure C - 9. A Virtual Array Formed From Three Radiators And 153 Discrete Frequencies.

In the previous section on experimental results, an ultra narrow band signal was radiated in a tomographic sensor using 60 transmit/receive locations and 420 receive only locations to image complex targets in the field of view central to the tomographic sensor. However with 480 spatial degrees of freedom, a tomographic sensor would be impractical for fielding except in urban centers or areas

Figure C - 10. Fourier Sampling Associated With Figure C - 9.

of high military value. Using 480 ultra narrow band tones, and the three element sparse array defined above, we can create a number of phase centers which result in a virtual tomographic array. The Fourier sampling of the resulting virtual array has excellent support in the Fourier domain, and this is essential for detection and discrimination because of the impact on image quality. Reciprocity permits the three element virtual tomographic array concept to be applied on receive as well. With as few as three elements, a multi-tome ultra-narrow band virtual tomographic array can replicate the results achieved with an array containing 60 transmit/receive and 420 receive only elements.

REFERENCES

[C-1]   H. Li, F. Lin, Y. Shen, N. Farhat, "A Generalized Interpretation and Prediction in Microwave Imaging Involving Frequency and Angular Diversity," Journal of Electromagnetic Waves and Applications, vol 4, no 5, pp 415-430, 1990.

[C-2]   Michael C. Wicks, et. al., "Ultra Narrow Band Adaptive Tomographic Radar", IEEE CAMPSAP 2005, Puerto Vallarta, Mexico, 13-16 Dec 2005.

[C-3]   B. Himed, H. Bascom, J. Clancy and M. Wicks, "Tomography of Moving Targets (TMT)", Proceedings of SPIE Vol. 4540 (2001)

[C-4]   K. Magde, M. Wicks, "Waveforms in Virtual Tomographic Arrays", 2007 Waveform Diversity & Design Proceedings, Pisa, Italy, 2007.

APPENDIX D
SENSOR MANAGER SIMULATION (SMS) SYSTEM

SMS OVERVIEW

The SMS System was designed to integrate various simulation components and sensor management algorithms to enable performance evaluation of multiple sensor resource managers. The simulation architecture and defined interfaces between each module allow for switching of system components for evaluation purposes. A high-level overview of the SMS System can be seen below[D-1].
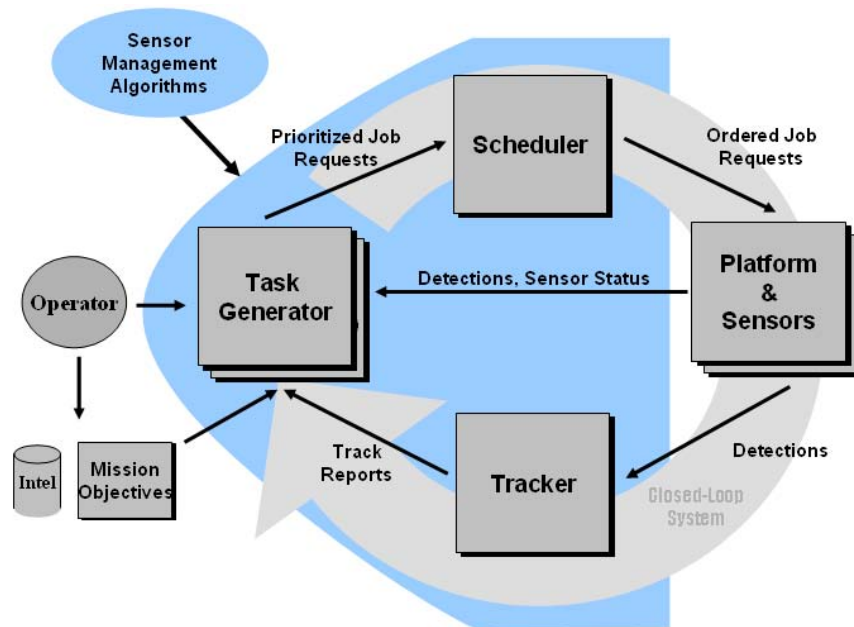
Figure D - 1. SMS Architecture

This architecture provides a closed-loop system which allows sensor manager algorithms, along with operator input, to dynamically task multiple sensors to meet mission goals and objectives. The module operation is as follows. The operator can interact with the system loop when desired by optionally controlling mission objectives, submitting operator tasks, and nominating targets as threats. The Task Generator is responsible for creating prioritized job requests based on situational assessment, operator input, and mission goals and objectives. The Scheduler orders tasks in a dynamically modifiable time window and submits them to the corresponding sensor. The Platform and Sensors are responsible for servicing the requests from the scheduler and producing detections based on truth data. The Tracker produces track reports from the detections received and passes them on to the Task Generator, completing the System Loop.

SMS Components Overview

The SMS system has several system components available for each module. These components can be set up in multiple configurations for the desired simulation. The entire simulation architecture along with all available components and dataflow can be seen below.
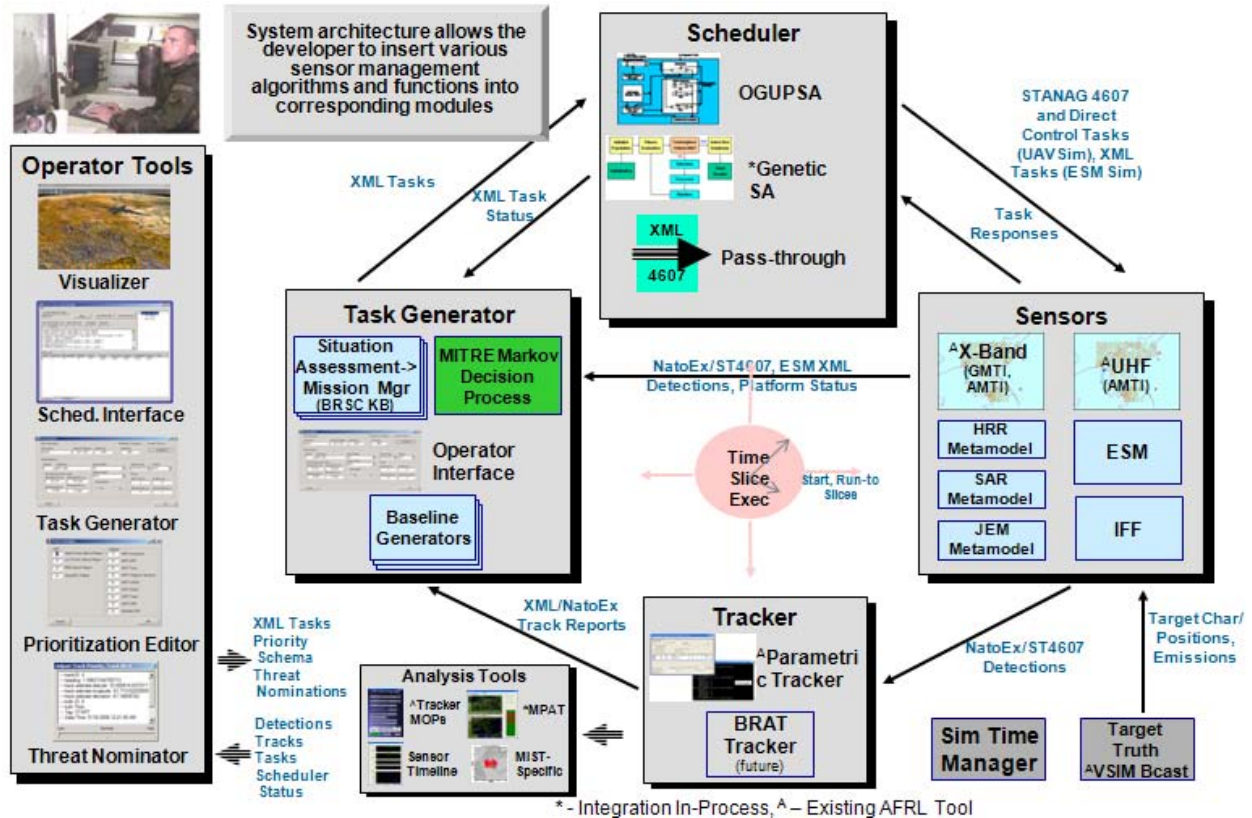
Figure D - 2. SMS Components

The simulation architecture allows the user to insert various sensor management algorithms and functions into corresponding modules. The system components will be discussed briefly below, with lower level descriptions of developed components to follow in later portions of the document.

Operator Tools

The **SMS Visualizer** provides the operator with visual feedback of what is currently occurring in the simulation. It also provides for user interaction by allowing them to change the prioritization scheme and nominate threats.

The **Scheduler** Interface is part of the SMS Scheduler package. It displays the current Scheduler status along with all tasks that have been submitted and their status, and allows the operator to submit tasks to the system as desired.

The **Prioritization Editor** allows the operator to modify the current prioritization scheme used by the sensor manager. The operator has the option of filling in individual values for the available mode priorities or selecting from pre-define schemes.

The **Threat Nominator** provides the operator with the ability to modify the threat levels of existing tracks. The operator can click on a track through the Visualizer, causing this tool window to appear. Upon selection of a threat level, the sensor manager will be notified of the change.

Task Generator

The **Task Generator** maps situational needs to sensor tasks based on the requirements defined by AFRL. The current requirements are based on the AFRL MIST Notional System document. The Task Generator consists of the **Threat Assessment** and **Mission Manager** modules. When run together they will provide Wide Area Surveillance (WAS), Wide Area Ground Surveillance (WAGS), and Narrow Area Ground Surveillance (NAGS), as well as a limited set of threat handling capabilities. If the Mission Manager is run alone without the Threat Assessment module (and thus not receiving system feedback), it will act as the **Baseline Generator** only submitting WAS tasks.

Scheduler

The **SMS Scheduler** architecture contains well-defined interfaces for incorporating various scheduling algorithms into the system.

The **OGUPSA** is based on the algorithm developed by McIntyre and Hintz in "Sensor Measurement Scheduling: An Enhanced Dynamic, Preemptive Algorithm."[D-2] It is a rules-based algorithm that orders the incoming tasks and submits them to the corresponding sensors.

The **Pass-through** algorithm was developed to allow sensor manager algorithms that contain their own integrated scheduling to simply pass their tasks on to the sensors. It performs the necessary interpretation/encoding of sensor-specific tasks and submits them to the corresponding sensors in the required format. For example, the MITRE algorithm has an integrated scheduler and utilizes this component.

Sensors

UAV Simulator (**UAVSim**) is the main sensor simulation tool. It models the UHF, X-Band, and IFF sensors with all required modes, including meta-models for SAR, HRR and Jet Engine Modulation (JEM).

This **MIST ESM Simulation Tool** receives electromagnetic emissions and produces ESM detections based on an algorithm developed by Lockheed Martin for AFRL.

Tracker

The **Parametric Tracker** is a tunable tracker that is configurable to the desired performance level. It accepts detection streams and produces realistic track streams with selectable association and track accuracy performance.

Other Tools

Truth data is broadcast using the Vehicle **STA/DYN to DIS Broadcaster** tool. It broadcasts target positions and emissions to be read by the sensor simulation tools and Visualizer. Note: STA/DYN are from VSim (the truth generator) – STA is a static file, and DYN is a dynamic file, both of which define the truth and their trajectories. DIS is Distributed Interactive Simulation and is the data format/definitions for the truth entities. DIS Protocol Distribution Units (commonly referred to as PDUs) are the information that is sent around the simulation for truth targets.

The **SMS Time-slice Executive** synchronizes simulation operation and time. It serially distributes "run-to" time slices to the system components, coordinating their operation and allowing each component the necessary time to complete operation of a given slice.

The **ARFL Tracking Measures of Performance** (MOPS) tool is available for post-processing of data for tracking performance evaluation.

SMS as Knowledge-Based Controller

The SMS is a knowledge-based (KB) controller and is a multi-threaded application that consists of Situational Assessment, Mission Management, and Task Scheduling. Its main objective is to map situational needs into intelligently-ordered sensor tasks. The controller utilizes situational awareness, system feedback, AFRL-defined rules, and needs identification to adapt its functionality to meet mission goals and objectives. An overview of its operation can be seen in **Figure D - 3**, with detailed descriptions to follow.
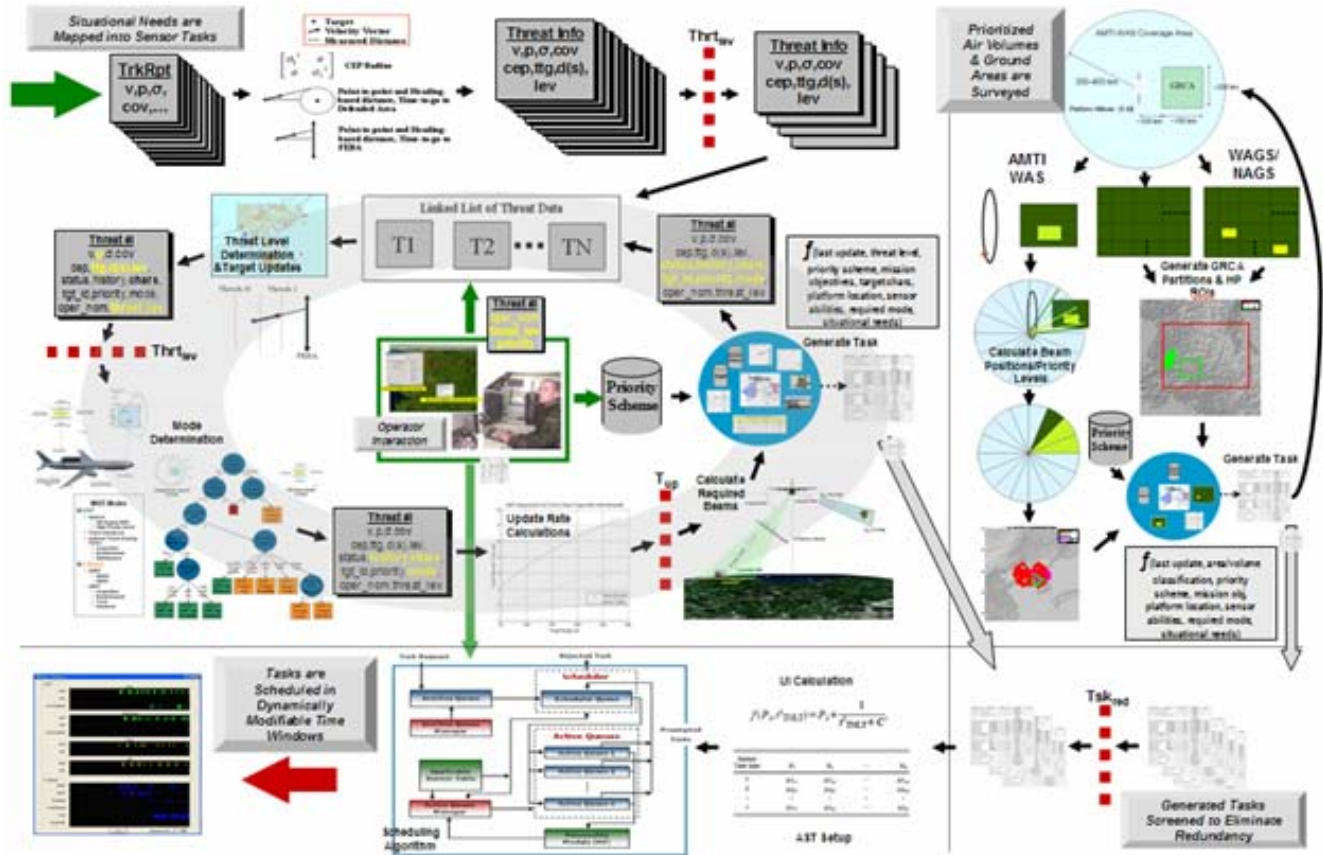
Figure D - 3. SMS KB Controller Operation

The threat handling processing begins by receiving track reports from a global tracker. Mission-specific calculations are performed on the track reports to extract threat data. Currently available are calculations for Complex Event Processing (CEP) radius, distance and time to a specified circular region (ex. defended area) based on heading and closest-point-of-attack, and distance and time to a specified boundary (ex. Forward Edge of the Battle Area (FEBA)) based on heading and closest-point-of-attack. The configurable calculations are stored with the track report data and initial high-level thresholding is performed to eliminate definite non-threats (ex. out of area). This data is stored in a linked list of track records. New records are formed for first-time targets and records are updated for existing monitored targets. The main threat-handling loop iterates over this list of target records to determine if and how it should handle the targets. It begins by updating target data and calculating a threat level based on mission-specific criteria, e.g. time-to-go to a FEBA. If the threat level is above a configurable threshold then the target is considered a threat that potentially requires action. Based on the target characteristics and threat-handling history, mode determination logic assigns a sensor mode to satisfy the current target needs. This present logic has evolved through several iterations based on evolving requirements and new modes available to the system. **Figure D - 4** displays the current mode handling logic that has been developed based on the current MIST Notional System rules/requirements and sensor modes available.
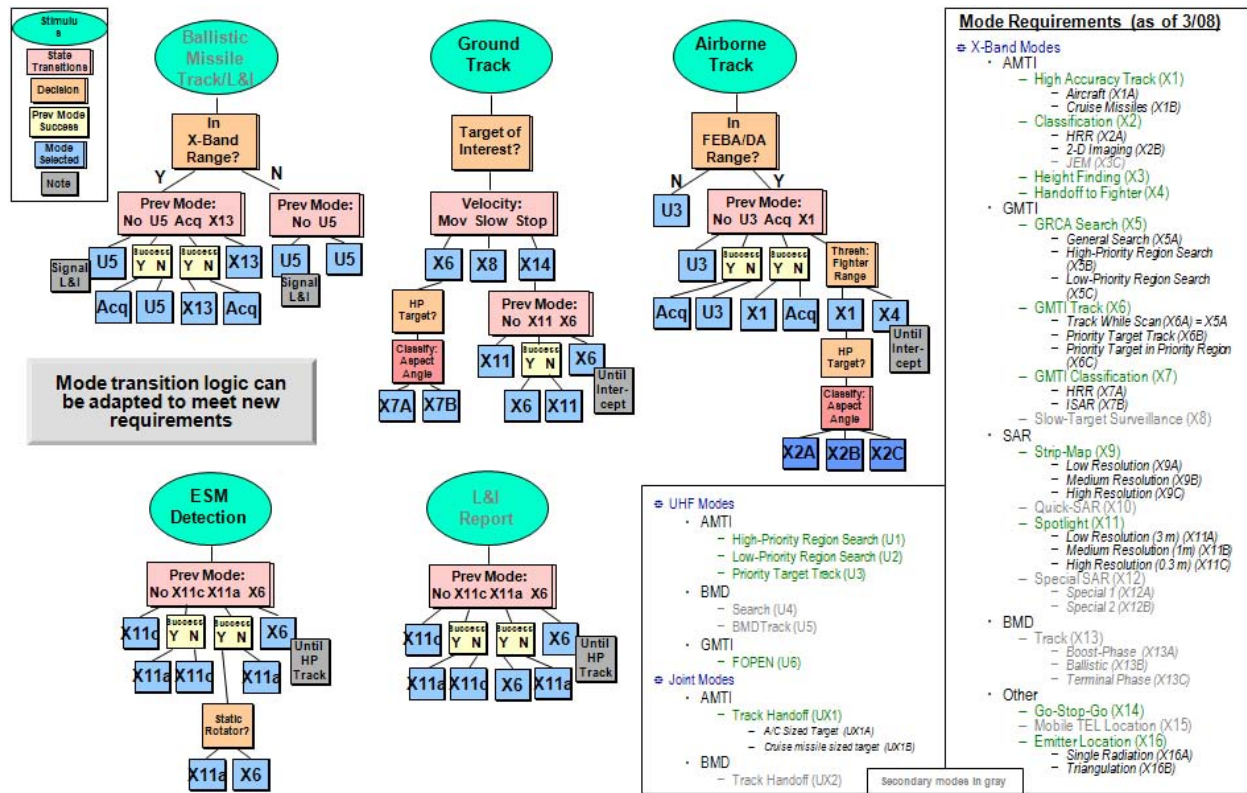
Figure D - 4. SMS Mode Determination Logic Based On MIST National Systems (MNS) Requirements

Figure D - 4 displays how the threat handling logic will assign modes based on the various stimuli that can be present in the simulation system. A list of the available sensor modes is displayed on the right. For an example, the Airborne Track handling functions as follows. UHF Low Accuracy Track (U3) will be used to handle airborne targets until they reach a configurable distance threshold to the FEBA or an Area of Interest (AOI, ex. Defended Asset). Once inside this range, the logic looks at the previous mode that handled this target. If the target has not yet been handled, then U3 will be used. Upon the next target evaluation, if U3 was successful in tracking the target then X-band Acquisition will be used, if not then U3 will again be attempted. If the Acquisition mode is successful in acquiring the target then X-band High Accuracy Track (X1) will be used to maintain track on the target. Once the track is maintained by the X-band subsystem, the target is evaluated to see if it is inside the configurable weapons handoff distance (ex. in range of a blue attack fighter). If it is not in weapons range, classification opportunities are evaluated based on the current aspect angle of the target and its classification status. The SRM evaluates the benefits of using HRR, 2-D Imaging, and JEM modes to classify the target. It can choose to submit all or none of the modes as desired. Once the target is inside the weapon's range, the X-band Handoff to Fighter (X4) mode is used until the target is intercepted. This developed mode logic will be updated as necessary as MNS requirements evolve. After a mode has been selected, the threat handling logic will determine if an update is necessary. This is based on the target characteristics (e.g. velocity, range), determined target type (e.g. attack fighter), and the time since the last threat-handling was performed on the target. Target type-specific curves consisting of target range versus update time are available for update time lookups. If the update time is satisfied then radar beam parameters are

generated for radar service requests (Risers). The parameters can be for single dwell bearing referenced tasks (azimuth angle, elevation angle, near range, far range, dwell duration, etc.) or for GRCA (coordinates, duration, etc.). After the beam parameters have been calculated, a priority is assigned to the task. The priority is calculated from an adaptable priority scheme (operator and/or configuration modifiable), target type, target handling history, threat level, and mission objectives. The priority can shrink or grow over time depending on how well the target has been handled. Following this, a radar service request is generated with the parameters necessary to task the desired sensor. Feedback is received from the scheduling portion of the controller informing the threat handler whether the task was successfully completed or not completed, which influences future threat handling of the target. A human operator has the ability to influence and adapt the threat handling process as desired. They may adjust target threat levels and/or modify the priority scheme through the simulation operator interfaces at any time during the simulation. The threat handling logic reads the operator requests and modifies the applicable objects as necessary.

The surveillance processing is responsible for performing WAS over specified ground and air regions at configurable update rates and priorities. Details of its major operations are shown in **Figure D - 5**

The surveillance processing is divided into two main areas, AMTI WAS and WAGS / NAGS. The AMTI WAS consists of partitioning the airspace into configurable low priority, high priority, and ballistic missile defense volumes. Three-dimensional rectangles are generated based on the configuration file inputs, and at each situational assessment, the surveillance processing determines which beam

Figure D - 5. Surveillance Processing

positions fall over which regions. If it is determined that the beam position requires an update then a radar task is generated based on the region/beam position history, required update time for the region, priority scheme, platform location, sensor abilities, and mission objectives. The WAGS/NAGS consists of partitioning the GRCA into a configurable grid with low and high priority regions. The surveillance processing evaluates each section of the grid at each situational assessment and determines which areas require updating. The radar tasks generated to satisfy the updates are computed based on the grid history, grid section classification, required update time, priority scheme, platform location, sensor abilities, and mission objectives. As in the threat handling processing, the operator can modify the priority scheme as desired.

All tasks generated by the threat handling and surveillance processing are monitored by the task screener. Its purpose is to eliminate redundant tasks. For example, if the threat handling has submitted a task for an update of an airborne target that coincides with a surveillance update of a beam position, only the higher priority task will be passed along if it can satisfy both needs.

The scheduling portion of the controller is responsible for ordering radar tasks in dynamically modifiable time windows. It is currently based on a modified version of the OGUPSA [D-2]. The simulation allows various scheduling algorithms to be used, OGUPSA is the one currently being used. A close-up of the scheduling processing is shown in **Figure D - 6**.
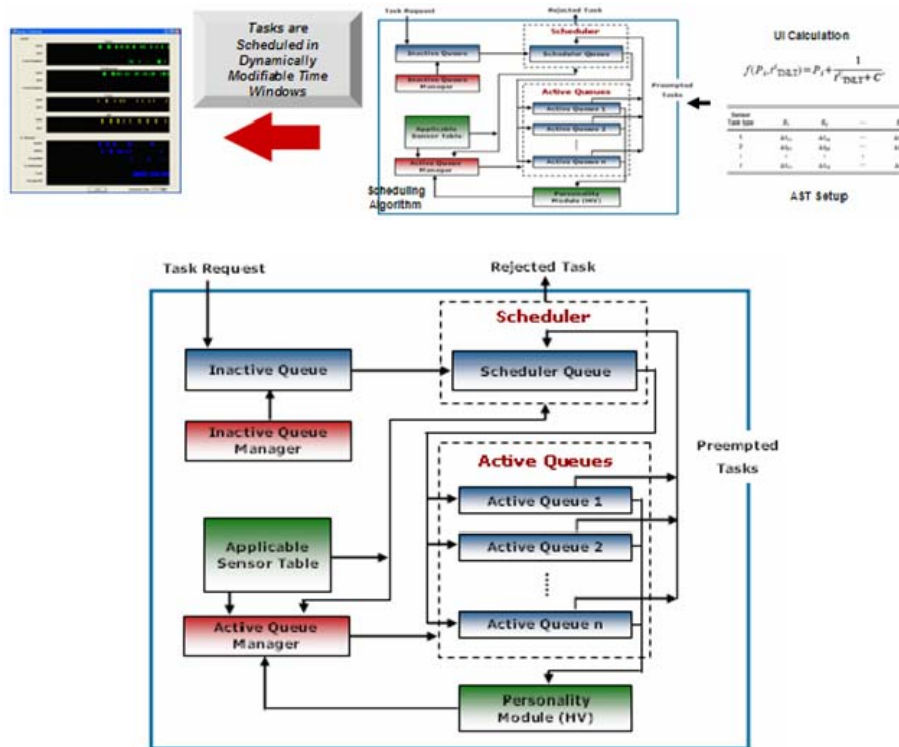
Figure D - 6. Scheduling Processing

The scheduling processing begins by generating a table consisting of the modes assigned to each sensor and initializing sensor timeline queues. As tasks arrive from the threat handling and surveillance portions of the controller, it assigns them an Urgency Index (UI). UI is a measure of priority with a tie-breaker for completion time. Tasks with the highest UI are moved into the Scheduler Queue. The task with the highest UI in the Scheduler Queue is moved into the appropriate sensor's Active Queue as determined by OGUPSA. The algorithm allows for prioritized preemption, removing interruptible tasks from a sensor's Active Queue if it is necessary for a higher priority task to be able to be completed. If a task cannot be scheduled to meet a deadline, it is rejected and notification is passed back to the appropriate portion of the controller. Upon successful completion of the tasks, tasks are removed from their assigned Active Queues and notification is passed back to the appropriate portion of the controller.

This is a high-level overview of the Knowledge-Based Controller operation. More details are available as desired. The controller logic will continue to evolve with evolving MNS requirements and as new sensors and modes are incorporated into the system.

REFERENCES

[D-1]   "MIST National Systems (MNS) for Multi-Sensor Controller Development", Version 1.0, 24 Jun 2009; AFRL/RYRD, J. Carlo/AFRL; Black River Systems Co, Helios Remote Sensing Systems, Inc., L-3 Communications and Research Associates for Defense Conversion (RADC).

[D-2]   G. McIntyre, K. Hintz, "Sensor Measurement Scheduling: An Enhanced Dynamic, Preemptive Algorithm", 1998 Society of Photo-Optical Instrumentation Enginneers, Vol 37 (2), pages 517-523 (Feb 1998).

APPENDIX E
KNOWLEDGE-AIDED CFAR

BACKGROUND

The classical approach to radar signal processing was developed for target detection by a ground-based radar looking high above near-range clutter. Interference is suppressed by the use of canceller-based filters such as MTI, assuming pulse to pulse invariance of the ground clutter. Additionally, Doppler processing is employed to further suppress clutter returns and improve SNR. Fast Fourier Transform (FFT) based filtering provides for excellent results. Typically, the output of the zero Doppler filter is ignored. The largest source of interference is the return from near-in ground clutter, within the first few miles of the radar. At the long detection ranges of interest, ground clutter is almost non-existent and the only limitation to detection is thermal noise, generally accepted to behave as a complex Gaussian random vector. The output of the MTI canceller and/or Doppler filter is processed most appropriately using Cell Averaging-CFAR (CA-CFAR) [E-1].

Now consider modern long range airborne surveillance radars operating in a complicated interference environment. The steep grazing angles associated with down looking radar may produce clutter returns of far greater magnitude than in ground based systems. As such, clutter backscatter often mask returns from targets flying above these regions. Also, clutter statistics change dramatically as the platform moves. For example, within one scan, we may have to content with clutter returns ranging from calm sea which we observe to behave as a Rayleigh distributed random vector, while at other locations within the surveillance volume we may encounter clutter returns from a land sea interface. Since terrain clutter backscatter often behaves as a K-distributed random vector, we ultimately must perform detection processing along a clutter edge where the statistics vary unpredictably. Clearly, the classical CA-CFAR detection used in ground based radar is not adequate. Further complicating this problem are spectrally spread sidelobe clutter returns which broaden the Doppler spectrum occupied by clutter, making AMTI less effective. Also, FFT-based Doppler filtering is suboptimum because the clutter returns are no longer confined to the zero Hertz filter. Platform motion and sidelobe returns broaden the clutter spectrum, spreading clutter energy into adjacent Doppler bins. This further complicates detection processing. It is in situations such as this that the use of a single combination of filtering and CFAR algorithms will produce excessive false alarms, because it cannot be designed to be optimum for each and every scenario to which it must be applied. In light of the many constraints imposed upon radar systems, improvements in detection performance are most likely to be a result of advanced processing techniques able to recognize the existence of these situations and apply appropriate processing while effectively maintaining a constant false alarm rate and an adequate detection probability.

Description and Operation of the ES-CFAR Processing

The ES-CFAR processor presented here is based upon the combined use of algorithmic and heuristic (artificial intelligence) techniques designed to assess the characteristics of the environment in order to apply the most appropriate filtering and CFAR detection algorithms [E-2]. The concept and structure of an Expert System is illustrated in **Figure E - 1**. Here, input data is compared to a data base where like or similar data sets are identified. These characteristics and descriptors of the data set are analyzed by a knowledge base which utilizes an extensive rule base to make inferences about the data. These inferences are then interpreted to ascertain their meaning in the context of the decision problem, and applied to a control structure which makes adjustments to the system under control based upon the nature of the input data. Feedback may also be incorporated where outputs of the control structure are input to the database providing additional sources of knowledge. The control structure relays decisions and actions to the user. The structure of the ES-CFAR Processor as well as the many functions performed by it, is based on this design, and is to be discussed below.
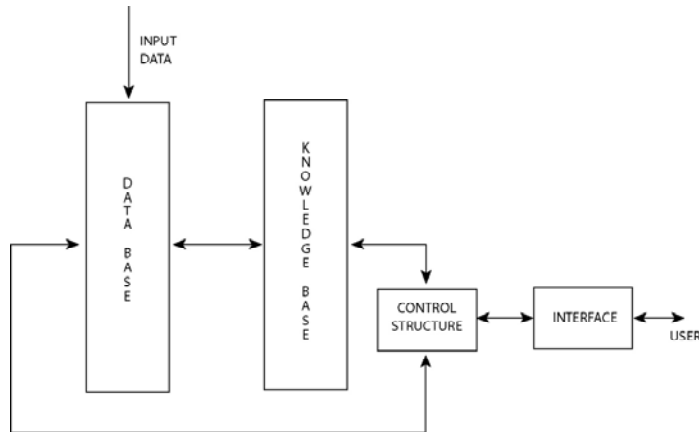
Figure E - 1. Basic Structure of an Expert System

The basic structure of the Expert System presented above can be extended to a more detailed level of sophistication by adding specific functions and knowledge sources. **Figure E - 2** illustrates the ES-CFAR Processor with specific functions added to provide additional knowledge about target detection and false alarm control. For this particular problem there are five functions to be performed, as described below.
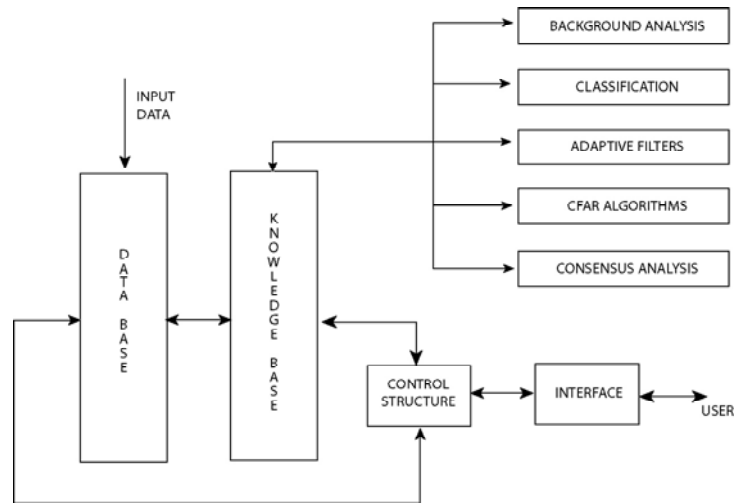
Figure E - 2. Expert System CFAR Processor

First consider the background analysis problem. As radar returns (data) are processed, one of the first tasks to be performed is determination of the statistical characteristics of the clutter. This entails identifying the probability density function (pdf) of the data as well as the associated parameters of the distribution. Standard histogram techniques, Quantile-Quantile and Percent-Percent (plot) analysis, moment techniques and various hybrid combinations are employed for this analysis.

Next, consider clutter classification (type). Also of importance in the selection of an appropriate CFAR detection algorithm are the physical attributes of the clutter (i.e., urban, sea, desert, etc.). For example, extensive research has resulted in numerous clutter and interference models which associate physical clutter features with particular statistical distributions. In fact, many CFAR algorithms are designed for detection processing in clutter behaving according to these statistical distributions. This is a priori knowledge provides the rule base which dictates the use of one CFAR algorithm over another in a given interference environment. Knowing the physical and statistical nature of the clutter environment, combined with performance measures for various CFAR algorithms as a function of clutter type, aids in the selection of the most appropriate CFAR algorithm. For example, it was stated previously that in a Gaussian white noise interference environment, CA-CFAR processing is optimum. If we consider performing detection along a clutter edge such as a transition from a thermal noise limited environment to sea clutter limited environment, the same CA-CFAR will exhibit excessive false alarms with a corresponding degradation in detection probability. A more prudent choice may be Greatest Of-CFAR (GO-CFAR) which will abate the effects of the clutter edge on our ability to perform CFAR detection processing.

The adaptive filtering algorithm library is also important. As discussed above, various forms of clutter suppression and Doppler filtering schemes are available (MTI cancellers, Doppler filtering, space-time processing, etc.), but generally only one is used. Here, based on the assessment of the environment, we cannot only choose the most appropriate CFAR algorithm, but also the most appropriate filtering technique to precede the CFAR detector.

A complete library of CFAR algorithms is critical. Many of the rules in the knowledge base control the utilization of CFAR algorithms. For each algorithm in the library, performance under the dynamic conditions of interest to the radar system engineer must be available. The relative performance of each CFAR algorithm must be quantified as a function of clutter type/statistic, detection probability, false alarm probability and CFAR processing loss. CFAR algorithm performance will vary widely considering the variety of backgrounds likely to be encountered in an airborne radar system. It is for this reason that the library must contain CFAR algorithms with variable parameters such as Cell Averaging, Greatest-Of, Ordered Statistic, and Trimmed Mean. Each of these algorithms exhibit performance advantages that can be exploited in an attempt to maintain an adequate level of detection and false alarm probability. One conventional performance measure of a detector is the receiver operating characteristics (ROC) which is a plot of detection probability versus false alarm probability. Intuitively, one would expect that as detection probability is increased, the threshold must be lowered, and consequently, false

alarm probability will be increased. **Figure E - 3** is a sample plot of the ROC for two different CFAR algorithms. This illustrates the very different behavior of two CFAR algorithms under the same conditions. We may also observe detection performance as a function of pdf, or more specifically, the variation of the parameters of a given pdf. **Figure E - 4** is a plot of detection probability versus Weibull shape parameters for two (arbitrary) CFAR algorithms. Again, we can see the very different behavior of these algorithms under identical background conditions. These are examples of the factors affecting detection and false alarm probability and the extent to which they dictate the use of one CFAR algorithm over another.
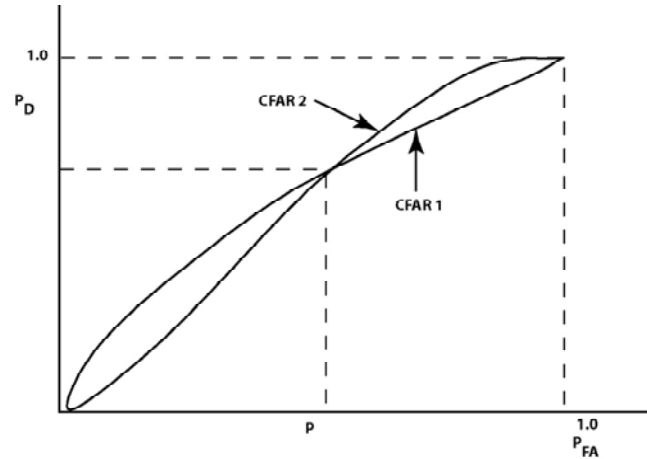
Figure E - 3. Receiver Operating Characteristic for 2 CFAR Algorithms

Finally, consensus analysis must be considered. After selection of the most appropriate algorithms, detection processing is performed and decisions from the selected CFAR algorithms must be weighted and fused to produce a satisfactory global detection decision.
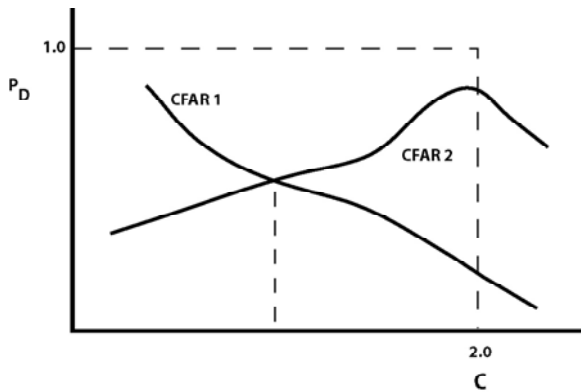
Figure E - 4. Probability of Detection vs. Weibull shape parameter for 2 CFAR Algorithms

The knowledge sources are not limited to the five listed above, but may also include exogenous variables such as temperature, wind speed, and precipitation. These factors are not directly related to target detection, but can certainly play a role in altering the statistics of the background we are trying to suppress.

A conceptual diagram of the ES-CFAR system is illustrated in **Figure E - 5**. The input is applied to an expert system where analysis (heuristic and algorithmic) produces the statistical and physical characteristics of the   This information is used in conjunction with a library of CFAR algorithms, containing algorithms such as Cell Averaging, Greatest Of, Smallest Of, Ordered Statistic, and Trimmed Mean.   Within each of these individual CFAR algorithms there are many subclasses with various combinations of rank, order, window size and multiplicative gain factor.   Preceding each of the CFAR algorithms is a filter and detector matched to that particular CFAR algorithm.   In this way one ensures that the filtering of radar data corresponds to the method of CFAR detection processing that follows. Based on the characteristics of the input data, the expert system assigns weights to the outputs of the various CFAR algorithms corresponding to their suitability given the input data.   The weighted outputs are then summed to produce a cumulative or global detection output.   This output could be, in simplest form, the decision or just one of the CFAR algorithms.   Alternatively, the output could be more complex such as a summation of the weighted outputs of all CFAR algorithms.   In this way the most appropriate combination of CFAR algorithms and parameters are used to perform CFAR detection processing.
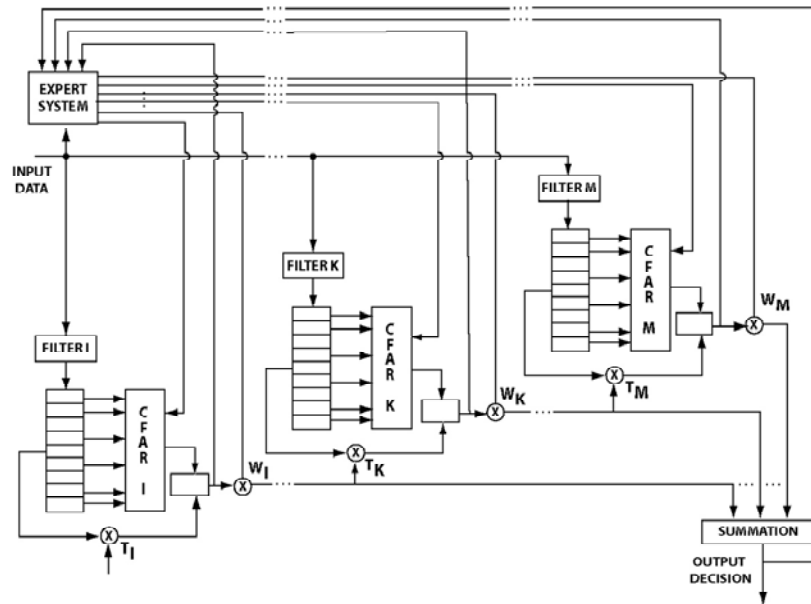
Figure E - 5. Expert System CFAR Processor

ES CFAR SUMMARY

The conflicting requirements for a high probability of detection and low probability of false alarm are rarely met in a wide area surveillance radar, due to spatial variations in the clutter. Any single algorithm is likely to be inadequate in a dynamically changing environment. The approach suggested in this paper is to select the filtering and CFAR algorithm(s) being executed at any one time based upon the observed characteristics of the interference. This requires sensing the environment, employing the most suitable filtering and CFAR algorithms, and applying a consensus algorithm to produce a global detection decision. Based on advances in expert systems, adaptive processing and CFAR algorithms, this approach has the potential to provide significant performance improvements to future wide area surveillance radars. This could also be utilized as part of a signal processor upgrade to an existing radar system.

REFERENCES

[E-1]   "Artificial Intelligence Applications to Constant False Alarm Rate (CFAR) Processing", W. Baldygo, R. Brown, M. Wicks, P. Antonoik, G. Capraro; 1993 IEEE 0-7803-0934-0/93; 1993.

[E-2]   "Expert System Constant False Alarm Rate (CFAR) Processor"; M. Wicks, W. Baldygo, R. Brown; US Patent Number 5,499,030, March 12, 1996.

APPENDIX F
NON-HOMOGENEITY DETECTION

INTRODUCTION

STAP has been proposed as a means for improving detection performance of airborne surveillance sensors [F-1-F-3]. To date, theoretical developments and computer simulation comprise much of the existing STAP literature. The Multichannel Airborne Radar Measurements (MCARM) program is a recently completed airborne data collection effort aimed at facilitating the development of field- capable STAP approaches. A very important, practical issue in fielding a STAP-based system concerns accurately estimating the interference covariance matrix and then computing an improved adaptive weight vector.

Nonhomogeneous interference, a feature of real-world airborne radar, complicates interference covariance matrix estimation and adaptive weight formulation. Wang anticipated the problem of nonhomogeneous interference on STAP in [F-4]. Ward also briefly mentions the difficulties nonhomogeneous interferences poses for STAP [F-3]. In [F-5-F-6], the authors discuss the difficulties of applying STAP to nonhomogeneous interference in the context of "undernulling". Recently, Melvin, Wicks and Brown demonstrated the impact of training data selection on STAP performance using MCARM data [F-7]. In addition, [F-7] discusses a scheme to excise nonhomogeneous interference from adaptive weight computation, leading to improved STAP performance using measured airborne radar data.

We discuss potential nonhomogeneity detection methods based on ranking and selection [F-8] of the generalized inner product [F-7, F-9-F-10], the inner product [F-5-F-6], and the sample matrix inversion (SMI) test statistic [F-1], to improve STAP performance. This effort considerably extends our previous analysis in [F-7]. We employ measured data from the MCARM program to illustrate the importance of sample selection and the capabilities of the aforementioned nonhomogeneity detectors for adaptive airborne radar.

NONHOMOGENEOUS AIRBORNE ENVIRONMENTS

The output of the space-time adaptive processor is

$$y_{k\,=\,W_k^H X_k,} \tag{F-1}$$

where $W_k^H = s^H \hat{R}_k^{-1}, s^H$ is the conjugate transpose of the target steering vector, $\hat{R}_k$ is the space-time interference covariance matrix estimate for X_k, and

$$X_k = [x_k(1,1), x_k(1,2), \ldots, x_k(1,M), x_k(2,1), \ldots, x_k(2,M), \ldots x_k(N,1), \ldots x_k(N,M)]^T \tag{F-2}$$

is the MNxl complex signal vector for the *kth* range cell [F-1]. In this case, *M* equals the number of receive channels and *N* indicates the number of coherent receive pulses. The adaptive filter equations appear similar to (F-1) - (F-2) for reduced dimension STAP methods (e.g., see [F-2 - F-4]).

A fundamental issue, evident from (F-1), concerns accurately estimating the true, unknown covariance matrix. The true, space- time covariance matrix is, $\hat{R}_k = E[X_{k/Ho}X_{k/Ho}^H]$, where $X_{k/Ho}$ is X_k under the null hypothesis (interference only). We typically estimate the covariance matrix via the minimum mean squared- error (MMSE) estimate as [F-l - F-3],

$$\hat{R}_k = \frac{1}{P}\sum_{i=k-P/2-G}^{k+P/2+G} X_i X_i^H; \ i \neq k-G, k, k+G, \tag{F-3}$$

where G indicates the use of guard cells. The X_i in (F-3) are referred to as secondary data. Similarly, we refer to the data to be filtered, X_k, as the test data. It is necessary that the *P* secondary data vectors in (F-4) appear independent and identically distributed (iid) to the interference in the test cell for the MMSE estimate to be accurate. When the interference is Gaussian-distributed, a general "rule of thumb" states that choosing $P \approx 2 \bullet MN$ iid secondary data vectors yields a loss ratio of less than 3dB between adaptive and optimal systems with a probability of fifty percent [F-11]. In practical adaptive airborne radar, complications arise due to nonhomogeneous signal environments.

Nonhomogeneous interference violates the iid assumption required to accurately compute the unknown covariance matrix via (F-3). It was shown in [F-7] that measured airborne data can appear quite nonhomogeneous and that adaptive filter performance varies dramatically with secondary data selection in such instances. Thus, an important issue arises regarding which secondary data should be selected to improve STAP performance in realistic airborne radar environments. In light of the iid assumption, a sensible approach is to screen and excise nonhomogeneous secondary data from the MMSE estimate of (F-3).

We designate two secondary data vectors appearing similar in covariance structure as homogeneous. Otherwise, the data vectors appear nonhomogeneous. The following definition clarifies the distinction between homogeneous and nonhomogeneous signal vectors.

Definition I (*Homogeneous Vectors*) Consider two multi-dimensional signal vectors, X_i and X_j, of form similar to (F-2). The true covariance matrices of X_i and X_i appear as

$$R_i \approx E[X_i X_i^H]; \ R_j \approx E[X_j X_j^H], \tag{F-4}$$

respectively. Under the Gaussian assumption, signal vectors X_i and X_j are approximately homogeneous provided

$$R_i R_j^{-1} \approx I_{MN}, \tag{F-5}$$

94

where I_{MN} is the MN x MN identity matrix. As the product of the two distinct covariance matrices deviates from the identity matrix, the signal vectors appear nonhomogeneous.

It is important to note from Definition 1 that both amplitude and phase information determine homogeneity between multi- dimensional secondary data vectors. Further note that in a strict sense, only when testing scalar quantities can amplitude power completely distinguish homogeneity among available data.

Definition 2 (***Distinguishing Secondary Data for STAP***) We assume the majority of secondary data appear homogeneous over limited range intervals. Homogeneous secondary data take the form,

$$X_i = X_{i/Ho} = C_i + N_i + I_i \ , \tag{F-6}$$

where C_i is the homogeneous clutter component, I_i is white noise jamming, and N_i is uncorrelated noise. A minority of the secondary data may appear nonhomogeneous with respect to (F-6). The nonhomogeneous secondary data appear as,

$$X_i = C_i + N_i + I_i + O_i \tag{F-7}$$

where O_i is the signal component appearing nonhomogeneous in covariance structure.

Factors making the environment appear nonhomogeneous include spatially varying clutter, system errors exacerbating spatial clutter variation, shadowing effects, moving scatterers including targets, multiple interfering targets, deceptive jamming and so forth. Since we assume in Definition 2 that the homogeneous clutter comprises the majority, computing (F-3) from the identified homogeneous secondary data ensures acceptable STAP performance for the majority of the test cells. To avoid cancellation of tactically significant signal returns, particularly weak, low velocity targets, the nonhomogeneous component of (F-7) should pass through the adaptive processor. Latter stages of signal processing, especially the tracker, should make the final determination whether O_i in (F-7) represents nonhomogeneous clutter or corresponds to a target.

NONHOMOGENEITY DETECTORS

In this section we discuss three methods one may consider for assessing relative homogeneity among available secondary data.

Inner Product

The inner product does not represent a general approach for nonhomogeneity detection in the adaptive airborne filtering problem. In other words, its value remains limited to specific instances which may be routinely violated in practice. We now briefly point out the reasons for the preceding statement. The inner product, defined as,

$$Y_i \approx X_i^H X_i \approx \sum_{i-1}^{NM} x_i^* \ x_i \ , \tag{F-8}$$

is a measure of power in signal vector, X_i. Similarly, this interpretation holds if we consider the inner product of the reduced-dimension signal vector. For example, we might take the inner product of X_i after Doppler decomposition. Notice that two signal vectors, X_k, and X_j, may have similar inner products while exhibiting dramatically different covariance matrices, R_k, and R_j. The expected value of (F-8) is,

$$E[\gamma_i] = trace \ (R_i) \ . \tag{F-9}$$

Complications arise since distinct covariance matrices may have the same trace, yet possess entirely different off-diagonal elements. The inner product serves as a suitable discriminant in testing homogeneity of scalar quantities, such as in a CFAR processor. However, nonhomogeneity detection for the adaptive filtering problem concerns assessing vector quantities and discriminating variation in both amplitude and phase.

Generalized Inner Product (GIP)

Next, consider the GIP,

$$z_i = X_i^H R_C^{-1} X_i \ , \tag{F-10}$$

where R_C, is the test covariance matrix. Chen studied and proposed (F-10) as a test of covariance structure in the context of ranking and selection for the radar problem in [F-9 - F-10]. Next, we used (F-10) as the basis for characterizing and excising outliers in [F-7] to demonstrate the importance of sample selection on STAP performance. In this section, we provide a physically intuitive description to complement Chen's analysis and further justify selection of the GIP as a nonhomogeneity detector.

Define the whitening filter output as the MN x 1 vector,

$$\tilde{X}_i = R_C^{-1/2} X_i \ . \tag{F-11}$$

The MN x MN test covariance matrix, R_C, is Hermitian. It can also be shown that $R_C^{-1/2}$ is Hermitian provided R_C is positive definite, which is almost always true. Next, observe that (F-10) can be written as the inner product,

$$Z_i = \tilde{X}_i^H \tilde{X}_i \ , \tag{F-12}$$

which equals the sum of the squares of $\tilde{X}_i$. Thus, (F-12) measures the power in the signal vector, X_i, after being whitened by $R_C^{-1/2}$. The covariance matrix of $\tilde{X}_i$ is given as

$$\tilde{R}_i = E[\tilde{X}_i \tilde{X}_i^H] = E\left[R_C^{-1/2} X_i X_i^H R_C^{-1/2}\right]. \tag{F-13}$$

Defining the true, unknown covariance matrix of X_i as $R_i = E[X_i X_i^H]$, we may express (F-13) as

$$\tilde{R}_i = R_C^{-1/2} R_i R_C^{-1/2}. \tag{F-14}$$

If $R_i \approx R_C$, then $\tilde{R}_i \approx I_{MN}$ and $E[z_i] \approx MN$. When the true covariance matrix of X_i deviates from R_C, the expected value of z_i deviates from the product MN. Thus, the GIP test in (F-10) can be used to assess similarity between the unknown covariance matrix of a selected signal vector and a test covariance matrix. Alternatively, we regard signal vectors with similar values of z_i as homogeneous with covariance matrices similar to R_C. A signal vector with z_i significantly varying from the mean is nonhomogeneous to those signal vectors with like GIP values. Note that this test directly assesses both amplitude and phase information critical to defining covariance structure.

In practice, we replace R_C, with a MMSE estimate as in (F-3). Notice that (F-3) is typically a normalized sum of the outer products of consecutively selected secondary data over a given range interval. Thus, an averaging process exists. We attempt to find those secondary data vectors significantly deviating from this average result. Then, we excise such vectors from further iterations as we refine the computation in (F-3) to best represent the majority of secondary data vectors defining the homogeneous set.

SMI Test Statistic

Letting $R_k = R_C$ in (F-1), the SMI test statistic becomes

$$\eta_i = |y_i|^2 = y_i y_i^* = W^H X_i X_i^H W, \tag{F-15}$$

where $W = R_C^{-1} s$ and R_C is Hermitian. Using (F-6), we recognize the expected value of the SMI test statistic in the homogeneous case to be,

$$E[\eta_i] \approx W^H R_C W$$
$$R_C = E[(C_i + N_i + I_i)(C_i + N_i + I_i)^H]. \tag{F-16}$$

In the nonhomogeneous case we have, from (F-7) and (F15),

$$E[\eta_i] \approx W^H R_C W + W^H(R_{OC} + R_{CO} + R_O) W$$
$$R_{OC} = E[O_i(C_i + N_i + I_i)^H]; \tag{F-17}$$

97

$$R_{CO} = R_{OC}^H; \ R_O = E[O_i O_i^H].$$

One may observe, after comparing (F-16) and (F-17) that the nonhomogeneous component leads to a shift in the SMI test statistic from the homogeneous case. The relative power of the nonhomogeneous interference and its location in the angle-Doppler domain (i.e. its two-dimensional power spectral density) influences the magnitude of the shift. This occurs since the two- dimensional (2-D) Fourier transform of the weight vector, W, defines the 2-D filter response. The filter suppresses the homogeneous component of X_i characterized by R_C while passing nonhomogeneous components outside the filter notch. Therefore, the SMI filter discriminates both amplitude and phase variation in the covariance structure of data vector, X_i, from the homogeneous condition.

As previously, we replace R_C with a MMSE estimate and seek those secondary data vectors significantly varying from the expected value of the SMI test statistic. We then recompute the MMSE estimate using the more homogeneous set of training data. If necessary, we then iterate the procedure to refine the result.

REDUCING COMPUTATION COMPLEXITY

The GIP of (F-10), or the SMI test statistic of (F-15), requires computing the inverse of the MMSE estimate of the covariance matrix given in (F-3). This computation is the most burdensome step in the adaptive filtering problem. Using appropriate techniques, we must initially compute the inverse covariance matrix. However, after this initial computational expense, a more efficient approach exists for updating the inverse covariance matrix estimate after excising or adding secondary data. We point out two simple formulations based on the matrix inversion lemma [F-12], also known as Woodbury's identity, to improve the efficiency of integrating nonhomogeneity detection with STAP.

First consider the case of adding a sample to the covariance matrix estimate. Define $\hat{R}_k(P)$ as the MMSE estimate of the interference covariance matrix using P samples. Further, let $\hat{R}_k(P+1)$ represent the MMSE estimate using P+l samples, computed as

$$
\begin{aligned}
\hat{R}_k(P+1) &= \frac{1}{P+1}\left(\sum_{i-1}^{P} X_i X_i^H + X_{P+1} X_{P+1}^H\right) \\
&= \frac{1}{P+1}\left(P\, \hat{R}_k(P) + X_{P+1} X_{P+1}^H\right).
\end{aligned}
\tag{F-18}
$$

Then, via the matrix inversion lemma, we may write,

$$
\hat{R}_k^{-1}(P+1) = \frac{P+1}{P}\left[R_k^{-1}(P) - \frac{R_k^{-1}(P)\, X_{p+1} X_{P+1}^H R_k^{-1}(P)}{P + X_{P+1}^H R_k^{-1}(P)\, X_{p+1}}\right]
\tag{F-19}
$$

Similarly, if we let $\hat{R}_k(P-1)$ represent the MMSE estimate after removing a sample from the estimate using P samples, then

$$\hat{R}_k^{-1}(P-1) = \frac{P-1}{P}\left[R_k^{-1}(P) - \frac{R_k^{-1}(P)\,X_E\,X_E^H R_k^{-1}(P)}{X_E^H R_k^{-1}(P)\,X_E - P}\right], \tag{F-20}$$

where X_E represents the excised secondary data vector and $P \neq X_E^H R_k^{-1}(P)\,X_E$.

ILLUSTRATION

We use measured airborne radar data from the MCARM Program to illustrate enhanced STAP capability resulting from the use of a NHD. The NHD leads to enhanced adaptive weight computation via improved secondary data selection.

The radar data under consideration is a single CPI of 128 pulses taken from MCARM Flight 5, Acquisition 575. Twenty-two independent channels comprise the array, organized in an eleven over eleven planar configuration. We inject a synthetic target at Doppler bin 10 (41.5 mph), range cell 290 (16.4 miles from the airborne platform and less than half the unambiguous range of 41.6 miles), and at the transmit azimuth of zero degrees (broadside). This injected target has a signal-to-clutter plus noise ratio (SCNR) of -56 dB with respect to the mainlobe clutter and an SCNR of -25 dB with respect to the competing sidelobe clutter in Doppler bin 10.

Figure F - 1 overviews the basic signal processing chain applied to the measured data [F-13]. We compare the three NHDs described in the preceding section. The factored-time space (FTS) algorithm [F-2 - F-3] represents the specific STAP algorithm

Figure F - 2. MSMI Test Statistic Versus Range Using SW Method And GIP And SMI-Based Nonhomogeneity Detection Schemes.

used in this analysis, thereby dictating the data structure used in the nonhomogeneity detection scheme. Initialization of the GIP and SMI-based NHDs uses a covariance matrix, $R_C(0)$, computed from the available secondary data using (F-3). Homogeneous secondary data result in NHD outputs falling between the upper and lower thresholds, V_{lo}, and V_{hi}. The range indices of identified homogeneous secondary data comprise the vector, $Q(n)$, in Figure F - 1. We only consider a single-pass through the secondary data set (i.e., $n_{max} = 1$). An improved covariance matrix is computed using a minimum subset of the homogeneous secondary data. This minimum subset size is forty-four samples, or twice the data vector length. Then, the processor applies the adaptive weight vector computed from this homogeneous secondary data set to filter the test data.
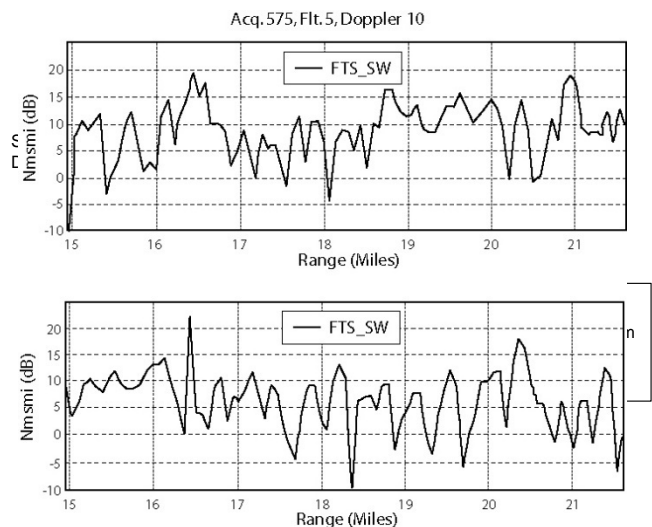
99

Figure F - 2 and **Figure F - 3** compare the performance of the FTS algorithm with varied sample selection and adaptive weight computation. Each subplot shows the output of the FTS algorithm for Doppler 10 versus range, normalized by $s^H \hat{R}_i^{-1} s$. The literature refers to this normalization of the SMI test statistic as the modified SMI (MSMI) algorithm [F-14]. Under the Gaussian assumption, it yields an embedded CFAR characteristic such that a fixed threshold may be applied over all range for a fixed probability of false alarm. This allows us to assess detection performance improvement or degradation resulting from the different nonhomogeneity detection schemes.

The top plot in **Figure F - 2**, labeled "FTS_SW", corresponds to the most commonly accepted approach for sample selection. In this case, a symmetric window (SW) about the test cell defines

Figure F - 3. MSMI Test Statistic Versus Range Using SW Method And Inner Product (IP)-Based Nonhomogeneity

the secondary data to be used in the MMSE estimate of (F-3) and the ensuing adaptive weight computation. The SW approach uses a total of twenty-two range cells and two guard cells on each side of the test cell, for a total of forty-four secondary data. The basic idea behind this approach is that data most local to the test cell will appear most statistically similar. Notice in this scenario that the injected target at a range of 16.4 miles goes undetected. The mean signal power computed over all range depicted in the plot is 11.2 dB. On the other hand, the bottom plot in **Figure F - 2** shows the normalized adaptive filter output computed following the nonhomogeneity detection stage of Figure F - 1. The GIP of (F-10) is used as the NHD. Thresholding the output of the NHD normalized to its mean with $V_{lo} = 0.7$ and $V_{hi} = 1.1$ yields forty-four secondary data identified as most homogeneous according to their GIP values. The processor computes an adaptive weight vector from this set of forty-four homogeneous secondary data and applies it to all test range cells in the subject interval. Observe that the injected target is clearly visible! Another signal peak at 20.3 miles corresponds to a highway appearing in the radar field of view, and thus we speculate it represents vehicular motion. In this case, the mean power over the range interval shown in the plot is 9.5 dB.

Next, consider **Figure F - 3**. The top plot shows the resulting FTS output that uses the SMI-based nonhomogeneity detector. The injected target is clearly visible, yet the potential target at range 20.3 miles disappears in comparison with the "FTS_GIP" result in **Figure F - 2**. Thresholds for the NHD output normalized to its mean are $V_{lo} = 0.1$ and $V_{hi} = 0.5$, resulting in the selection of forty-four homogeneous secondary data. We compute the mean power of the normalized FTS output over range to be 9 dB.
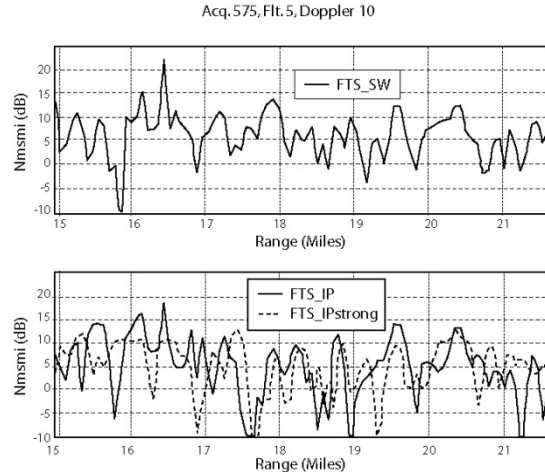
In a similar fashion, the bottom plot in **Figure F - 3** shows the FTS output when the Doppler inner product (section A of preceding section) assesses relative homogeneity. The "FTS_IP" curve corresponds to the case where values of $V_{lo} = 0.2$ and $V_{hi} = 1.0$ serve to threshold the normalized NHD output, identifying the forty-four most homogeneous secondary data in terms of their Doppler inner product. The injected target cannot be detected in this instance without a dramatic increase in the number of false alarms. Alternatively, the "FTS_IPstrong" curve corresponds to selecting the secondary data appearing strongest in power (or, most nonhomogeneous with respect to the Doppler inner product), as proposed in [F-5-F-6]. This appears to provide improved results over the "FTS_IP" case. The computed mean power values are 8.5 dB and 7.8 dB, respectively, for "FTS_IP" and "FTS_IPstrong" processing.

To further analyze the different processing methods leading to the results shown in **Figure F - 2** and **Figure F - 3**, we plot the corresponding adapted patterns. **Figure F - 4** depicts the adapted patterns for the processor selecting secondary data using the SW method and the GIP and SMI-based nonhomogeneity detection schemes. Note that the adapted patterns remain the same over all range for the GIP and SMI-based results, yet changes for the SW method since the secondary data set varies over range. Due to the nonhomogeneous nature of the interference environment, we observe that these patterns can change quite dramatically over relatively limited range extent. One conclusion from **Figure F - 4** is that the adapted patterns appear quite different for all three approaches shown.
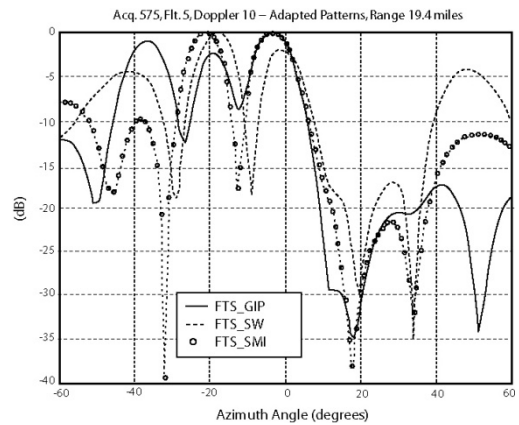
Figure F - 4. Adapted Patterns For SW Method And GIP And SMI- Based Nonhomogeneity Detection Techniques.
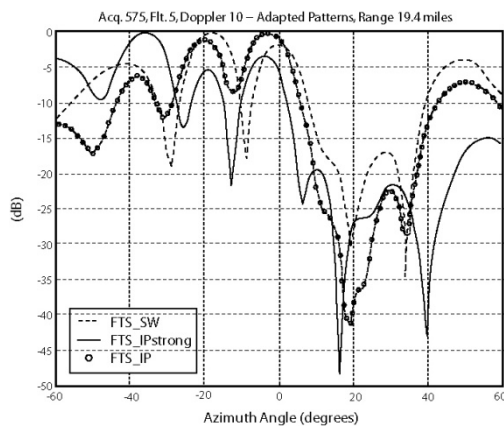
Figure F - 5. Adapted Patterns For SW Method And Inner Product (IP)-Based Nonhomogeneity Detection Schemes.

Figure F - 5 shows the adapted patterns for the SW method and the two cases where the secondary data is selected based on the inner product as the NHD. Again notice the dramatic variation in the adapted patterns. Also, observe that while the "FTS_IPstrong" results appear better than the FTS_IP"' results in **Figure F - 3**, the related adapted pattern is seriously distorted, revealing significant loss in gain in the desired signal direction of zero degrees. Nulling in the desired signal direction further suggests that training on the most powerful secondary data, in terms of the inner product measure, can lead to disaster in an electronic countermeasure (ECM) environment.

IMPROVING PRACTICAL SPACE TIME ADAPTIVE RADAR CONCLUSIONS

In this section we show the impact of sample selection on the performance of space-time adaptive processing for airborne radar. Furthermore, we discuss a scheme to improve sample selection, referred to as (multipass) nonhomogeneity detection, and consider several potential nonhomogeneity detectors. The nonhomogeneity detectors discussed include the inner product, generalized inner product and the sample matrix inversion test statistic. Analysis of measured airborne radar data shows, at least for the specific data considered, that incorporating nonhomogeneity detection with the space-time adaptive filter dramatically improves detection performance.

Our results indicate that perhaps no single nonhomogeneity detector provides superior performance, but that capability is situation dependent. In the future we will analyze more measured data so that we may better identify those scenarios when a given nonhomogeneity detector yields superior performance, or adequate performance combined with reduced computational complexity. Furthermore, we plan to investigate other possible nonhomogeneity detectors.

REFERENCES

[F-1]   L.E. Brennan and I. S. Reed, "Theory of adaptive radar," IEEE Trans. AES-9, Issue 2, pp237-252, March 1973.

[F-2]   A.G. Jaffar, M.H. Baker, W.P. Ballance, J.R. Staub, "Adaptive space-time processing techniques for airborne radars," Rome Laboratory Technical Rept. TR-91-162, July 1991.

[F-3]   J. Ward, "Space-time adaptive processing for airborne radar," MIT Lincoln Laboratory Technical Rept. ESC-TR-94-109, 13 December 1994.

[F-4]   H. Wang and L. Cai, "On adaptive spatial-temporal processing for airborne surveillance radar systems," *IEEE Trans. AES,* Vol. 30, No. 3, pp. 660-670, July 1994.

[F-5]   D. Marshall, 'Evaluation of STAP training strategies with Mountaintop data, "MIT Lincoln Lab, TR MTP-5, 1996.

[F-6]   D.J. Rabideau and A.O. Steinhardt, "Improving the performance of adaptive arrays in nonstationary environments through data-adaptive training," *Proc. 30th Asilomar Conf on Signal, Systems and Computers,* Pacific Grove, CA, 3-6 November 1996, in press.

[F-7]   W.L. Melvin, M.C. Wicks, and R.D. Brown, "Assessment of multichannel airborne radar measurements for analysis and design of space-time processing architectures and algorithms," *Proc. 1996 IEEE Nutl. Radar Con,* Ann Arbor, MI, pp. 130-135, May 13-16, 1996.

[F-8]   M.C. Wicks, "Application of ranking and selection theory to radar signal processing," Rome Laboratory Internal Tech. Memo, unpublished, October 1993.

[F-9]   P. Chen, "On testing the equality of covariance matrices under singularity," Report for AFOSR Summer Faculty Research Program, Rome Laboratory, Rome, NY, August 1994.

[F-10] P. Chen, "Partitioning procedure in radar signal processing problems," Final Report for AFOSR Summer Faculty Research Program, Rome Laboratory, Rome, NY, August 1995.

[F-11] I.S. Reed, J.D. Mallett and L.E. Brennan, "Rapid convergence in adaptive arrays," JEEE Trans. AES, Vol. 10, No. 6, pp. 853-863, November 1974.

[F-12] S. Haykin, *Adaptive Filter Theory, Third Edition,* Upper Saddle River, NJ: Prentice-Hall, 1996.

[F-13] W.L. Melvin, M.C. Wicks and P. Chen, "Nonhomogeneity detection method and apparatus for improved adaptive signal processing," USA Patent Application No. 694577, filed 9 August 1996.

[F-14] W.S. Chen and I.S. Reed, "A new CFAR detection test for radar," *Digital Signal Processing,* Vol. 1, Academic Press, pp. 198-214, 1991. Vol. 9, No. 2, pp. 237-252, March 1973.

APPENDIX G
KNOWLEDGE AIDED DETECTION AND TRACKING

By: C. Capraro, G. Capraro (Capraro Technologies); and M. Wicks (AFRL, Sensors Directorate)

INTRODUCTION

Sensor performance may be enhanced by selecting algorithms adaptively as the environment changes. It has been shown [G-1 – G-7], that if an airborne radar system uses prior knowledge concerning certain features of the earth (e.g. land-sea interfaces) intelligently, then performance in the filtering, detection and tracking stages of a radar processing chain improves dramatically. As an example the performance of an intelligent radar can be increased if the characteristics and location of electromagnetic interference, mountainous terrain, and weather conditions are known. The Sensors Directorate of the AFRL conducted and sponsored research and development in the use of prior knowledge for enhancing radar performance, as did the DARPA under the KASSPER program.

One design of an intelligent radar system that processes information from the, filter, detector, and tracker stages of a surveillance radar, investigated by AFRL and under the KASSPER program, was specifically designed for an AIRS. This architecture design leveraged advancements pursued by the World Wide Web Consortium (W3C) and DARPA Agent Markup Language (DAML) program for constructing the next generation internet. Futuristic advanced intelligent radar systems will

Figure G - 1. Airborne Intelligent Radar System (AIRS)

cooperatively perform signal and data processing within and between sensors and communications systems while utilizing waveform diversity and performing multi-sensor processing, for reconnaissance, surveillance, imaging and communications within the same radar system. A high level description of AIRS is shown in Figure G - 1 and is described in detail, [G-6, G-8], in the literature.

There are other efforts concerned with dynamically controlling the emission and reception of radio frequencies in addition to AIRS, for example, the XG Communications program sponsored by DARPA. This program developed an architecture that will open up the spectrum for more efficient use by first sensing and then using portions of the spectrum for XG radio transmissions adaptively.

The goals of the XG program are: 1. Demonstrate through technological innovation the ability to utilize available (unused, as opposed to unallocated) spectrum more efficiently, and 2. Develop the underlying architecture and framework required to enable the practical application of such technological advances.

Figure G - 2 is a diagram representing the operational concepts of an XG policy-agile spectrum user, which employs a computer understandable spectrum policy capability, [G-9].

Another effort related to communications, and having similar goals to the XG program, is the Cognitive Radio [G-10]. Its objectives are to efficiently utilize the radio frequency spectrum and to provide reliable communications at all times. A basic cognitive cycle view of the radio is illustrated in Figure G - 3.
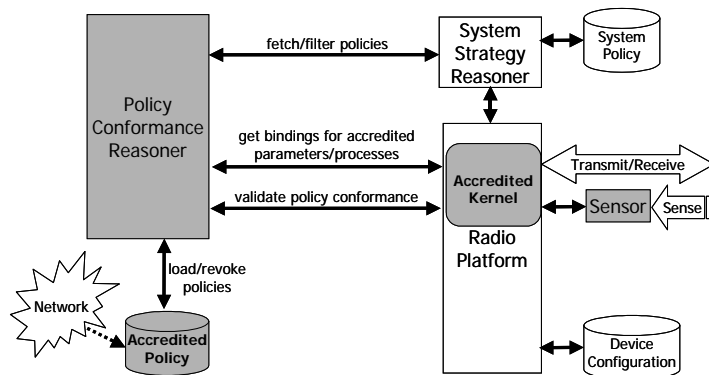
Figure G - 2. Policy-Agile Operation Of XG Spectrum-Agile Radio

Figure G - 3. Basic Cognitive Cycle

All of the aforementioned efforts are using advanced technologies being developed in the artificial intelligence and user community to manage processing resources. In addition, most of the efforts sponsored by the KASSPER program leveraged outside sources of knowledge to enhance the performance of a radar system. Most of these efforts were related to ground looking radar systems on board one or more aircraft. Some of the efforts used measured radar data to develop and demonstrate algorithms. Other efforts used simulated data provided by DARPA. Our investigations have primarily been concerned using map data to assist in selection of the best training data for STAP in airborne radar. We used radar data taken from the MCARM program sponsored by AFRL Sensors Directorate [G-3, G-4, G-5, G-11]. The prior knowledge we used consisted of land use and land cover (LULC) map data provided by the US Geological Survey (USGS). Other researchers have used digital line graph (DLG) data to take into consideration ground traffic on roads [G-11]. The MCARM data used in these works were taken in the Delaware, Maryland and Virginia region within the USA, where the terrain is relatively flat.

105

Within this effort our goal was to determine how DTED could be used in a very mountainous environment where the LULC data was relatively unchanged from location to location. In Section II a description of the terrain and our algorithm for registering the location of the radar range cell is provided. In Section III our performance measure is described, and the results from the analysis of experiment radar data are presented. Section IV provides a summary and conclusions.

DIGITAL TERRAIN DATA AND REGISTRATION

There is a large assortment of geospatial data available to assist in the development of Knowledge Aided (KA) radar signal processing algorithms. The National Geospatial-Intelligence Agency (NGA) and the USGS offer digitized geospatial data containing terrain elevation, classification (urban, agricultural, forested, etc.), and feature (roads, power lines, railroads, etc.) information. These publicly available datasets cover most of the United States as well as other parts of the world. The majority have a resolution of about 90 meters although more are being offered at 10 meters. Other data such as terrain radar cross-section measurements, synthetic aperture radar imagery and satellite imagery also aid in KA radar signal and data processing.

For this effort we used National Elevation Data (NED) [G-12]. The NED data was obtained from the USGS with a resolution of 10 meters. This data was collected between 1999 and 2001. The datasets were in a binary grid-cell format. Each value corresponded to an elevation in meters abo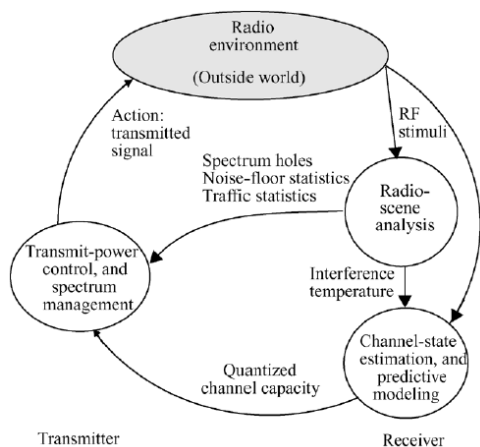ve mean sea level. A header file was included that contained the number of columns, number of rows, geographic location of the lower left corner and the size of each cell. As part of this effort, the data was converted to a non-projected global geodetic coordinate system (latitude, longitude, and elevation) and stored in a relational database for flexible search and retrieval.

Registration Techniques

Registering the radar with the terrain data is a complex task and requires an advanced knowledge of geographic science. Data sources are geo-referenced using various geodetic datums (frames of reference), reference ellipsoids, and map projections.

Geo-coordinate System:

An Earth-Centered Earth-Fixed (ECEF) Cartesian system was chosen for registration of the radar with the earth. **Figure G - 4** shows a diagram of the ECEF coordinate system in contrast with the standard geodetic coordinate system. The x-axis of the ECEF system lies in the equatorial plane and intersects the Prime Meridian. The z-axis points through the axis of rotation of the earth (geographic North pole) and the y-axis lies in the equatorial plane, forming a right-handed global coordinate system. The origin of this system corresponds to the center of mass of the earth.

This coordinate system was chosen because it is a non-projected system and, therefore, it is not distorted as in planar map projections. It is also a global three-dimensional system with values measured in length, not degrees. This makes it easier to calculate distances between points.

Earth Model:

A more accurate model of the earth is a geoid defined as the shape of the gravitational equipotential of the earth's surface. However, geoid models are often complex, computationally intensive to implement, and are constantly being refined as technology improves.

Figure G - 4. ECEF And Geodetic Coordinate Systems (Latitude, Longitude, Height).

As a result, a spherical earth model is typically used because it simplifies the calculations and it provides a good approximation at shorter slant ranges. However, at longer slant ranges, the spherical approximation can be in error by hundreds of feet. A better approximation is to model the earth as an ellipsoid where its curvature flattens near the poles.

After choosing an ellipsoidal model, the frame of reference used was the 1984 World Geodetic System (WGS84) which globally approximates the mean sea level of the earth. In certain areas of the world, more accurate local frames of reference are available and are easily substituted.

Registration Equations:

A system of three nonlinear equations was developed to calculate the position of a point on the earth given a slant range, either a Doppler or spatial frequency, and an ellipsoidal model of the earth. It is assumed that the earth is smooth (no elevation) and that the radar data is unambiguous in Doppler. Figure G - 5 illustrates the registration geometry. Under conditions where the terrain varies significantly, the registration equations shown below are used in conjunction with digital elevation data.

Figure G - 5. Registration Geometry

In Figure G - 5, the point $P_r(x_r, y_r, z_r)$ represents the position of the radar, and the point $P_e(x,y,z)$ designates the point on the earth to be determined. Also shown is the slant range of the lth range sample, R_l, and the iso-frequency (Doppler or spatial) contour of interest. The intersection of the slant range with the iso-frequency contour and the earth surface occurs at two points: P_e and a mirror point on the contour.

The first equation is related to the slant range and is simply the squared Euclidian distance between the points, P_e and P_r. The functional form of the equation is given as

$$F_1(x, y, z) = (x - x_r)^2 + (y - y_r)^2 + (z - z_r)^2 - R_l^2 = 0 \tag{G-1}$$

The second equation models the earth surface as an ellipsoid and is defined as

$$F_2(x, y, z) = \frac{x^2}{a^2} + \frac{y^2}{a^2} + \frac{z^2}{b^2} - 1 = 0 \tag{G-2}$$

where a and b are the semi-major and semi-minor radii of the earth, respectively. Values for these parameters were obtained from the WGS84 world geodetic datum. The last equation represents the iso-frequency contour as mapped onto the earth. One of the following two equations may be used in conjunction with (1) and (2) to complete the system of equations.

Doppler Frequency Equation

For a given Doppler frequency, f_d, the third registration equation was derived from

$$f_d = \frac{2(\mathbf{k} \cdot \mathbf{v_r})}{\lambda} \tag{G-3}$$

where, after normalizing by R_l, $\mathbf{k}$ is the unit vector pointing from the radar to the earth, $\mathbf{v_r}$ is the radar velocity vector and λ is the wavelength of the radar. After some manipulation, the third equation is

$$F_3(x, y, z) = (x - x_r)v_{rx} + (y - y_r)v_{ry} + (z - z_r)v_{rz} - \left(\frac{f_d \lambda R_l}{2}\right) = 0 \tag{G-4}$$

where v_{rx}, v_{ry}, v_{rz} are the components of the radar velocity vector.

Spatial Frequency Equation

For a given spatial frequency, υ, assuming a one-dimensional linear array, the third registration equation was derived from

$$\upsilon = \frac{(\mathbf{k} \cdot \mathbf{d})}{\lambda} \tag{G-5}$$

where $\mathbf{d}$ is the interelement spacing vector along the array horizontal axis. After some manipulation, the third equation is

$$F_3(x,y,z)=(x-x_r)d_x+(y-y_r)d_y+(z-z_r)d_z-(\upsilon\lambda R_s)=0 \qquad \text{(G-6)}$$

where d_x, d_y, d_z are the components of **d**.

In order to find solutions for x, y and z, an iterative Newton-Raphson method [G-13] was used until the method converged. The initial point for the iteration was calculated from a spherical earth model and was chosen to be near the point of interest, P_e. This helped the Newton-Raphson method rapidly converge to a solution for P_e, and not to its mirror point.

Assuming a smooth earth, a grid with a resolution matching that of the digital elevation data was created for each range-Doppler cell. These cell grid-points were then registered to the earth using [G-1] – [G-5], [G-8]. In order to determine the elevation at each grid-point in a cell, a 2-D nearest neighbor interpolation was performed with the elevation terrain grid. Because of the inclusion of elevation data, the slant ranges to each cell grid-points were recomputed, and the cells were sorted into their proper range bins by the average slant range of their grid-points. Next, a mesh of triangular patches for each cell was created using Delaunay triangulation [G-14]. This produced an approximate three-dimensional surface which modeled the actual terrain.
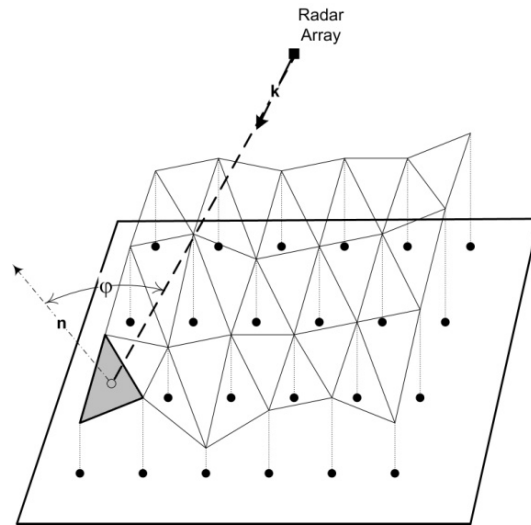
Figure G - 6. Surface Model Of Range-Doppler Cell Generated From Digital Elevation Data. The Backscattering Angle, Φ, Is The Angle Between A Patch Normal, N, And The Unit Vector, K, Pointing To The Patch From The Radar. The Black Dots Represent Cell Grid-Points Registered On A Smooth Earth.

In order to make comparisons between cells based upon their surface models, the backscattering angle of each patch contained within a cell was determined (see Figure G - 6). A 3-element terrain vector for each cell was developed which included the average backscattering angle of its patches, the standard deviation of the backscattering angles, and the percent of shadowed (obscured from radar due to terrain) patches. The shadowed patches were ascertained by determining if the terrain obstructed the line of sight from the radar to the patch. Diffraction or atmospheric refraction were not taken into account. Figure G - 7 is an example of some shadowed regions computed by the KA elevation algorithm.

KA SECONDARY DATA SELECTION APPROACH

An airborne phased array radar was used to experiment and test our algorithm [G-5]. The radar is located at approximately 60 kilometers from the illuminated earth at an elevation of approximately 30,000 feet. Six different CPIs were evaluated with three different filtering algorithms. A CA-CFAR detector algorithm was used. The probability of detection threshold level was the same for each CPI, and the number of false alarms was computed for each filtering algorithm. A false alarm was defined as any detection that occurred where truth data indicated there were no ground targets. The number of false alarms for each of the three different STAP filtering algorithms and CA-CFAR detector is shown in **Table G - 1**. Also shown is the number of false alarms for the same CPIs after the KA algorithm eliminated those detections whose locations were within shadowed
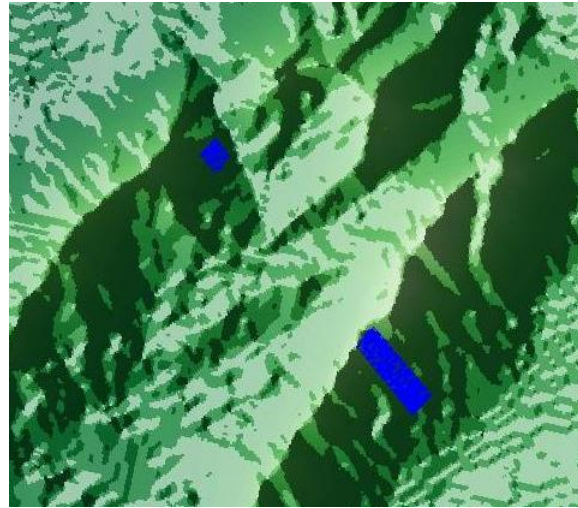
Figure G - 7. Shadow Region Example Using The KA Elevation Algorithm. Shadowed Cells (Blue) In A Mountainous Terrain Are Highlighted. The Radar Is Located North-West Of This Area With Its Main Beam Pointing South-East.

regions. Averaging the number of false alarms for the three different filtering algorithms and the CA-CFAR detector and comparing it to the average number of false alarms for the KA algorithm; a reduction of approximately 9.4 dB was obtained, i.e. 10Log(52/18)/(2/6) = 9.4 dB. As shown, the KA algorithm still exhibited two false alarms. It is conjectured that these may have occurred because of multipath and/or strong reflections from sidelobe regions of the antenna that were not shadowed.

Table G - 1. KA Performance Results

CPI No.	Filter Algorithm 1 - No. of False Detections	Filter Algorithm 2 - No. of False Detections	Filter Algorithm 3 - No. of False Detections	KA Filter No. of False Detections	KA Gain
09	3	3	3	1	
11	0	0	0	0	
13	12	12	10	1	
15	0	0	0	0	
17	1	1	1	0	
20	2	2	2	0	
Total	18	18	16	2	9.4 dB

As demonstrated, performing a post detection filtering of potential targets utilizing digital elevation data in mountainous regions can significantly reduce the number of false alarms passed on to the tracker portion of a radar. This same approach can also be used in urban environments where buildings rather than mountains can obstruct or shadow targets. In general, knowledge of the environment can significantly increase the performance of a radar.

SUMMARY AND CONCLUSIONS

This paper has provided a brief introduction to some of the work sponsored by the AFRL and DARPA related to KA algorithms for airborne ground looking radar systems. It briefly describes three different architectures for using artificial intelligence technologies for controlling the reception and analysis of electromagnetic signals for radar and communication systems. The paper describes an algorithm for registering the main beam of a radar to the earth, and identifying those areas where the beam is shadowed because of terrain elevation. The paper concludes with the development of a new algorithm which performs post detection filtering of false targets prior to track processing. This approach will reduce errors in tracking. Identifying shadowed regions may also be used to determine where, why, and for how long targets may be obscured. The results of an experiment are presented where three different filtering algorithms and a cell averaging CFAR detector are compared to our KA post detection filtering algorithm. The limited results computed using experimental radar data demonstrates a 9.4 dB average reduction of false alarms passed to the tracker.

The use of this advanced filtering algorithm in regions of mountainous terrain significantly enhances radar performance. This algorithm requires more testing, verification and numerical processing optimization before fielding. It should also be investigated for applicability in other shadowed environments such as urban terrain. Computer models of these dense urban environments can be used in a manner similar to the DTED model constructed herein to register the main beam of a radar and detect and eliminate false alarms before passing them on to the tracker.

REFERENCES

[G-1] W. Baldygo, M. Wicks, R. Brown, P. Antonik, G. Capraro, and L. Hennington, "Artificial intelligence applications to constant false alarm rate (CFAR) processing", *Proceedings of the IEEE 1993 National Radar Conference*, Boston, MA, April 1993.

[G-2] R. Senn, "Knowledge Base Applications To Adaptive Space-Time Processing", AFRL-SN-TR-146, Final Report, July 2001.

[G-3] P. Antonik, H. Shuman, P. Li, W. Melvin, and M. Wicks, "Knowledge-Based Space-Time Adaptive Processing", *Proceedings of the IEEE 1997 National Radar Conference*, Syracuse, NY, May 1997.

[G-4] C. Capraro, G. Capraro, D. Weiner, M. Wicks, and W. Baldygo "Improved STAP Performance Using Knowledge-aided Secondary Data Selection, Proceedings 2004 IEEE Radar Conference, Philadelphia, PA, April 2004, pp. 361 - 365.

[G-5] C. T. Capraro, G. T. Capraro, D. D. Weiner, and M. Wicks, "Knowledge Based Map Space Time Adaptive Processing (KBMapSTAP)," Proceedings of the 2001 International Conference on Imaging Science, Systems, and Technology, June 2001, Las Vegas, Nevada.

[G-6] A. Farina, H. Griffiths, G. Capraro, and M. Wicks, "Knowledge-Based Radar Signal & Data Processing", NATO RTO Lecture Series 233, November 2003.

[G-7] G. T. Capraro, A. Farina, H. Griffiths, and M. C. Wicks, "Knowledge-Based Radar Signal and Data Processing", IEEE Signal Processing Magazine, vol. 23, no. 1, pp. 18-29, January 2006.

[G-8] G. Capraro and M. Wicks, "An Airborne Intelligent Radar System (AIRS)", Proceedings of the Radar 2004 – International Conference on Radar Systems, Paris, France.

[G-9] G. T. Capraro, P. J. Baskinger, M. C. Chruscicki, and D. Hague, "Communications and Sensor Management A Net-Centric Semantic Web Approach", Proceedings of the 2006 International Conference on Artificial Intelligence, June 2006, Las Vegas, Nevada.

[G-10] S. Haykin, "Cognitive Radio: Brain-Empowered Wireless Communications", IEEE Journal on Selected Areas in Communications, vol. 23, no. 2, pp. 201 – 220, February 2005

[G-11] R. S. Adve, T. B. Hale, and M. C. Wicks, "Joint domain localized adaptive processing in homogeneous and non-homogeneous environments, Part I: homogeneous environments," and "Joint domain localized adaptive processing in homogeneous and non-homogeneous environments, Part II: homogeneous environments," Proc. Inst. Elect. Eng. (Radar Sonar Navig.) vol. 147 pp. 57-73, April 2000.

[G-12] United States Geological Survey, "National Elevation Data (NED)", Oct. 28, 2004, Sept. 6, 2006: http://seamless.usgs.gov/.

[G-13] W. H. Press, S. A. Teukolsky, W. T. Vetterling, and B. P. Flannery, *Numerical Recipes in C: The Art of Scientific Computing*, 2nd Ed., New York, NY: Cambridge University Press, 1992.

[G-14] D. T. Lee, B. J. Schachter, "Two Algorithms for Constructing a Delaunay Triangulation," *Int. J. Computer Information Sci.*, Vol. 9, pp. 219-242, 1980.

APPENDIX H
IMPLEMENTING DIGITAL TERRAIN DATA IN KNOWLEDGE-AIDED STAP

By: C. Capraro, G. Capraro, I. Bradaric, Capraro Technologies; D. Weiner, Syracuse University;
M. Wicks, W. Baldygo, AFRL Sensors Directorate

INTRODUCTION

In order to estimate the clutter covariance matrix needed for STAP, range samples located close to the sample under test are normally chosen as secondary (or training) data. If N samples are required for estimation, $N/2$ above the test sample and $N/2$ below the test sample, excluding guard samples, are typically chosen. It is assumed that this sliding window method of secondary data selection chooses samples that are representative of the clutter in the test sample. However, in a nonhomogeneous terrain environment this assumption may not be valid. The amount of secondary data required for proper estimation of the covariance matrix in a stationary environment is between 2 and 5 times the number of degrees of freedom (DOF) of the radar assuming the clutter is Gaussian distributed [H-1]. As a result, the sample support needed may geographically span hundreds of meters, or even kilometers, depending on the range resolution and the DOF of the radar. Terrain boundaries such as land-water or urban-grassland interfaces are likely to occur. This nonstationarity due to nonhomogeneous terrain can lead to poor estimation of the clutter covariance matrix and, in turn, poor cancellation of the clutter.

Several authors [H-2]-[H-4] have proposed statistical nonhomogeneity detectors, in both Gaussian and non-Gaussian distributed clutter environments, to excise outliers contained within the secondary data. They have shown the deleterious effects of nonhomogeneous secondary data and have improved STAP performance by filtering the outliers in the selection process. Melvin [H-5] has modeled STAP performance with respect to heterogeneous clutter and has demonstrated that, in specific cases, loss in signal-to-interference plus noise ratio (SINR) can be greater than 16 dB. Other researchers [H-6] have also recognized the limitations of STAP and have investigated new methods for incorporating *a priori* knowledge as part of DARPA's KASSPER program. Some knowledge sources have already proven valuable when integrated into other portions of the radar signal processing chain such as detection [H-7] and tracking [H-8].

We propose an approach, in the area of KA-STAP, which employs digital terrain data to aid in choosing representative secondary data. The assumption is that estimation of the covariance matrix will improve by choosing secondary data whose terrain characteristics match the range sample under test. Properly utilized *a priori* knowledge in STAP will enable the adaptive filter to use limited degrees of freedom more effectively thereby improving clutter rejection. This approach can also be implemented in conjunction with other data independent and data dependent secondary data selection algorithms in order to remove any unknown nonhomogeneities.

Implementing digital terrain data in KA STAP requires a wide breadth of knowledge in several areas. In this paper we extend our prior work [H-9]-[H-11], identify some of the practical problems that arise, and present numerical solutions.

In Section H-2.1, a description of the measured radar data and the digital terrain data used is provided. In Section III an approach to knowledge-aided secondary data selection is presented. In Section H-3.1 techniques for registering the radar return data with the terrain data are described. In Section H-3.2, an analysis leading to an understanding of the conditions needed for equivalent secondary data is presented. In Section H-3.3, a description of the STAP algorithm that was chosen is provided. In Section H-3.4, corrections for certain factors affecting STAP performance such as array misalignment, range, reflectivity, atmospheric propagation, and vertical gain are developed. In Section H-3.5, a method for producing a rudimentary terrain image from actual surveillance radar returns is described. The terrain image helps in evaluating how well the terrain data represents the environment and also aids with registration. In Section H-3.6, a KA secondary data selection algorithm for both digital land classification data and digital elevation data are described. In Section H-3.7, an approach for improving sample support using terrain data is given. In Section H-3.8, a simple method for mitigating the effects of range spread is provided. In Section H-4, results are presented that compare our KA approach to the standard sliding window method. Finally, in Section H-5, we provide our conclusions.

BACKGROUND

Measured Radar Data

Measured airborne radar data was obtained from the AFRL Sensors Directorate's MCARM program [H-12]. The datasets consist of multi-channel clutter data collected by an airborne platform with a side looking radar. The radar was configured with a 2 by 11 channel linear array including sum and delta analog beamformers. MCARM operated at L-Band in low, medium and high PRF modes. It had a range resolution of approximately 120 meters with about 500 range samples of data. Each coherent processing interval (CPI) consisted of 128 pulses and the clutter was typically unambiguous in Doppler. Northrop Grumman collected the data during flights over the Delmarva Peninsula and the East coast of the US in the mid-1990s. There were eleven flights with an in-scene moving target simulator (MTS) in some of the data collection experiments. The MTS transmitted five "Doppler" tones (0, -200, -400, -600, -800 Hertz) and was used as the basis for evaluating our results. Table H - 1 provides some of the MCARM radar's system parameters.

Table H - 1. MCARM Radar System Parameters

Symbol	Description	Value
N	Number of array elements	22
M	Number of pulses per CPI	128
L	Number of usable range samples	500
P_t	Peak transmit power	1.5 kW
T_p	Transmit pulse width (uncompressed)	50.4 μs
B	Instantaneous bandwidth	800 kHz
f_r	Pulse repetition frequency (PRF)	1984 Hz
D	Interelement spacing	0.109 m
f	Radar frequency	1.24 GHz
ΔR	Range resolution	120

Digital Terrain Data

There is a large assortment of geospatial data sources available that can assist in the development of KA radar signal processing algorithms. The NGA and the USGS offer digitized geospatial data containing terrain elevation, classification (urban, agricultural, forested, etc.), and feature (roads, power lines, railroads, etc.) information. These publicly available datasets cover most of the US and other areas of the World. The majority have a resolution of about 90 meters although more are being offered at 10 meters. Other data such as terrain radar cross-section measurements, synthetic aperture radar imagery and satellite imagery could also aid in KA radar signal processing algorithms.

For this paper two types of digital terrain data were used in the development of our KA approach. The first called National Land Cover Data (NLCD) [H-13] was used to classify the ground environment illuminated by the MCARM radar. The second called NED [H-14] contained elevation measurements of the terrain.

The NLCD data was obtained from the USGS with a spatial resolution of 30 meters. In the NLCD format the terrain is hierarchically grouped by 9 major classifications such as urban areas, barren land, water, etc., and subgrouped into 21 minor classifications such as high intensity residential urban areas, low intensity residential urban areas, etc. (see Table H - 2). These data were collected in the 1990s at about the same time as the MCARM experiments.

Table H - 2. NLCD Land Cover Classifications

Code	Major Classifications	Minor Classifications
11	Water	Open Water
12	Water	Perennial Ice/Snow
21	Developed	Low-Intensity Residential
22	Developed	High-Intensity Residential
23	Developed	Commercial/Industrial/Transportation
31	Barren	Bare Rock/Sand/Clay
32	Barren	Quarries/Strip Mines/Gravel Pits
33	Barren	Transitional
41	Forested Upland	Deciduous Forest
42	Forested Upland	Evergreen Forest
43	Forested Upland	Mixed Forest
51	Shrubland	Shrubland
61	Non-natural Woody	Orchards/Vineyards/Other
71	Herbaceous Upland	Grasslands/Herbaceous
81	Herbaceous Planted/Cultivated	Pasture/Hay
82	Herbaceous Planted/Cultivated	Row Crops
83	Herbaceous Planted/Cultivated	Small Grains
84	Herbaceous Planted/Cultivated	Fallow
85	Herbaceous Planted/Cultivated	Urban/Recreational Grasses
91	Wetlands	Woody Wetlands
92	Wetlands	Emergent Herbaceous Wetlands

The NED data was also obtained from the USGS with a resolution of 10 meters. It was collected between 1999 and 2001.

Both datasets were in a binary grid-cell format although other data formats were available. Each value corresponded to either a land classification code for NLCD or an elevation in meters above mean sea level for NED. A header file was included that contained the number of columns, number of rows, geographic location of the lower left corner and the size of the cells. As part of this effort, the data was converted to a non-projected global geodetic coordinate system (latitude, longitude, and elevation) and stored in a relational database for flexible search and retrieval.

116

KA SECONDARY DATA SELECTION APPROACH

Registration Techniques

Registering the radar with the terrain data is a complex task and requires a good knowledge of geographic science. Data sources are geo-referenced using various geodetic datums (frames of reference), reference ellipsoids, and map projections. Careful attention to how data sources are geo-referenced is required in order to perform accurate registration.

Geo-coordinate System:

An ECEF Cartesian system was chosen for registration of the radar with the earth. **Figure H - 1** shows a diagram of the ECEF coordinate system in contrast with the standard geodetic coordinate system. The x-axis of the ECEF system lies in the equatorial plane and intersects the Prime Meridian. The z-axis points through the axis of rotation of the earth (geographic North pole) and the y-axis lies in the equatorial plane forming a right-handed global coordinate system. The origin of this system corresponds to the earth's center of mass.

This coordinate system was chosen because it is a non-projected system and, therefore, it is not distorted like planar map projections. It is also a global three-dimensional system with its values measured in length, not degrees, which makes it easier to calculate distances between points.

Figure H - 1. ECEF And Geodetic Coordinate Systems (Latitude, Longitude, Height).

Addendum A contains methods for converting between the standard geodetic system and the ECEF Cartesian system.

Earth Model

The most accurate model of the earth is a geoid defined as the shape of the gravitational equipotential of the earth's surface. However, geoid models are often complex, computationally intensive to implement, and are constantly being refined as technology improves.

As a result, a spherical earth model is typically used because it simplifies the calculations that need to be performed and it provides a good approximation at shorter slant ranges. Though at longer slant ranges, the spherical approximation can be in error by hundreds of feet. A better approximation is to model the earth as an ellipsoid where its curvature flattens near the poles.
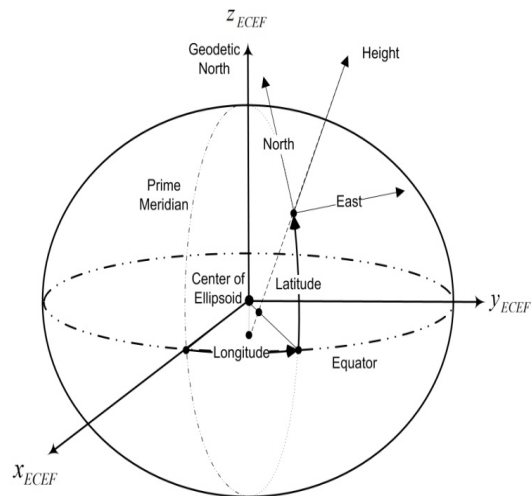
117

After choosing an ellipsoidal model, the frame of reference used was the WGS84 which globally approximates the mean sea level of the earth. In certain areas of the world though, more accurate local frames of reference are available and can easily be substituted.

Registration Equations

A system of three nonlinear equations was developed to calculate the position of a point on the earth given a slant range, either a Doppler or spatial frequency, and an ellipsoidal model of the earth. It is assumed that the earth is smooth (no elevation) and that the radar data is unambiguous in Doppler. Figure H - 2 illustrates the registration geometry.

In Figure H - 2 the point, $P_r(x_r, y_r, z_r)$, represents the position of the radar and the point, $P_e(x,y,z)$, designates the point on the earth to be determined. Also shown is the slant range of the lth range sample, R_l, and the iso-frequency (Doppler or spatial) contour of interest. The intersection of the slant range with the iso-frequency contour and the earth's surface occurs at two points, P_e and a mirror point on the contour. However, since the radar data was gathered by a side looking radar, the location of the point on the same side as the radar is of interest.
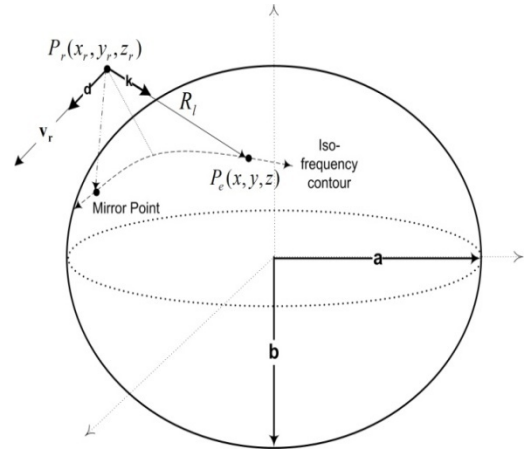
Figure H - 2. Registration Geometry

The first equation is related to the slant range and is simply the squared Euclidian distance between the points, P_e and P_r. The functional form of the equation is given as

$$F_1(x, y, z) = (x - x_r)^2 + (y - y_r)^2 + (z - z_r)^2 - R_l^2 = 0 \tag{H-1}$$

The second equation models the earth's surface as an ellipsoid and is defined as

$$F_2(x, y, z) = \frac{x^2}{a^2} + \frac{y^2}{a^2} + \frac{z^2}{b^2} - 1 = 0 \tag{H-2}$$

where a and b are the semi-major and semi-minor radii of the earth, respectively. Values for these parameters were obtained from the WGS84 world geodetic datum. The last equation represents the iso-frequency contour on the earth. One of the following two equations may be used in conjunction with (1) and (2) to complete the system of equations.

Doppler Frequency Equation

For a given Doppler frequency, f_d, the third registration equation was derived from

$$f_d = \frac{2\left(\mathbf{k}\cdot\mathbf{v_r}\right)}{\lambda}$$
(H-3)

where, after normalizing by R_l, $\mathbf{k}$ is the unit vector pointing from the radar to the earth, $\mathbf{v_r}$ is the radar's velocity vector and λ is the wavelength of the radar. After some manipulation, the third equation is

$$F_3(x,y,z)=(x-x_r)v_{rx}+(y-y_r)v_{ry}+(z-z_r)v_{rz}-\left(\frac{f_d\lambda R_l}{2}\right)=0$$
(H-4)

where v_{rx}, v_{ry}, v_{rz} are the components of the radar's velocity vector.

Spatial Frequency Equation

For a given spatial frequency, υ, assuming a one-dimensional linear array, the third registration equation was derived from

$$\upsilon = \frac{\left(\mathbf{k}\cdot\mathbf{d}\right)}{\lambda}$$
(H-5)

where $\mathbf{d}$ is the interelement spacing vector along the array's horizontal axis. After some manipulation, the third equation is

$$F_3(x,y,z)=\left(x-x_r\right)d_x+\left(y-y_r\right)d_y+(z-z_r)d_z-\left(\upsilon\lambda R_s\right)=0$$
(H-6)

where d_x, d_y, d_z are the components of $\mathbf{d}$.

In order to find solutions for x, y and z, an iterative Newton-Raphson method [H-15] was used until the method converged to a solution. The initial point for the iteration was calculated from a spherical earth model and was chosen to be near the point of interest, P_e. This helped the Newton-Raphson method rapidly converge to a solution for P_e as opposed to its mirror point. A check was performed to ensure that the result for a side looking radar was on the correct side of the platform.

Atmospheric Propagation Model

Typically the 4/3rd earth-radius model [H-16] is used as an approximation to compensate for normal atmospheric refraction. This model, however, is only accurate for altitudes up to 1 or 2 km. Ray-tracing and parabolic equation methods are more accurate but are often computationally intensive. As a result, we turned to propagation models developed for the GPS. In general these models are empirically based, are more accurate than the 4/3rd earth-radius model, and are relatively easy to implement. Also, the MCARM radar's operating frequency is within the range of frequencies (1-2 GHz) supported by the models.

In the GPS literature excess path delay (EPD) refers to the difference in time it takes for an electromagnetic wave (ray) to travel between two points in free-space versus the time it takes the wave to travel between the same two points through the atmosphere. EPD occurs because the velocity of an electromagnetic wave decreases when propagating through the atmosphere, thereby increasing the time it takes for it to travel. EPD also includes the delay that occurs at smaller elevation angles due to atmospheric bending. Even though these two phenomena are referred to as delays, they are often given in measurements of length.

Since the MCARM radar flew at an altitude of 3 km we were only interested in propagation models of the tropospheric layer (from the ground to about 12 km). Therefore, assuming a neutral (nondispersive) atmosphere, the tropospheric EPD is expressed as the sum of two terms: the first represents the delay due to the velocity decrease and the second denotes the delay due to bending. The EPD is given in meters as

$$D_{trop}^{total} = \int \left[n(r) - 1 \right] dr + \delta_b \tag{H-7}$$

where $n(r)$ is the refractive index along the ray path, r, and δ_b denotes the ray path bending term.

Equation (H-7) has been widely studied and is dependent on the index of refraction or its more common representation called refractivity, N, where $N = (n - 1)10^6$. The refractivity is composed of two parts, hydrostatic refractivity and nonhydrostatic refractivity, often referred to as wet refractivity. These components, and thus the refractivity, are dependent on a variety of atmospheric factors such as temperature, dry air pressure, water vapor density, etc.

The current empirical models used for modeling the first term in (H-7) have the general form given by

$$D_{trop} = D_{hyd}^{'} M_{hyd}(\theta) + D_{wet}^{'} M_{wet}(\theta) \tag{H-8}$$

where D'_{hyd} is the hydrostatic zenith delay, M_{hyd} is the hydrostatic mapping function, D'_{wet} is the wet zenith delay, M_{wet} is the wet mapping function, and θ is the elevation angle [H-17]. The zenith delays are the delays incurred by a ray traveling perpendicular to the earth's surface and the mapping functions modify the zenith delays to include elevation angle for rays traveling at a slant to the earth's surface. The most accurate models of the form given by (H-8) were developed by Herring [H-18] and Neill [H-19] and are valid for elevation angles as small as 2-3 degrees. These models have an error of less than 1 meter under normal conditions.

Typically, the amount of tropospheric delay that can be expected is about 25 meters starting from the top of the troposphere at an elevation angle of 5 degrees [H-20]. The delay decreases with decreasing altitude or increasing elevation angle. For our research, the tropospheric delay was ignored because the MCARM radar flew at a low altitude and its range resolution was 120 meters. On the other hand, the delay might become significant for KA STAP algorithms using data having a resolution of 25 meters or less.

Next, in order to evaluate the significance of, δ_b, the second term in (H-7), a numerical analysis was performed. It is known that significant ray path bending can occur especially at higher altitudes and low elevation angles. To estimate the effect of tropospheric bending on registration, we determined the displacement, Δx, between where a straight-line path hits the ground and a bent path starting from the same position hits the ground.

Consider two ray paths of the same length, R, that start from the same point (x_0, h_0), but have different initial elevation angles as shown in Figure H - 3. The path of the first ray was determined without considering bending while bending was considered for the second.
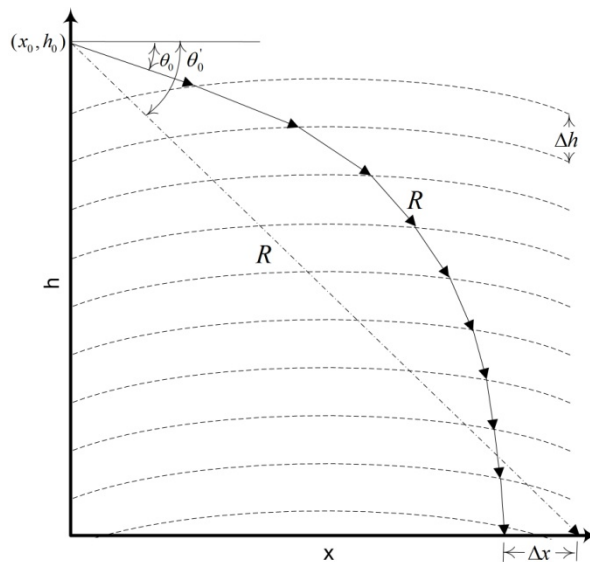

Figure H - 3. Model For Numerical Analysis Of Tropospheric Bending.

To model tropospheric bending it was assumed that the refractive index has an exponential profile as expressed by

$$n(h) = 1 + \alpha e^{-\beta h}$$

(H-9)

where h is height in meters, $\alpha = 315 \times 10^{-6}$ and $\beta = 0.136 \times 10^{-3}$ m^{-1} (α and β are derived from standard atmospheric parameters) [H-21]. Since the refractive index is only dependent upon height, a two-dimensional spherical earth model was employed. Subsequently, the troposphere was modeled by dividing it into sub-layers with each sub-layer having a thickness, Δh, and a constant index of refraction determined by (H-9). Then a ray path with a starting height of h_0 and an initial elevation angle of θ_0 was calculated using Snell's Law in spherical coordinates which is given by

$$n_{i+1} r_{i+1} \sin z_{i+1} = n_i r_i \sin z_i$$

(H-10)

where n_i is the refractive index of the ith sub-layer, r_i is the distance of the ray to the earth's center of mass from the ith sub-layer, and z_i is the zenith angle ($90^\circ - \theta_i$) at which the ray leaves the ith sub-layer.

Figure H - 4 is a plot of the displacement between a straight-line ray path and a bent ray path as a function of the straight-line path's initial elevation angle for an altitude of 12 km (worst case scenario). The results show that the displacement and, therefore, δ_b is negligible. Even for the small elevation angles (long trajectories) the displacement is only a few of centimeters.
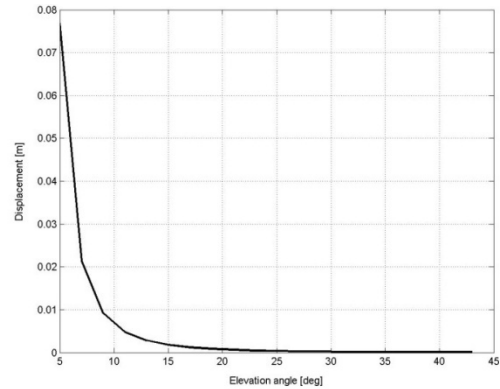

Figure H - 4. Plot Of Displacement Due To Tropospheric Bending (Altitude 12 Km).

EQUIVALENT SECONDARY DATA

Ward's general clutter model [H-22] is employed to determine whether or not available secondary data may be useful in estimating the clutter covariance matrix of a test range sample. Ward approximates a continuous field of clutter by modeling the clutter return from each range sample as the superposition of a large number of independent point scatterers that are evenly distributed in azimuth about the radar. For simplicity, we assume unambiguous range.

As illustrated in Figure H - 5, let a range sample be subdivided into a total of N_c clutter patches such that each patch has an angular extent given by $\Delta\phi = 2\pi/N_c$. The location to the center of the kth clutter patch in the lth range sample is specified by a slant range, R_l, and an azimuthal angle, ϕ_k. The slant range is determined by the elevation angle, θ_l. The airborne radar platform is assumed to be moving along the x-axis with a velocity, $\mathbf{v_r}$.
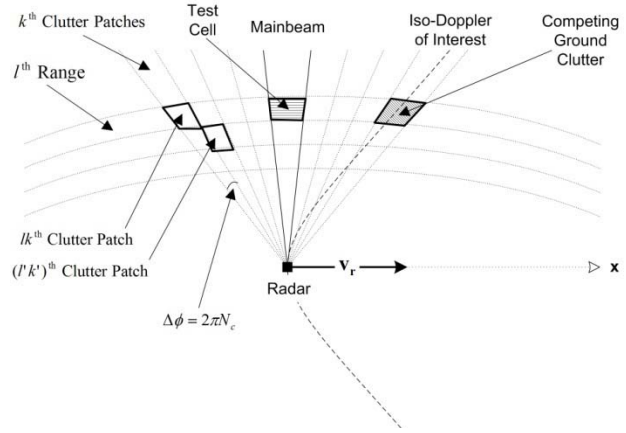
Figure H - 5. Diagram Of Ward's General Clutter Model And The Location Of Competing Ground Clutter For Single-Bin Post-Doppler STAP.

Consider the clutter return from the kth clutter patch in the lth range sample. Treating the patch as a point scatterer, the down-converted and match filtered response in the nth spatial channel due to the mth pulse of the coherent processing interval is given by

$$x_{nmlk} = \alpha_{lk}\, e^{j2\pi(m\,\omega_{lk}\, +\, n\,\upsilon_{lk})}$$

(H-11)

where the normalized Doppler frequency is

$$\omega_{lk} = \frac{2\,v_r}{f_r\,\lambda}\cos\theta_l\,\sin\phi_k$$

(H-12)

the normalized spatial frequency is

$$\upsilon_{lk} = \frac{d}{\lambda}\cos\theta_l\sin\phi_k$$

(H-13)

α_{lk} is the complex amplitude of the lk^{th} clutter patch, f_r is the pulse repetition frequency, λ is the wavelength of the transmitted wave, and d is the horizontal interelement spacing of the radar array.

123

Summing over all of the clutter patches in the lth range sample, the total response in the nth channel due to the mth pulse is

$$x_{nml} = \sum_{k=1}^{N_c} \alpha_{lk} \, e^{j2\pi(m\omega_{lk} + n\upsilon_{lk})} . \qquad \text{(H-14)}$$

Note that the various clutter patches contribute to the total response separately, with different normalized Doppler and spatial frequencies and complex amplitudes determined by the scattering properties of each patch.

The clutter covariance matrix for the lth range sample is expressed as

$$\mathbf{M}_l = \sum_{k=1}^{N_c} \mathrm{E}[\,|\alpha_{lk}|^2\,] \, \mathbf{v}_{lk} \, \mathbf{v}_{lk}^{\text{H}} \qquad \text{(H-15)}$$

where E[•] denotes the expectation operator, H is the conjugate transpose and $\mathbf{v}_{lk}$ is the space-time steering vector expressed by

$$\mathbf{v}_{lk} = \mathbf{b}(\omega_{lk}) \otimes \mathbf{a}(\upsilon_{lk}) \qquad \text{(H-16)}$$

which is the Kronecker matrix product of the temporal steering vector,

$$\mathbf{b}(\omega_{lk}) = \left[1, e^{j2\pi\omega_{lk}}, \ldots, e^{j(M-1)2\pi\omega_{lk}} \right]^{\text{T}} \qquad \text{(H-17)}$$

and the spatial steering vector,

$$\mathbf{a}(\upsilon_{lk}) = \left[1, e^{j2\pi\upsilon_{lk}}, \ldots, e^{j(N-1)2\pi\upsilon_{lk}} \right]^{\text{T}} \qquad \text{(H-19)}$$

Hence, estimation of the clutter covariance matrix reduces to the estimation of $\mathrm{E}[|\alpha_{lk}|^2]$, the mean-squared value of the complex amplitude magnitude for each clutter patch in the range sample, assuming there is no mismatch in the steering vectors.

Next, assume the test sample in which a target is to be detected is located in the lth range sample. Since $\mathbf{M}_l$, the clutter covariance matrix of the lth range sample is unknown, the objective is to select secondary data from other range samples in order to estimate $\mathbf{M}_l$. Suppose attention is focused on the $(l')^{th}$ range sample where $l' \neq l$. The question that arises is, "Is the clutter in the $(l')^{th}$ range sample representative of the clutter in the lth range sample?" This will be the case provided that for each clutter patch in the lth range sample having a specific mean-square complex amplitude magnitude and a specific pair of normalized Doppler and spatial frequencies there is a corresponding clutter patch in the $(l')^{th}$ range sample having approximately the same mean-square complex amplitude and approximately the same normalized Doppler and spatial frequencies.

Consider the $(k')^{th}$ clutter patch in the $(l')^{th}$ range sample. The normalized Doppler and spatial frequencies are $\omega_{l'k'}$ and $\upsilon_{l'k'}$, as given by (H-12) and (H-13). Assume $\omega_{l'k'} = \omega_{lk}$. This implies that $cos\theta_{l'} sin\phi_{k'} = cos\theta_l sin\phi_k$. As a result, $\upsilon_{l'k'} = \upsilon_{lk}$. We see that if two clutter patches, each in a different range sample, have the same normalized Doppler frequency, then they also have the same normalized spatial frequency.

Let the normalized Doppler and spatial frequencies for a clutter patch equal ω_0 and υ_0, respectively. Assuming a flat earth, the constant Doppler frequency contour for ω_0 is a hyperbola given by

$$\left[\left(\frac{2v_r}{f_r \lambda}\right)^2 - \omega_0^2\right] x_c^2 - \omega_0^2 \, y_c^2 = \omega_0^2 \, h^2 \qquad \text{(H-20)}$$

where h is the height of the radar platform and (x_c, y_c) are the coordinates of the clutter point scatterer. Similarly, the constant spatial frequency contour for υ_o is a hyperbola given by

$$\left[\left(\frac{d}{\lambda}\right)^2 - \upsilon_0^2\right] x_c^2 - \upsilon_0^2 \, y_c^2 = \upsilon_0^2 \, h^2 \qquad \text{(H-21)}$$

It can be shown that the hyperbola given by (H-19) is identical to the hyperbola given by (H-20) using the fact that $\omega_o = (2v_r/f_r d)\upsilon_o$.

Even though the pairs of normalized Doppler and spatial frequencies remain invariant from one range sample to another and even if clutter patches are identified such that $\omega_{l'k'} = \omega_{lk}$, it is unlikely in a nonhomogeneous clutter environment that $\text{E}[|\alpha_{l'k'}|^2] = \text{E}[|\alpha_{lk}|^2]$ for all N_c pairs of clutter patches in the two range samples.

STAP Algorithm

The concept of equivalent secondary clutter data is still meaningful though, on a selective basis. For example, consider post-Doppler adaptive beamforming in which non-adaptive Doppler filtering is first performed separately on the *M* pulses from each array element. Because the residual clutter in normalized Doppler and spatial frequencies is confined to a localized region along the clutter ridge, it is no longer necessary that the range sample from which secondary data is being collected be equivalent in its entirety to the range sample in which the test is located. Now the clutter in only a few patches of each range sample need to be equivalent, as illustrated in Figure H - 5, for our approach to be successful in canceling the dominant ground clutter.

Corrections for Deleterious Factors

One of the advantages of the sliding window method of secondary data selection is that the data, including the test sample, are close in range. As a result, they are less susceptible to deleterious factors such as differences in power due to range, clutter reflectivity, and vertical gain and differences in phase due to array misalignment. Since our post-Doppler secondary data selection algorithm may choose data which extend over a larger range, corrections were performed to account for these factors. The following is a description of these corrections which were applied to each CPI in a preprocessing step before Doppler filtering and STAP were done. More specifically, the corrections were applied to each space-time snapshot. A space-time snapshot for a radar with *N* elements and *M* pulses per CPI is an *MN* x 1 vector defined as

$$\chi_l = \left[\mathbf{x}_{0,l}, \mathbf{x}_{1,l}, \ldots, \mathbf{x}_{M-1,l} \right]^{\mathrm{T}}$$

(H-22)

where $\mathbf{x}_{m,l}$ is an *N* x 1 vector of array element outputs of the mth pulse and l^{th} range sample also known as a spatial snapshot.

Other factors including internal clutter motion (ICM), channel mismatch and range walk are discussed in [H-23].

Array Misalignment

One of the assumptions made in the analysis of equivalent secondary data was that the Doppler frequency contours and the spatial frequency contours were aligned. However, in practice, this is usually not true.

In order for the array to be aligned properly the velocity vector of the radar, $\mathbf{v_r}$, should point in the same direction as the horizontal axis of the array, $\mathbf{d}$. This causes the Doppler and spatial frequency contours to overlap. On the other hand, when the two vectors point in different directions, because of crabbing or pitch of the radar platform, the contours do not overlap and cause an increase in the rank of the clutter. Figure H - 6 shows a normalized angle-Doppler plot produced from the MCARM radar data for two range samples.

To correct for misalignment, the ground position of the 0 Hertz spatial frequency contour (mainbeam) for each range sample,
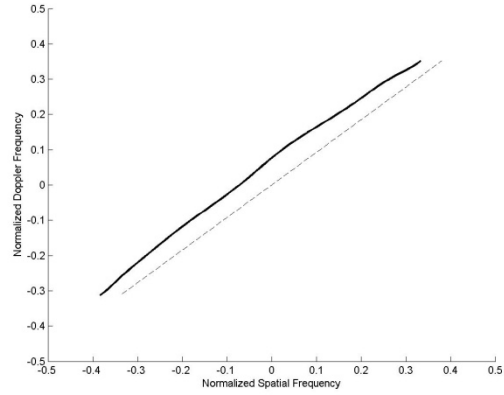

Figure H - 6. Clutter Ridge (Backlobe Not Shown) Plotted From MCARM Flight 5, Acquisition 575 Radar Return Data Before Array Misalignment Correction. The Dashed Line Represents Theoretical Clutter Ridge With No Misalignment.

using (H-1), (H-2), and (H-6), was calculated. Next, a unit vector from the radar's location pointing to each ground position is created. Then, using (H-3), the Doppler frequency of the iso-Doppler contour passing through each ground position was determined (0 Hertz if no misalignment). From [H-24], an M x N correction matrix is formed using a linear phase taper and is defined as

$$
\mathbf{C}_l^{align} = \begin{bmatrix} 1 & e^{j2\pi\Delta\omega_l} & \cdots & e^{j2\pi(M-1)\Delta\omega_l} \\ 1 & e^{j2\pi\Delta\omega_l} & \cdots & e^{j2\pi(M-1)\Delta\omega_l} \\ \vdots & \vdots & \ddots & \vdots \\ 1 & e^{j2\pi\Delta\omega_l} & \cdots & e^{j2\pi(M-1)\Delta\omega_l} \end{bmatrix}
\tag{H-23}
$$

where $\Delta\omega_l$ is the amount of normalized Doppler frequency shift from 0 Hertz calculated for the lth range sample. The correction matrix was reshaped into an MN x 1 vector and applied to each space-time snapshot as defined by

$$
\tilde{\boldsymbol{\chi}}_l = \boldsymbol{\chi}_l \circ \mathbf{C}_l^{align}
\tag{H-24}
$$

where $\circ$ is the Hadamard matrix product. This shifts the Doppler frequency of the radar return data thereby compensating for the misalignment and aligning the two frequency contours (see Figure H - 7).
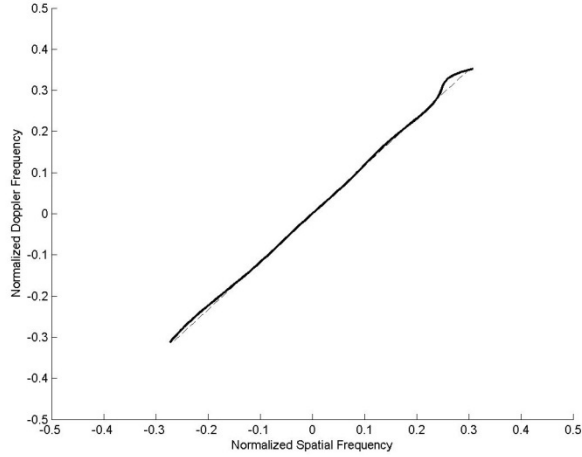
Figure H - 7. Clutter Ridge Plotted From MCARM Flight 5, Acquisition 575 Radar Return Data After Array Misalignment Correction. The Dashed Line Represents Theoretical Clutter Ridge With No Misalignment Which Is Almost Covered By The Corrected Measured Clutter Ridge.

Power and Reflectivity

Consider two of the kth clutter patches, one in the lth range sample and one in the $(l')^{\text{th}}$ range sample, and assume there is no array misalignment. Using Ward's general clutter model [H-22], the mean-squared value of the complex amplitude magnitude of the lk^{th} clutter patch given by $\text{E}[/\alpha_{lk}/^2] = \sigma^2 \xi_{lk}$ where σ^2 represents the thermal noise power per element and ξ_{ik} is the clutter-to-noise ratio (CNR). The CNR is given by

$$\xi_{lk} = \frac{P_t T_p G_t(\phi_k, \theta_l) g(\phi_k, \theta_l) \lambda \, \sigma_{lk}}{(4\pi)^3 N_o L_s R_l^4} \tag{H-25}$$

where

$$\sigma_{lk} = \sigma_o(\phi_k, \theta_l) R_l \Delta\phi \Delta R \sec\psi_l \tag{H-26}$$

$G_t(\phi_k, \theta_l)$ is the transmit gain, $g(\phi_k, \theta_l)$ is the element pattern, N_o is the spectral density of the receiver noise power, L_s accounts for system losses, $\sigma_o(\phi_k, \theta_l)$ is the area reflectivity and ψ_l is the grazing angle.

128

We are interested in formulating a correction, c_{lk}, such that $\xi_{l'k} = c_{lk}\xi_{lk}$. If we presume that

$$\frac{G_t(\phi_k,\theta_{l'})g(\phi_k,\theta_{l'})}{G_t(\phi_k,\theta_l)g(\phi_k,\theta_l)} \approx 1 \qquad \text{(H-27)}$$

it follows that

$$c_{lk} = \frac{\xi_{l'k}}{\xi_{lk}} = \frac{\sigma_o(\phi_k,\theta_{l'})R_l^3 \sec\psi_{l'}}{\sigma_o(\phi_k,\theta_l)R_{l'}^3 \sec\psi_l} \qquad \text{(H-28)}$$

The area reflectivity, σ_o, for the lkth clutter patch was approximated using the constant gamma model [H-25] given by

$$\sigma_o = \gamma \sin\psi_l \qquad \text{(H-29)}$$

where γ is a terrain dependent parameter. It is important to note that (H-28) is invariant with respect to azimuthal angle and, therefore, is the same for all k clutter patches in a range sample. Substituting (H-28) into (H-27) and assuming $\gamma_{l'} = \gamma_l$ (same type of terrain in each cell) produces the following correction for power and reflectivity given by,

$$c_l^{power} = \frac{R_l^3 \tan\psi_{l'}}{R_{l'}^3 \tan\psi_l} \qquad \text{(H-30)}$$

where a range sample from the middle of the range represents the $(l')^{th}$ range sample in (H-29) and was fixed for all other samples. This correction was then applied to each space-time snapshot creating a corrected snapshot defined by

$$\tilde{\chi}_l = \chi_l \sqrt{c_l^{power}} \qquad \text{(H-31)}$$

The square root of the correction was taken since the radar return data was in voltage and not power.

Vertical Gain Correction

In the previous section we assumed that the gain in different range samples was approximately the same (as implied by (H-26)). For horizontal gain this is a good assumption since the iso-Doppler contours lie along azimuthal angles. However, depending on the vertical beamwidth of the radar, the orientation of the array, the roll of the airborne platform, and atmospheric propagation, the vertical gain can vary with range. Consequently, this would impact our approach.

129

To correct for this problem, an estimate of the vertical gain pattern was calculated and the result was used to normalize the return data. Alternatively, we could have used the measured gain patterns that were provided. Though they were measured on the ground under controlled conditions, and may not be representative of the actual gain pattern when airborne.

In order to determine the vertical gain pattern, the return data was non-adaptively filtered in space and time. This was accomplished by first filtering the data in Doppler. Then an estimate of the power returning from each range-Doppler cell was obtained by using

$$P_{ml} = \left| \mathbf{a}(\upsilon_{lk})^{\mathrm{H}} \mathbf{x}_{m,l} \right|^2 \tag{H-32}$$

where υ_{lk} is the spatial frequency in the kth patch of the lth range sample corresponding to the same angle of arrival (AOA) as the iso-Doppler contour of the mth Doppler bin. The powers were then averaged over all M Doppler bins for each range sample as given by

$$\hat{P}_l^{VG} = \frac{1}{M} \sum_{m=0}^{M-1} P_{ml} \tag{H-33}$$

A polynomial fit of the results of (H-32) was made in order to smooth any anomalies. The correction for vertical gain in the lth range sample was then normalized by the maximum average power across all range samples and is defined as

$$c_l^{vgain} = \frac{\hat{P}_l^{VG}}{\max\left\{ \hat{P}_0^{VG}, \hat{P}_1^{VG}, \ldots, \hat{P}_{L-1}^{VG} \right\}} \tag{H-34}$$

It was applied to each space-time snapshot creating a corrected snapshot expressed by

$$\tilde{\chi}_l = \frac{\chi_l}{c_l^{vgain}} \tag{H-35}$$

Figure H - 8 is a plot of the relative estimated vertical gain of a MCARM CPI. It can be seen from Figure H - 8 that the returns from range samples near the radar have significantly less gain then those beyond range sample 300. This occurred even though the array for this acquisition was tilted down from horizontal over 10 degrees due to roll of the platform and array orientation.

RADAR TERRAIN IMAGE

It is important to realize that digital terrain data is time dependent. There are several factors that can modify the terrain environment over time such as: weather, seasonal changes, man-made development, etc. As a result, digital terrain data may not represent the terrain being illuminated by the radar.

In order to gain some insight into how well the terrain data compared with what the radar "saw", a rudimentary image of the terrain was created from the radar return data. If there was a correlation between the digital land classification data and the clutter returns, then it

Figure H - 8. Relative Estimated Vertical Gain Pattern From MCARM Flight 5, Acquisition 575.

should be evident from the image. On the other hand, if the terrain image did not correlate well with the terrain data it would serve as an indicator that other factors, as mentioned above, might have altered the environment such as a weather front.

The terrain image was produced by using the results from (H-31) since they represent the estimated power returned from each range-Doppler cell. Given the relationship between the Doppler of ground clutter and azimuthal angle, it was possible to map the powers. However, because of the narrow beamwidth of the radar, the horizontal gain pattern was estimated and used to normalize the powers similar to the vertical gain correction.

To estimate the horizontal gain, the powers from (H-31) were averaged over all L-1 range samples for each mth Doppler bin as defined by

$$\hat{P}_m^{HG} = \frac{1}{L} \sum_{l=0}^{L-1} P_{ml} \tag{H-36}$$

A polynomial fit of the results of (H-35) was made (see Figure H - 9). Then gain corrections given by

$$c_m^{hgain} = \frac{\hat{P}_m^{HG}}{\max\left\{\hat{P}_0^{HG}, \hat{P}_1^{HG}, \ldots, \hat{P}_{M-1}^{HG}\right\}} \tag{H-37}$$

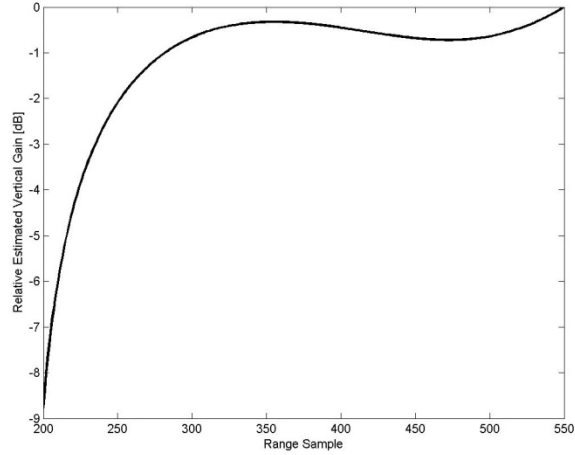and (H-33) were applied to the powers thereby normalizing them as defined by

$$\tilde{P}_{ml} = \frac{P_{ml}}{c_m^{hgain} c_l^{vgain}}$$ (H-38)

The final results from (H-37) were registered using (H-1), (H-2), and (H-4) and geographically plotted.

The resolution of the terrain image using a single CPI is dependent on the DOF of the radar. Yet, a composite image using multiple CPIs can be produced, by normalizing the results of (H-37) for each CPI by the average of all the individual CPI results.

Figure H - 10 and Figure H - 11 shows a comparison of a terrain image generated from multiple MCARM CPIs with the digital land classification map of the same area. It can be seen from these images that large homogeneous terrain features such as bodies of water (blue in color) can clearly be identified. Other features such as urban areas and some possible discretes (red in color) are evident as well.
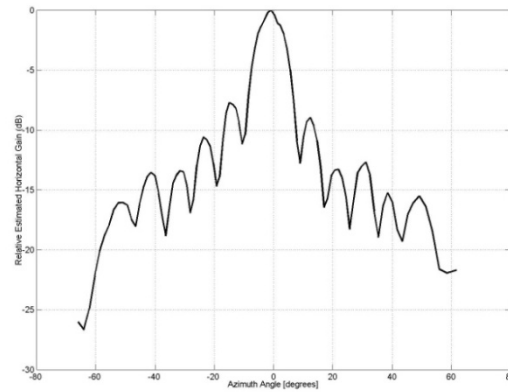

Figure H - 9. Relative Estimated Horizontal Gain Pattern From MCARM Flight 5, Acquisition 575.

Figure H - 10. NLCD Terrain Data Representing Terrain Illuminated By MCARM Flight 5, Acquisition 575.
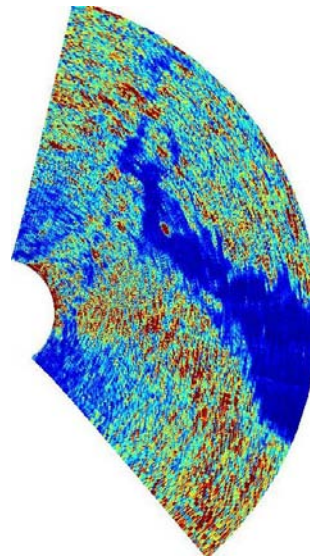

Figure H - 11. Radar Terrain Image Generated Using 3 Cpis From MCARM Flight 5 (Acquisitions 575, 576, And 577).

The terrain image can also aid in evaluating and possibly correcting for errors in registration assuming enough distinguishing features can be identified between the terrain image and the digital terrain data.

Secondary Data Selection Algorithm

The secondary data selection algorithm is dependent upon the environment of the area of interest and the type or types of digital terrain data used to represent the area. Presented are two algorithms: one using digital land classification data and one using digital elevation data.

Algorithm for land classification data

Given a Doppler of interest, the position of four boundary points defining the area of each range-Doppler cell was calculated using (H-1), (H-2), and (H-4) as illustrated in Figure H - 12. Since these boundary points will probably not align with latitude and longitude like the digital land classification cells, a rectangle bounding them was determined that does align. It should be noted that this provides an approximation to a range-Doppler cell's true boundary and was done for simplicity. However, more accurate results can be obtained by subdividing the range-Doppler cells and applying the same procedure on the sub-areas.
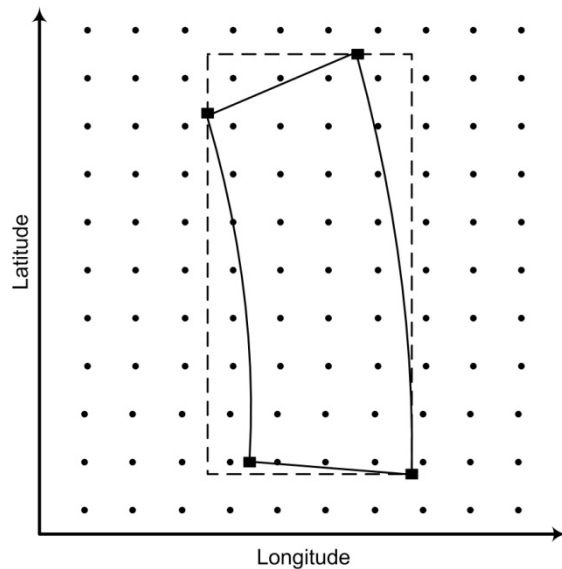

Figure H - 12. Determining Land Classifications Types Contained Within A Range-Doppler Cell For Secondary Data Selection Algorithm. Black Dots Represent Centers Of Land Classification Terrain Cells. Black Squares Represent Boundary Points Of Range-Doppler Cell. Dashed Rectangle Approximates Area Of Range-Doppler Cell.

Once the bounding rectangle for a range-Doppler cell was defined, the database was queried to determine the terrain cell count for each type of land classification contained within the rectangular area. The results were stored in a 21-element vector with each element corresponding to a land classification type (see Table H - 2). The vector was then normalized by dividing it by the total number of terrain cells contained in the range-Doppler cell. This was necessary in order to account for the variation in area of the range-Doppler cells. The normalized vector for the lth range sample is represented by

$$\mathbf{t}_l = \left[t_{l,1}, t_{l,2}, \ldots, t_{l,21} \right]^{\text{T}} \tag{H-39}$$

Once this was performed for all of the range-Doppler cells at the Doppler of interest, the vectors of potential secondary data cells were compared with the vector of the test cell by computing the squared error between their elements. This gave a measurement or grade of how close the $(l')^{th}$ range-Doppler cell matched the test cell and is defined by

$$grade_{l'} = \sum_{i=1}^{21} \left(t_{l,i} - t_{l',i} \right)^2 \qquad \text{(H-40)}$$

where $t_{l,i}$ is the ith element of the test cell terrain vector and $t_{l',i}$ is the ith element of the of the potential secondary data terrain vector. Cells with lower grades matched the test cell more closely. The grades were then sorted and the top cells were chosen as secondary data.

Although we chose a squared error minimal distance estimator for grading, others may be used. Also, our algorithm equally weights each of the land classification types. In practice, certain types of land classifications produce stronger clutter than others. Therefore, a weight vector, perhaps derived from terrain radar cross-section (RCS) measurements, could be applied to the terrain vectors before grading. This would create an adjusted terrain vector defined as

$$\tilde{\mathbf{t}}_l = \mathbf{t}_l \circ \mathbf{w}_t \qquad \text{(H-41)}$$

where

$$\mathbf{w}_t = \left[w_1, w_2, \ldots, w_{21} \right]^{\text{T}} \qquad \text{(H-42)}$$
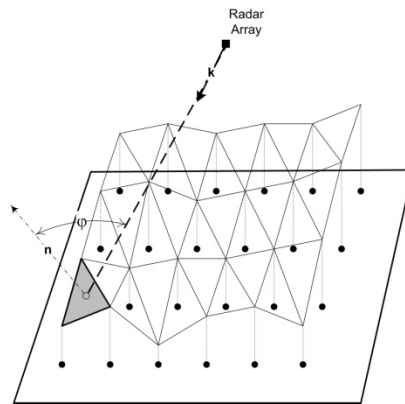

Figure H - 13. Surface model of range-Doppler cell generated from digital elevation data. The backscattering angle, φ, is the angle between a patch normal, *n*, and the unit vector, *k*, pointing to the patch from the radar. The black dots represent cell grid-points registered on a smooth earth.

134

Algorithm for Elevation Data

Assuming a smooth earth, a grid with a resolution matching that of the digital elevation data was created for each range-Doppler cell. These cell grid-points were then registered to the earth using (H-1), (H-2), and (H-4). In order to determine the elevation at each grid-point in the cell, a nearest neighbor interpolation was performed with the elevation terrain grid corresponding to each cell. Because of the inclusion of elevation data, the slant ranges to each cell's grid-points were recomputed and the cells were sorted into their proper range bins by the average slant range of their grid-points. Next, a mesh of triangular patches for each cell was created using Delaunay triangulation [H-26]. This produced an approximate three-dimensional surface which modeled the actual terrain.

In order to make comparisons between cells based upon their surface models, the backscattering angle of each patch contained within a cell was determined (see Figure H - 13 above). A 3-element terrain vector for each cell was developed which included the average backscattering angle of its patches, the standard deviation of the backscattering angles, and the percent of shadowed (obscured from radar due to terrain) patches. The potential secondary data terrain vectors were then compared to the test cell vector using a squared error measure as was done in (H-39), and the top cells were chosen as secondary data.

Figure H - 14 and Figure H - 15 are examples of how the KA elevation algorithm chose secondary data in a mountainous region.
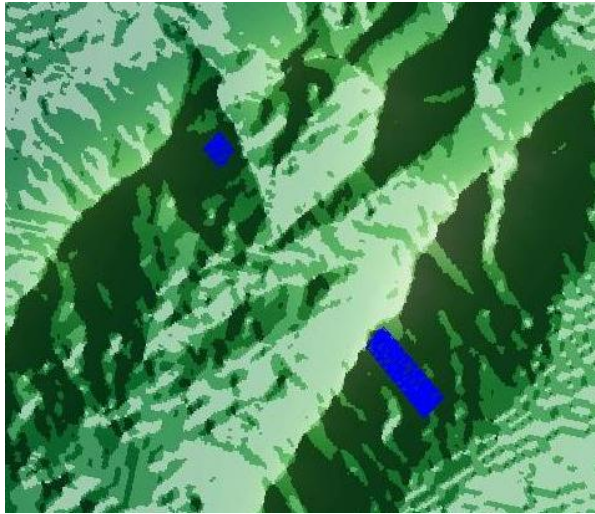

Figure H - 14. Example Of KA Secondary Data Selection Algorithm Using Elevation Data To Identify Shadowed Cells (Blue) In A Mountainous Terrain. The Radar Is Located North-West Of This Area With Its Mainbeam Pointing South-East.

Figure H - 15. Example Of KA Secondary Data Selection Algorithm Using Elevation Data To Chose Secondary Data (Yellow) That Matches The Test Cell (Red) In A Mountainous Terrain. The Radar Is Located North-West Of This Area With Its Mainbeam Pointing South-East.

Improving Sample Support

One of the practical limitations of STAP is the amount of sample support required for proper estimation of the covariance matrix as analyzed in [H-1]. Although the amount of potential samples to choose from is fixed by the radar's operating parameters, there is a way to improve the sample quality using terrain data and some of the corrections previously described.

As mentioned previously, post-Doppler STAP confines the residual clutter in normalized Doppler and spatial frequencies along the clutter ridge. Instead of choosing secondary data along the Doppler of interest, which limits our KA selection algorithms to a small region of terrain, the search space can be expanded to include all range-Doppler cells. Therefore, secondary data with a higher quality match to the test cell should result (see Figure H - 16).
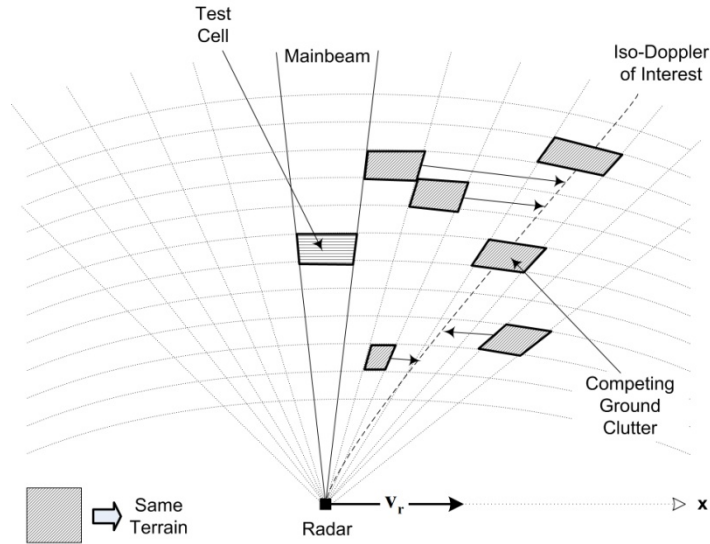

Figure H - 16. Improving Sample Support By Shifting Range-Doppler Cells To The Iso-Doppler Of Interest Which Have Similar Terrain As That Of The Competing Ground Clutter Patch.

Once the best matches are determined an M x N correction matrix for a range-Doppler cell in the mth Doppler bin and the lth range is expressed by

$$\mathbf{C}_{ml}^{shift} = \frac{1}{c_m^{hgain} c_l^{vgain}} \begin{bmatrix} 1 & \cdots & e^{j2\pi((N-1)\Delta\upsilon)} \\ \vdots & \ddots & \vdots \\ e^{j2\pi((M-1)\Delta\omega)} & \cdots & e^{j2\pi((M-1)\Delta\omega+(N-1)\Delta\upsilon)} \end{bmatrix} \tag{H-43}$$

where $\Delta\omega$ is the difference in normalized Doppler frequency between the secondary data cell and the Doppler of interest and $\Delta\upsilon$ is the difference in normalized spatial frequency between the secondary data cell and the spatial frequency of interest. The correction matrix can then be applied to the space-time snapshots for each secondary data cell and post-Doppler STAP may be subsequently performed.

Secondary Data Guard Cells

As part of our approach, issues concerning range-Doppler spread were addressed. During the analysis of the MCARM data containing the MTS simulated targets, we noticed that a certain amount of range-Doppler spread occurred. This may have been caused by numerous factors. As a result, cells experienced signal contamination from neighboring cells. This violates the requirement that secondary data be iid when used in estimating the clutter covariance matrix. In order to mitigate this effect, guard cells were placed around the range-Doppler cells selected for secondary data. Including these secondary data guard cells (SDGC) is analogous to the standard practice of placing guard cells around the test cell. The number of SDGC used was chosen by the amount of spread measured.

RESULTS WITH MEASURED DATA

The results presented compare the sliding window method of secondary data selection to our KA method. For both methods, the corrections in Section 3.4 were applied to the radar return data before STAP was performed. Only the KA algorithm utilizing digital land classification data was employed since the Delmarva area that the MCARM radar illuminated was flat (less than 90 meters between maximum and minimum elevations). It should be noted that in areas of homogeneous terrain, the KA method selected the same samples as the sliding window method. All secondary data was chosen from the same Doppler of interest as the competing ground clutter. Finally, a single-bin post-Doppler STAP algorithm was used with a 65-dB Chebyshev temporal taper.

A CPI from flight 5, acquisition 151, of the MCARM program, was processed which contained simulated target signals from the MTS. A modified sample matrix inversion (MSMI) test statistic [H-27] was plotted versus range bin for each of the results obtained. The ratio of the MTS signal's MSMI value to the range averaged MSMI value is our preferred performance measure (PPM) in this paper.
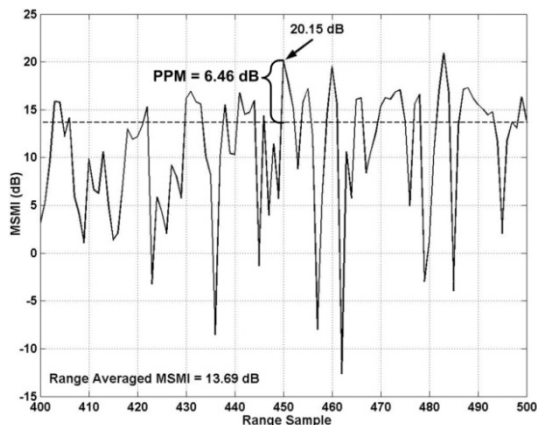

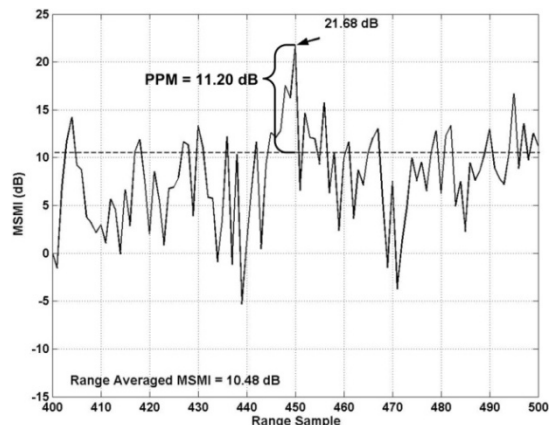**Figure H - 17. Sliding Window Method Using Full Array.**

Figure H - 18. Knowledge-Aided Approach Using Full Array.

137

In Figure H - 17 and Figure H - 18, all 22 channels of the MCARM array were used for STAP. A total of 44 secondary data samples were chosen for the estimation of the covariance matrix. Guard cells were placed around the cell under test. However, no secondary data guard cells were included. The simulated target is located at range bin 450 (see arrow) and its MSMI value and PPM are given in each figure. The range averaged MSMI value is also given and represented by a dashed line.

The PPM of our KA approach, as illustrated in Figure H - 17 and Figure H - 18, was approximately 4.7 dB better than the sliding window method. Notice that the KA approach not only raised the MSMI value of the target but it also lowered the range averaged MSMI statistic.

As mentioned above, there was some range-Doppler spread in the radar data. Figure H - 19 and Figure H - 20 show the results obtained when guard cells were placed around the secondary data as well as the cell under test. It can be seen that the range averaged MSMI value was significantly lowered, in both cases, by 6-8 dB. Furthermore, the PPM of the MTS target, using the sliding window method and SDGC, was almost 3 dB better. However, the KA approach did not do as well with SDGC. This may be caused by the reduction in sample support due to the inclusion of guard cells. The grading algorithm of the KA approach represented by (H-41) may need to be examined more closely when there is a small pool of potential secondary data.
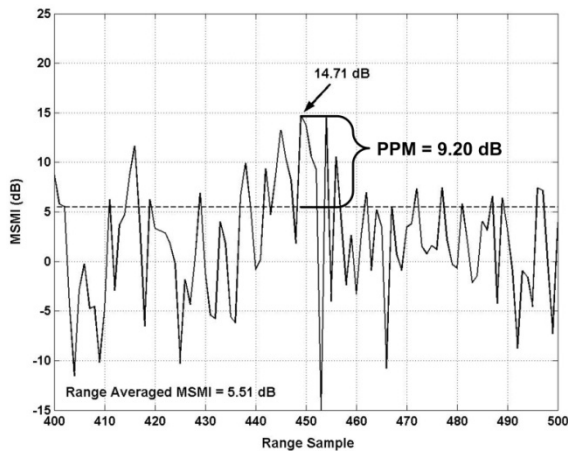

Figure H - 19. Sliding Window Method Using Full Array And Secondary Data Guard Cells.
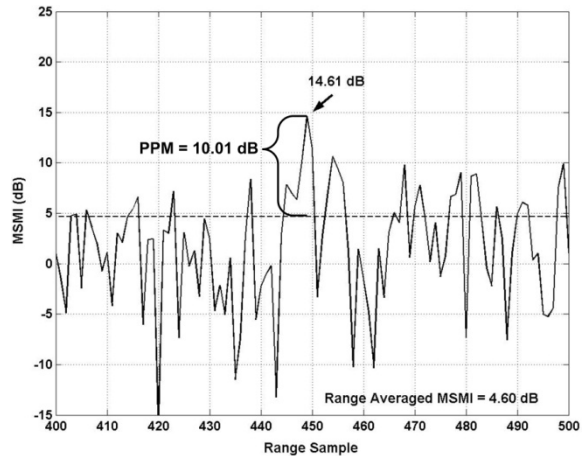
Figure H - 20. Knowledge-Aided Approach Using Full Array And Secondary Data Guard Cells.

In Figure H - 21 and Figure H - 22, the returns from only the top row of the MCARM array, consisting of 11 of the 22 available channels, were used for STAP to compensate for the reduction in available secondary data because of SDGC. Although this reduces the number of degrees of freedom for the adaptive filter, it also reduces the amount of sample support needed from 44 samples to 22. The results show an increase in performance, for both cases, and the KA approach performed best.

138
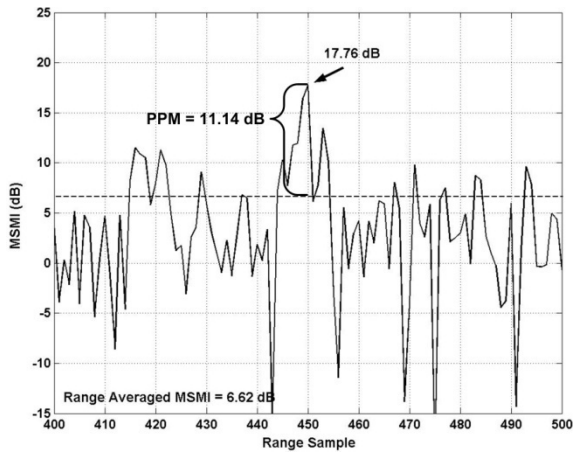
Figure H - 21. Sliding Window Method Using Top Half Of The Array And Secondary Data Guard Cells.
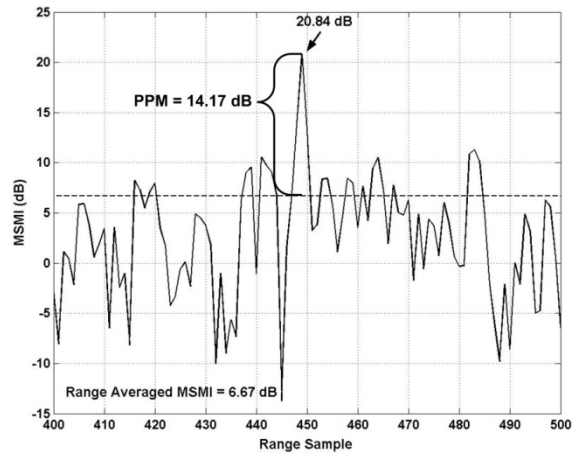
Figure H - 22. Knowledge-Aided Approach Using Top Half Of The Array And Secondary Data Guard Cells.

However, the most notable results can be seen when comparing Figure H - 17, the sliding window method using the full array and no SDGC, with Figure H - 22, the KA method using half of the array with SDGC. The range averaged MSMI value was lowered by 7 dB while the MTS MSMI value increased slightly, resulting in almost an 8 dB increase in the PPM. Similar results were obtained for other CPIs.

CONCLUSION

In this paper we present solutions to some of the practical problems that arise when trying to incorporate *a priori* digital terrain data into STAP. The issues addressed include spatially registering the radar data with the terrain data, correcting for factors that affect the performance of STAP, choosing secondary data based on land classification and elevation terrain data, generating a terrain image from the radar returns to evaluate the environment, improving the quality of sample support with the aid of terrain data, and mitigating the effects of range spread.

We compared our KA approach to the standard sliding window method of secondary data selection. It is important to note that the sliding window method has an inherent advantage over most selection algorithms because it chooses secondary data near in range to the sample under test. As a result, it does not suffer as much from factors such as differences in power due to range, clutter reflectivity, and vertical gain and differences in phase due to array misalignment, all of which vary as a function of range. Therefore, the corrections we presented will aid any secondary selection algorithm which may chose samples that are not close in range.

The results illustrate the benefits of using terrain information, a priori data about the radar, and the importance of statistical independence when selecting secondary data for improving STAP performance. We have demonstrated that almost an 8 dB improvement can be gained.

Further study is needed to determine how well terrain classification data correlates with airborne radar clutter statistics. In addition, research on fusing a radar terrain image with digital terrain data should be pursued, thereby producing a more accurate model of the terrain environment. The fused imaged will help, for example, to account for time varying effects such as weather. Other types of terrain data and knowledge sources should be studied as well in order to explore their potential as an aid for STAP and to determine how to integrate multiple knowledge sources. This will aid in excising additional types of clutter including discretes, moving vehicles, and known targets that affect STAP performance [H-29]. Further study is also required to establish if secondary sample support can be improved by using our approach described in Section H-5.2. This would be a preferable solution to the problem of limited sample support as oppose to reducing the DOF of the adaptive filter.

Future work will also include integrating this novel approach into the AFRL Signal Processing Evaluation, Analysis and Research (SPEAR) Testbed, configuring and evaluating it with several STAP algorithms and measured GMTI radar datasets. The SPEAR Testbed provides a means of assessing performance against a variety of signal processing metrics to aid in the comparison of multiple competing adaptive signal processing approaches.

An ultimate goal is to incorporate knowledge sources in the filter, detection, and tracking stages with the ability to share information between them [H-30]-[H-31].

ADDENDUM TO APPENDIX H.

CONVERSION BETWEEN STANDARD GEODETIC COORDINATES AND ECEF COORDINATES

This addendum presents the equations necessary to convert between standard geodetic coordinates (latitude, longitude, and height) and ECEF Cartesian coordinates (x, y, and z). Figure H - 1 is a diagram representing both coordinate systems.

To convert from geodetic coordinates to ECEF coordinates the following system of equations can be used and is given by

$$x = (v + h)\cos(lat)\cos(lon)$$

$$y = (v + h)\cos(lat)\sin(lon) \tag{H-44}$$

$$z = [(1 - e^2)v + h]\sin(lat)$$

where

$$v = \frac{a}{\sqrt{1 - e^2 \sin^2(lat)}} \tag{H-45}$$

a is the semi-major axis of the reference ellipsoid, h denotes height, lat is the latitude, lon is the longitude, e is the eccentricity defined as $e^2 = 2f - f^2$ with f being the inverse flattening of the ellipsoid.

To convert from ECEF coordinates to geodetic coordinates an iterative method from [H-28] was used. The conversion is giving by

$$lat = \tan^{-1}\left(\frac{z(1 - f) + e^2 a \sin^3(u)}{(1 - f)(p - e^2 a \cos^3(u))}\right)$$

$$lon = \tan^{-1}\left(\frac{y}{x}\right) \tag{H-46}$$

$$h = p\cos(lat) + z\sin(lat) - a\sqrt{1 - e^2 \sin^2(lat)}$$

where

$$p = \sqrt{x^2 + y^2} \qquad \text{(H-47)}$$

$$u = \tan^{-1}\left(\frac{z}{p}\left((1-f) + \frac{e^2 a}{r}\right)\right) \qquad \text{(H-48)}$$

and

$$r = \sqrt{p^2 + z^2} \qquad \text{(H-49)}$$

This method converges to an accurate result very quickly (usually within 2 iterations).

REFERENCES

[H-1]   S. Reed, J. D. Mallet, and L. E. Brennan, "Rapid Convergence Rate in Adaptive Arrays," *IEEE Transactions on Aerospace and Electronic Systems*, Vol. 10, No. 6, pp. 853-863, November, 1974.

[H-2]   W. Melvin and M. Wicks, "Improving Practical Space-Time Adaptive Radar," *Proceedings of the 1997 IEEE National Radar Conference*, pp. 48-53, Syracuse, NY, May 1997.

[H-3]   M. Rangaswamy, B. Himed, and J. Michels, "Performance Analysis of the Nonhomogeneity Detector for STAP Applications," *Proceedings of the 2001 Radar Conference*, pp. 193-197, Atlanta, GA, May 2001.

[H-4]   M. Rangaswamy, J. Michels, and B. Himed, "Statistical Analysis of the Nonhomogeneity Detector for Non-Gaussian Interference Backgrounds," *Proceedings of the 2002 IEEE Radar Conference,* pp. 304-310, Long Beach, CA, April 2002.

[H-5]   W. Melvin, "Space-Time Adaptive Radar Performance in Heterogeneous Clutter," *IEEE Transactions on Aerospace and Electronic Systems*, Vol. 36, No. 2, pp. 621-633, April, 2000.

[H-6]   J. R. Guerci, "Knowledge-Aided Sensor Signal Processing and Expert Reasoning," *Proceedings of the 2002 Workshop on Knowledge-Aided Sensor Signal Processing and Expert Reasoning (KASSPER)*, Washington, D.C., April 2002 (CD-ROM).

[H-7]   W. Baldygo, M. Wicks, R. Brown, P. Antonik, G. Capraro, and L. Hennington, "Artificial Intelligence Applications to Constant False Alarm Rate (CFAR) Processing," *Proceedings of the 1993 IEEE National Radar Conference*, Boston, MA, April 1993.

[H-8]   P. Antonik, H. Shuman, P. Li, W. Melvin, and M. Wicks, "Knowledge-Based Space-Time Adaptive Processing," *Proceedings of the 1997 IEEE National Radar Conference*, pp. 372-377, Syracuse, NY, May 1997.

[H-9]   D. Weiner, G. Capraro, C. Capraro, M. Wicks, "An Approach for Utilizing Known Terrain and Land Feature Data in Estimation of the Clutter Covariance Matrix," *Proceedings of the 1998 IEEE National Radar Conference*, pp. 381-386, Dallas, TX, May 1998.

[H-10] C. Capraro, G. Capraro, D. Weiner, M. Wicks, "Knowledge Based Map Space Time Adaptive Processing (KBMapSTAP), " *Proceedings of the International Conference on Imaging Science, Systems, and Technology*, Vol. 2, pp. 533-538, Las Vegas, NV, June 2001.

[H-11] C. Capraro, G. Capraro, D. Weiner, M. Wicks, W. Baldygo, "Improved STAP Performance using Knowledge-Aided Secondary Data Selection," *Proceedings of the 2004 IEEE Radar Conference,* pp. 361-365, Philadelphia, PA, April, 2004.

[H-12] Westinghouse Electronic Systems, "Multi-Channel Airborne Radar Measurement (MCARM) Flight Test," Contract F20602-92-C-0161, for Rome Laboratory/USAF, vol. 1, September 1995.

[H-13] National Land Cover Data (NLCD), http://landcover.usgs.gov/.

[H-14] National Elevation Data (NED), http:// seamless.usgs.gov/.

[H-15] W. H. Press, S. A. Teukolsky, W. T. Vetterling, and B. P. Flannery, *Numerical Recipes in C: The Art of Scientific Computing*, 2nd Ed., New York, NY: Cambridge University Press, 1992.

[H-16] M. I. Skolnik, *Introduction to Radar Systems,* 3rd Ed., New York, NY: McGraw-Hill, 2001.

[H-17] J. P. Collins, R. B. Langley, "Mitigating Tropospheric Propagation Delay Errors in Precise Airborne GPS Navigation," *IEEE Position Location and Navigation Symposium*, pp. 582-588, April 1996.

[H-18] T. A. Herring, "Modeling Atmospheric Delays in the Analysis of Space Geodetic Data," *Proceedings of Refraction of Transatmospheric Signals in Geodesy*, Netherlands Geodetic Commission Series, Vol. 36, The Hague, Netherlands, pp. 157-164, 1992.

[H-19] E. Neill, "Global Mapping Functions for the Atmosphere Delay of Radio Wavelengths," *J. Geophys. Res.*, Vol. 101, pp. 3227-3246, 1996.

[H-20] E. E. Altshuler, "Tropospheric Range-Error Corrections for the Global Positioning System," *IEEE Transactions on Antenna and Propagation*, Vol. 46, No. 5, pp. 643-649, May 1998

[H-21] ITU-R Recommendation P. 853-3, "Reference Standard Atmospheres," October, 1999.

[H-22] J. Ward, "Space-time adaptive Processing for Airborne Radar," *Technical Report 1015 – Lincoln Laboratory*, Massachusetts Institute of Technology, Lexington, MA, December 1994.

[H-23] J. R. Guerci, *Space-Time Adaptive Processing for Radar*, Norwood, MA: Artech House, 2003.

[H-24] G. K. Borsari, "Mitigating Effects on STAP Processing Caused By An Inclined Array, " *Proceedings of the IEEE 1998 National Radar Conference*, pp. 135-140, Dallas, TX, May 1998.

[H-25] F. E. Nathanson, *Radar Design Principles,* 2nd Ed., McGraw-Hill, Inc., 1991.

[H-26] D. T. Lee, B. J. Schachter, "Two Algorithms for Constructing a Delaunay Triangulation," *Int. J. Computer Information Sci.*, Vol. 9, pp. 219-242, 1980.

[H-27] W. S. Chen and I. S. Reed, "A New CFAR Detection Test for Radar," *Digital Signal Processing*, Vol. 1, pp. 198-214, 1991.

[H-28] R. Bowring, "The Accuracy of Geodetic Latitude and Height Equations," *Survey Review*, pp. 202-206, October, 1985.

[H-29] W. L. Melvin, J. R. Guerci, "Adaptive Detection in Dense target Environments," *Proceedings of the 2001 Radar Conference*, pp. 187-192, Atlanta, GA, May 2001.

[H-30] G. Capraro and M. Wicks, "An Airborne Intelligent Radar System", *Radar 2004, International Conference on Radar Systems*, Toulouse France, 2004.

[H-31] Farina, H. Griffiths, G. Capraro, and M. Wicks, "Knowledge-Based Radar Signal and Data Processing", *NATO RTO Lecture Series 233*, November 2003.

APPENDIX I

WAVEFORM DIVERSITY FOR DIFFERENT MULTISTATIC RADAR CONFIGURATIONS

By: I. Bradaric, G.T. Capraro, Capraro Technologies, Inc.; M. Wicks, AFRL Sensors Directorate

INTRODUCTION

Sensors as Robots is a US Air Force (USAF) project that is performing research in applying knowledge based techniques to radar signal processing. A sensor system's performance can be enhanced by changing a sensor's algorithms as the environment changes. It has been shown that if an airborne radar system is aware of certain features of the earth (e.g. land/sea interfaces) and its surroundings, then it can intelligently improve performance. We need to leverage this approach beyond a single sensor onboard a single platform to multiple sensors on multiple platforms performing distributed sensing.

The monolithic military adversary of the twentieth century is no longer the number one threat. Single function radar systems are necessary but not sufficient for combating terrorism. The desire to AF2T2EA4 by the USAF will require changes to how we modify, build, and deploy radar systems. Coherent signal level fusion of homogeneous sensors and data fusion of heterogeneous sensors are being studied and implemented in order to obtain sensor coverage consistent with AF2T2EA4. However, we must also integrate these radar systems with heterogeneous sensors (e.g. acoustic, IR, EO) located on the ground, in the air, in space, or even underground. The radar systems of the future must be intelligent and integrated within sophisticated systems of heterogeneous sensors that operate on many hypotheses at the same time. Within this paper we make a case that there are obtainable benefits of pre-detection fusion of multiple radar receivers. Our approach is based upon the development and use of a multistatic ambiguity function.

The ambiguity function is a widely used tool for the analysis of radar systems. In the case of monostatic radar systems, the ambiguity function was shown to play an important role in quantifying system performance measures such as probability of detection, probability of false alarm, estimation accuracy, resolution, clutter cancellation, etc. In recent years there have been considerable efforts to formulate the ambiguity function for bistatic and multistatic radar systems [I-1]-[I-6]. In [I-1] the authors developed the ambiguity function for bistatic radar systems. This work was extended in [I-2] to the case of multistatic radar systems. In [I-3]-[I-5] the multistatic ambiguity function was used for assessing waveform selection and coherent signal processing strategies. It was demonstrated through examples that multistatic radar system performances can be improved by shaping the multistatic ambiguity function through waveform selection and adequate weighting of different receivers during pre-detection fusion.

In this work we follow the approach presented in [I-3]-[I-5]. In [I-3] the shaping of the multistatic ambiguity function was achieved by solely relying on the waveform selection process. In [I-4] the shaping was accomplished by optimizing the weighting coefficients associated with different receivers, while in [I-5] these two approaches were combined. This time we add the third way of shaping the ambiguity function that might be at our disposal – the adequate repositioning of the sensors. In all works mentioned above the multistatic system configuration was assumed to be fixed. However, in some applications it might be possible to move the transmitter (and/or receivers) to achieve better performance. It is our goal in this paper to provide some preliminary simulation results that combine

Figure I - 1. Multistatic System Geometry

waveform selection, receiver weighting and sensor placement strategies. These results will hopefully be a good starting point and serve as a guideline for future multistatic fusion rule development.
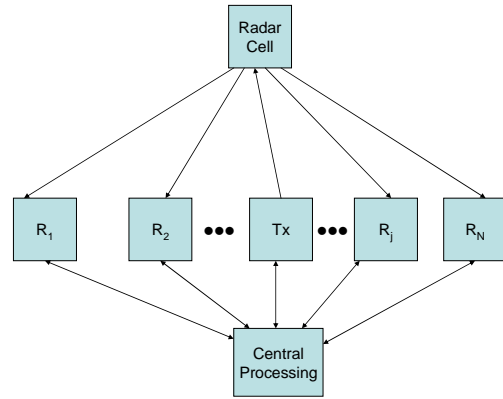
MATHEMATICAL BACKGROUND

In this section we will briefly outline the basic system assumptions and concept behind the multistatic ambiguity function. A more in depth mathematical framework can be found in [I-1]-[I-4]. We consider a single transmitter multiple receiver radar system as shown in **Figure I - 1**. The problem formulation for the case of multiple transmitters is in essence very similar but requires additional signal processing at each receiver to form a matched filter. The corresponding analysis can be found in [I-6].

We assume that a coherent processing interval consists of a single pulse $s(t)$ given as:

$$s(t) = \sqrt{2E}\,\mathrm{Re}\left\{\tilde{f}(t)e^{j\omega_c t}\right\},\ 0 \leq t \leq T_d \tag{I-1}$$

where $\mathrm{Re}\{\cdot\}$ denotes the real part operator, $\tilde{f}(t)$ is the complex envelope of the transmitted pulse, E and T_d are the energy and duration of the pulse, respectively , and $\omega_c = 2\pi f_c$ is the carrier frequency.

Let the complex envelope of the ith receiver input $(i = 1, 2, ..., N)$ be denoted by $\tilde{r}_i(t)$. According to whether a target is absent (H_o) or present (H_1), the two hypotheses are presented by:

$$H_0 : \tilde{r}_i(t) = \tilde{n}_i(t)$$
$$H_1 : \tilde{r}_i(t) = \tilde{a}_i \tilde{s}(t - \tau_{ai}) e^{j\omega_{Dai}t} + \tilde{n}_i(t) \tag{I-2}$$

where $\tilde{a}_i$ is a complex gain which accounts for propagation and scattering effects along the ith path between the transmitter, target and i^{th} receiver. τ_{ai} and ω_{Dai} denote the actual total delay and Doppler shift experienced by the transmitted signal along the ith path, and $\tilde{n}_i(t)$ denotes the complex envelope of the additive noise present at the ith receiver input.

Assuming additionally that the envelopes $\tilde{n}_i(t)$ are complex Gaussian random processes with zero-mean and white in quadrature components with power spectral densities $N_{0i}/2$, the signal at the output of the matched filter of the ith receiver becomes:

$$d_i = \left| \int_{-\infty}^{\infty} \frac{\tilde{r}_i(t)}{\sqrt{N_{0i}}} \tilde{f}^*(t - \tau_{Hi}) e^{-j\omega_{DHi}t} dt \right| \tag{I-3}$$

where $\tilde{f}^*(t)$ denotes complex conjugate of $\tilde{f}(t)$, and τ_{Hi} and ω_{DHi} denote the hypothetical total delay and Doppler shift experienced by the transmitted signal assuming a target present in the radar cell under test.

Signals d_i, $i = 1, 2, ... N$, represent local statistics obtained at each receiver. The ambiguity function for the ith receiver becomes [I-2]:

$$d_i = \left| \int_{-\infty}^{\infty} \frac{\tilde{r}_i(t)}{\sqrt{N_{0i}}} \tilde{f}^*(t - \tau_{Hi}) e^{-j\omega_{DHi}t} dt \right| \tag{I-4}$$

The global ambiguity function is then given as a weighted sum of the bistatic ambiguity functions:

$$\Theta\left(\underline{\tau}_H, \underline{\tau}_a, \underline{\omega}_{DH}, \underline{\omega}_{Da}\right) = \sum_{i=1}^{N} c_i \Theta_i \left(\tau_{Hi}, \tau_{ai}, \omega_{DHi}, \omega_{Dai}\right) \tag{I-5}$$

where

$$\underline{\tau}_H = \left[\tau_{H1}\tau_{H2}\ldots\tau_{HN}\right]^T$$
$$\underline{\tau}_a = \left[\tau_{a1}\tau_{a2}\ldots\tau_{aN}\right]^T$$
$$\underline{\omega}_{DH} = \left[\omega_{DH1}\omega_{DH2}\ldots\omega_{DHN}\right]^T \qquad \text{(I-6)}$$
$$\underline{\omega}_{Da} = \left[\omega_{Da1}\omega_{Da2}\ldots\omega_{DaN}\right]^T$$

and c_i, $i = 1,\ldots,N$ are the weighting coefficients that satisfy the relationship $\sum_{i=1}^{N} c_i = 1$.

The ambiguity function $\Theta\left(\underline{\tau}_H,\underline{\tau}_a,\underline{\omega}_{DH},\underline{\omega}_{Da}\right)$ for a given target (fixed $\underline{\tau}_a$ and $\underline{\omega}_{Da}$) is a $2N$-dimensional function. Since we are ultimately interested in target position (defined by its coordinates, e.g. x, y and z) and its velocity vector (defined by its components, e.g. $\dot{x}$, $\dot{y}$ and $\dot{z}$) it is more practical to express the ambiguity function as a function of these quantities. The highly nonlinear nature of mapping between the delays and Doppler shifts on one hand, and target coordinates and its velocity vector components on the other, makes the analysis of multistatic radar systems especially challenging and the system geometry very important. It should be pointed out that this nonlinearity does not exist in monostatic radar systems.

Thus, to simplify the analysis, but more importantly, to account for the system geometry when formulating the multistatic ambiguity function, we align all receivers with respect to the target position and velocity. In addition, in order to visualize the problem we usually select two fixed dimensions to present the multistatic ambiguity function. For example, in [I-3]-[I-5] the range between the transmitter and the target cell and true target velocity direction were used. More generally, we can define the multistatic ambiguity function as a function of any subset of coordinates needed to fully define target position and velocity in a 6-dimensional parameter space.

In this paper we will consider 2-D system geometries and concentrate on target position only. Thus, the multistatic ambiguity function will be presented as a function of x and y coordinates only.

148

The flexibility to arbitrarily select weighting coefficients gives us one way of shaping the multistatic ambiguity function. The second way of shaping the ambiguity function is by changing the waveform. Finally, the multistatic ambiguity function can also be shaped by changing the system geometry. In the next Section we will combine these three methods to improve desired system performance.

SIMULATION RESULTS AND ANALYSIS

We will illustrate the significance of adequate sensor placement, waveform selection and receiver weighting strategies with several examples. Let us first consider a 2-D multistatic system configuration with 4 receivers and one transmitter as shown in **Figure I - 2**.

Without the loss of generality, the target is placed at the origin (labeled *Tgt*), four receivers are shown as R_i, $i = 1, 2, 3, 4$ and the transmitter is shown as *T*. The distance between the target and all the sensors (transmitter and receivers) is assumed to be 10 km. We will assume that we are interrogating a relatively small area (100 m x 100

Figure I - 2. Multistatic System Geometry

m) as compared to distances between the sensors and that range resolution is our primary concern. In this example the transmitted waveform is a single pulse Barker 13 waveform with the pulse width of 44ns. We will also assume that all receivers are weighted equally (a reasonable assumption since all distances are the same).

The multistatic ambiguity function (presented in x-y plane) is shown in **Figure I - 3**, while the corresponding 3-dB main lobe contour plot is shown in **Figure I - 4**.
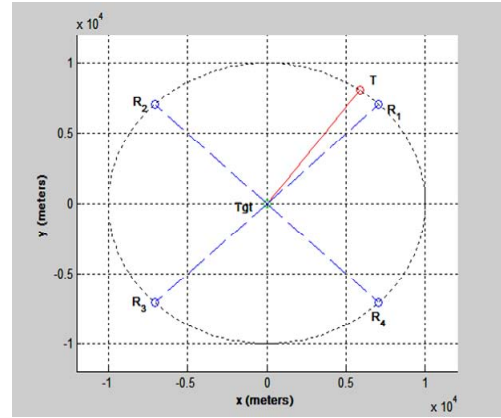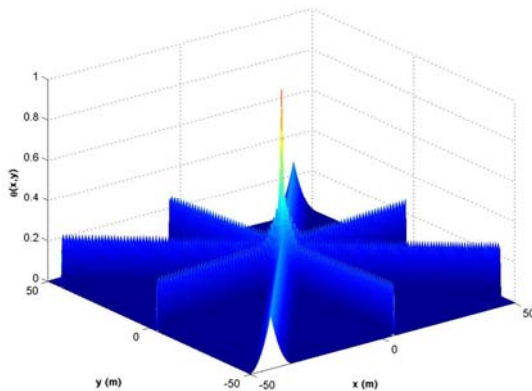
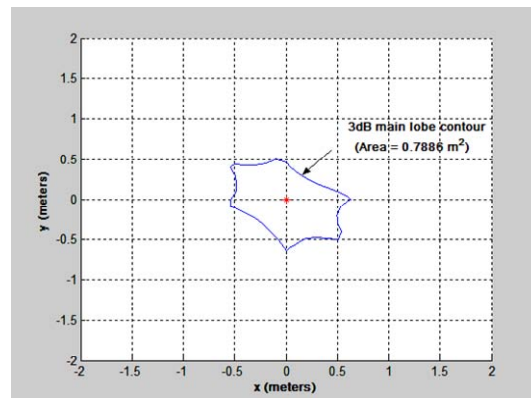

Figure I - 3. Multistatic Ambiguity Function

Figure I - 4. Multistatic Ambiguity Function (3-Db Contour Plot)

149

The area of the 3-dB main lobe contour in this example is 0.7886 m^2. We will try to improve this result by combining three different approaches discussed above.

First we will assume that positions of all receivers are fixed, while the position of the transmitter can change as long as the distance from the origin remains the same (10 km). Because of the symmetry it is sufficient to move the transmitter along the arc shown in **Figure I - 5**.

Figure I - 6 shows the 3-dB main lobe contour area results for different transmitter positions (angle α was varied between 0 and π/2 (see **Figure I - 5**).
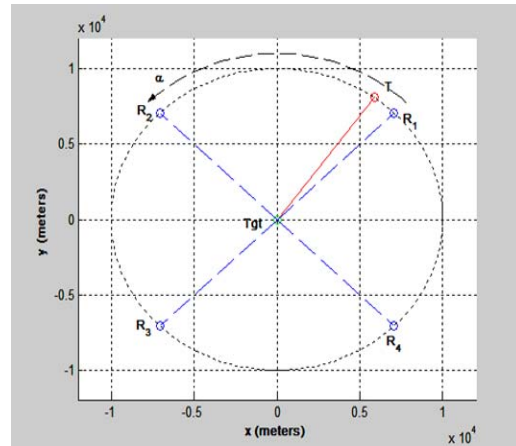
Figure I - 5. Multistatic System Geometry (Moving Transmitter)
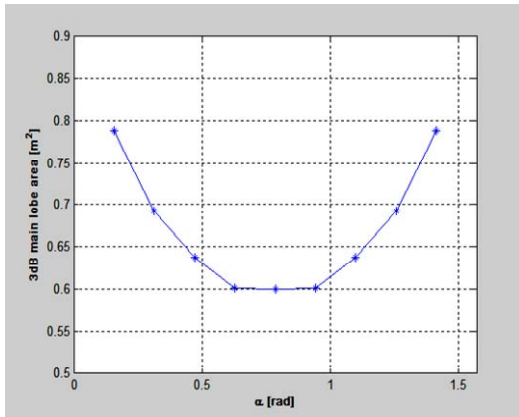
Figure I - 6. 3-dB Main Lobe Area Results (Moving Transmitter)

As can be seen in **Figure I - 6** in order to achieve the best range resolution, the transmitter should be placed right in the middle between receivers R_1 and R_2. This is a somewhat expected result. What might not be so expected is that by changing the position of the transmitter we can significantly improve the resolution. For example, for $\alpha = 0.1\pi$ the 3-dB area equals 0.7886 m^2, while for $\alpha = 0.25\pi$ (best case scenario), the 3-dB area equals 0.6012 m^2 (23.76% reduction). This comparison is shown in **Figure I - 7**.

150

We can additionally improve the resolution by changing the transmitted waveform. We evaluated the 3-dB contour area for two different waveforms – Barker 13 (a bi-phase waveform) and Frank 16 (a poly-phase waveform) and for different transmitter positions as in the previous example. Both waveforms were assumed to be a single pulse with the pulse width of 44ns. The results are shown in **Figure I - 8**.

As can be seen, Frank 16 waveform outperforms the Barker 13 waveform for the entire range of different transmitter positions.

Figure I - 7. 3-dB Contour Plot Comparison

Figure I - 8. 3-dB Area Results (Waveform Comparison)

Finally, the third way of improving the system resolution (shaping the multistatic ambiguity function) is by changing the weights associated with different receivers. So far we have assumed the all weights are equal ($c_1 = c_2 = c_3 = c_4 = 0.25$). For the Frank 16 waveform and for different positions of the transmitter we optimized the weighting coefficients to achieve the minimal 3-dB main lobe contour area. The optimization was performed using an exhaustive search on a finite grid with a step size of 0.05 and under the constraint that $\sum_{i=1}^{N} c_i = 1$.

151

The results of the optimization are shown in Table I-1. The corresponding 3-dB contour area results are shown in **Figure I - 9**.

Table I - 1. Optimal weighting coefficients

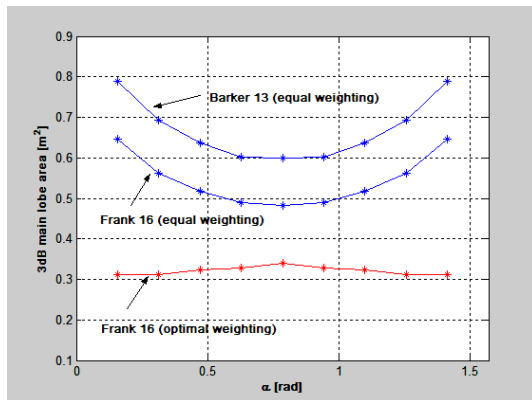| Transmitter Angle	Optimal Weighting Coefficients
α=0.05π	c1=0.35, c2=0.35, c3=0,00 c4=0.30
α=0.10π	c1=0.35, c2=0.40, c3=0.00, c4=0.25
α=0.15π	c1=0.40, c2=0.40, c3=0.00, c4=0.20
α=0.20π	c1=0.45, c2=0.45, c3=0.00, c4=0.10
α=0.25π	c1=0.45, c2=0.45, c3=0.05, c4=0.05
α=0.30π	c1=0.45, c2=0.45, c3=0.10, c4=0.00
α=0.35π	c1=0.40, c2=0.40, c3=0.20, c4=0.00
α=0.40π	c1=0.40, c2=0.35, c3=0.25, c4=0.00
α=0.45π	c1=0.35, c2=0.35, c3=0.30, c4=0.00

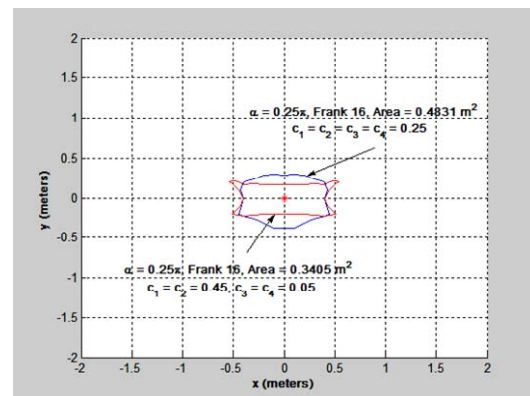**Figure I - 9. 3-dB area results (optimal and non-optimal weighting comparison)**

Figure I - 10. 3-dB contour plot comparison

One can see that a significant reduction in the 3-dB area is achieved by adequately changing the weighting coefficients associated with different receivers. For example, with $c_1 = c_2 = c_3 = c_4 = 0.25$ and $\alpha = 0.25\pi$ the 3-dB area equals 0.4831 m^2. On the other hand, for $c_1 = c_2 = 0.45$, $c_3 = c_4 = 0.05$ and $\alpha = 0.25\pi$, the 3-dB area equals 0.3405 m^2 (29.52% reduction). This comparison is illustrated in **Figure I - 10**

REFERENCES

[I-1]   T. Tsao, M. Slamani, P.K. Varshney, D.D. Weiner, and H. Schawarzlander, "Ambiguity Function for a Bistatic Radar," IEEE Transactions on Aerospace and Electronic Systems, Vol. 33, No. 3, July 1997.

[I-2]   D.D. Weiner, M.C. Wicks, and G.T. Capraro, "Waveform Diversity and Sensors as Robots in Advanced Military Systems," 1st International Waveform Diversity and Design Conference, Edinburgh, UK, November 2004.

[I-3]   G.T. Capraro, I. Bradaric, D.D. Weiner, R. Day, J. Perretta, and M.C. Wicks, "Waveform Diversity in Multistatic Radar," International Waveform Diversity and Design Conference, Lihue, HI, January 2006.

[I-4]   I. Bradaric, G.T. Capraro, D.D. Weiner, and M.C. Wicks, "Multistatic Radar Systems Signal Processing," IEEE Conference on Radar, Verona, New York, USA, April, 2006.

[I-5]   I. Bradaric, G.T. Capraro and P. Zulch, "Signal Processing and Waveform Selection Strategies in Multistatic Radar Systems," International Waveform Diversity and Design Conference, Pisa, Italy, June 2007, invited paper.

[I-6]   I. Bradaric, G.T. Capraro, D. D. Weiner, and M. C. Wicks, "A Framework for the Analysis of Multistatic Radar Systems with Multiple Transmitters," International Conference on Electromagnetics in Advanced Applications, Torino, Italy, September 2007.

APPENDIX J

AN AIRBORNE INTELLIGENT RADAR SYSTEM (AIRS)

By: G. Capraro, Capraro Technologies, Inc., and M. Wicks, AFRL Sensors Directorate

INTRODUCTION

A design of an intelligent airborne radar system that processes information from end-to-end, i.e. filter, detector and tracking stages of a surveillance radar is presented. This architecture design leverages advancements being pursued by the W3C and the DARPA DAML program for constructing the next generation Internet. In the near future, advanced intelligent radar systems will cooperatively perform signal and data processing within and between platforms of sensors and communication systems while exercising waveform diversity, performing multistatic processing, and performing reconnaissance, surveillance, imaging and communications within the same radar system.

The next section provides a global view of how a radar and sensor systems will be built in the near future, i.e. away from stove pipe systems to cooperative and sharing systems. The third section describes the major knowledge base components of an AIRS. The fourth section provides an overview of how the AIRS processes data within different states. The last section provides a summary. .

GLOBAL VIEW

A sensor system's performance can be enhanced by changing a sensor's algorithms as the environment changes. It has been shown in [J-1] – [J-2] that if an airborne radar system knows about certain features of the Earth (e.g. land sea interfaces) and its surroundings then it can use this information intelligently and increase its performance. The sharing of information in real-time with other sensors is beneficial. Radar performance is increased with information from other sensors, e.g. sensor fusion. Also an intelligent radar's performance can be increased if the characteristics and location of jammers are known.

If radar systems are going to share and receive information from multiple sources they must be able to communicate and understand the information. A solution for the exchange of information between heterogeneous sensors is for each sensor to publish information based upon an agreed upon format and protocol. For example, when a sensor publishes its track data multiple sensors interpret its contents without ambiguity.   Conformity must be established, e.g. one method for defining the Earth's surface, one coordinate system, synchronized clocks, and one standard time stamping method for all communications.

Each communication between sensors must include its time and its coordinates. Information regarding a track/target must include unique identifiers, the aircraft's velocity, pitch, yaw, and role and meta data describing the transmitted data along with encryption/decryption keys. The unique identifier will allow the receiving sensor to acquire, within its resident database management system, all of the sender's radar characteristics. Sensor characteristics include such things as nomenclature, power output, bandwidth, frequency, antenna pattern, pulse width, PRF, etc. Platform characteristics as to the position of the antenna on the platform, number of elements, the pattern of the elements, the pointing vector of the radar, etc. These data and numerous rules are used to understand information published by any sensor. This information can be used by the receiving sensor to perform functions such as sensor fusion, track correlation, and target identification.

How can this be obtained in the near future? One key in building an intelligent sensor system is leveraging the efforts of the AI, the Internet, and the software communities. The Internet community is building technologies that allow software agents not only to read, but to understand documents and resources available on the World Wide Web. Its goal is to enhance the exchange of information and to provide the tools for the Web to become more business friendly and more profitable. However, these technologies can also be used to build intelligent sensor systems where multiple sensors can communicate and understand each other with only minimum human intervention.

The Internet community is represented by an organization whose definition is found at www.w3c.org:

"The World Wide Web Consortium (W3C) develops interoperable technologies (specifications, guidelines, software, and tools) to lead the Web to its full potential. W3C is a forum for information, commerce, communication, and collective understanding." They, along with DARPA's Agent Markup Language (DAML) program, are building the next generation Internet, the Semantic Web. The goal of the Semantic Web is to provide mechanisms for Web publications that can be read and understood by software. Currently, most Internet content requires a human to understand its meaning, and is designed to push text, audio, and images to individuals. Search engines usually provide a wide array of varied results that must be filtered by a human. The Semantic Web is being designed in a manner similar to a large knowledge base such that a domain is defined specifically in an ontology, or series of ontologies that standardize the terms, relationships and meanings within the domain, such as radar or sensors in general. A radar or signal processing ontology may be defined in the same manner as other Internet ontologies. Dr. Tom Gruber defines an ontology at http://www-ksl.stanford.edu/kst/what-is-an-ontology.html:

"An ontology is a specification of a conceptualization….What is important is what an ontology is *for*. … For pragmatic reasons, we choose to write an ontology as a set of definitions of formal vocabulary. Although this isn't the only way to specify a conceptualization, it has some nice properties for knowledge sharing among AI software (e.g., semantics independent of reader and context). Practically, an ontological commitment is an agreement to use a vocabulary (i.e., ask queries and make assertions) in a way that is consistent (but not complete) with respect to the theory specified by an ontology. We build agents that commit to ontologies. We design ontologies so we can share knowledge with and among these agents."

Sharing information between sensors on the same platform is also required, especially if one or more sensors are adaptively changing its waveform parameters to meet the demands of a changing environment. **Figure J - 1** depicts a hypothesized intelligent sensor system. Each of the sensors has its own signal and data processing functional capability. In addition to this capability we have added an intelligent processor to address fusion between sensors, communication between sensors, and control of the sensors i.e. RF Intelligent Platform Network (IPN) or a System Strategy Reasoner (SSR) (XG Policy Language Framework in [http://www.darpa.mil/ato/programs/XG/]). The goal is to be able to build this processor so that it can interface with any sensor and communicate with the other sensors using ontological descriptions via the intelligent platform network. The IPN/SSR will be able to coordinate the communications between the sensors on board and to off platform sensor systems. There are approaches we can exploit to build this system by using fiber optic or wire links on board the platform. RF links using Bluetooth or 802.11 technologies can be exploited for linking these sensors on board the platform.

Between platforms other technologies may be exploited such as mobile Internet protocol over RF communications links. The communications issues need to be addressed for the sharing of information and for minimizing the potential of electromagnetic EM fratricide. The intelligent platform should determine if there is EM interference EMI potential when a sensor varies their antenna's main beam pointing vector, or changes its PRF and may thereby cause interference to a receiving sensor. Rather than have each sensor on a platform operate as an independent system we need to design our platform as a system of sensors with multiple goals managed by an IPN/SSR that can manage the dynamics of

Figure J - 1. An Intelligent Sensor System

each sensor to meet the common goal(s) of the platform. This is one of the major areas we are pursuing under our sensors as robots initiative. This initiative is addressing attended and un-attended sensor platforms.

The design presented in **Figure J - 1** has three levels of AI algorithms to share information. The first set of algorithms is contained within the Knowledge Based Signal and Data Processing (KBSADP) and represents the work being performed on the KASSPER program and by the USAF Sensors Directorate [J-1] –[J-7]. For communications equipment, this work is being pursued under DARPA's XG program [http://www.darpa.mil/ato/programs/XG/]. The next level of AI algorithms interfaces KBSADP with the intelligent platform network.

The Intelligent Fusion Communication Control, Plug & Play (IFC2P2) software module will share information with the KBSADP and XG modules and the IPN/SSR based on the ontologies. This sharing will allow each sensor and communication system to request/provide information from/to other sensor and communication systems for intelligent processing. The IFC2P2 could reside on a separate processor with a network connection to the IPN/SSR and a connection to KBSADP, or it could reside on the KBSADP (or XG) processor. For existing sensor and communication systems, software will be created to translate data to/from their own specific data formats to the formats defined by a common ontology. The IFC2P2 processor may have a graphical user front end, depending upon the sensor and communication system, to view information, control the KBSADP processor, and assess the results of the sensor fusion. Sharing information is valuable for new sensor systems in order to exercise waveform diversity functions, as well as for older systems lacking waveform diversity functions. For those non-adaptable equipment, the IPN/SSR will be preloaded with the appropriate ontology-based data. The following section provides a detail description of the KBSADP for an airborne radar system.

AN AIRBORNE INTELLIGENT RADAR SYSTEM (AIRS)

A KB signal and data processing portion shown in **Figure J - 1** represents one radar sensor system. If this radar system is built using knowledge based techniques then there exists intelligence to control its processing. A modified design obtained from the KB STAP effort [J-2] is shown in **Figure J - 2**. This section will describe the major components of this knowledge base radar design. The major components in the figure are labeled as processors with the knowledge base controller as the major integrator for communications and control of the individual processors. These processors operate independently and cooperatively. Each can be implemented on a separate computer or on the same computer and operate as separate software processes. The knowledge base controller (KBC) receives information from many sources. Data about the radar, its frequency of operation, antenna configuration, where it is located on the aircraft, etc. is provided by the block labeled in **Figure J - 2**, configuration information. The map data is preloaded before each mission for estimating clutter returns and for registering its location relative to the Earth and with other sensor platforms. It is also preloaded with its flight profile data and is updated continuously from the platform's navigation system. It also will receive information from the intelligence community both before a mission and throughout the mission. During flight, the KBC will receive information about weather, jammer locations, requests for information, discrete locations, fusion information, etc. The radar system is assumed to be aboard a surveillance aircraft flying a known and repeatable path over the same terrain. Therefore it can learn by monitoring the performance of different algorithms over repeatable passes of terrain.

The KBC performs the overall control functions of the AIRS. It assigns tasks to all processors, communicates with outside system resources, and "optimizes" the system's global performance. Each individual processor "optimizes" its individual performance measures, e.g. SNR and probability of detection. The tracker with the KBC, for example, "optimizes" the number of correct target tracks and "minimizes" the number of missed targets, incorrect tracks, and lost tracks. The KBC handles all interrupts from the User Interface Processor, assigns tasks to the individual processors based upon user requested jobs, generates information gathered from sources to enhance the performance measures of the individual processors, works with other sensors and outside sources for target identification, and provides the User Interface Processor periodic and aperiodic data for answering queries and requests from the user.
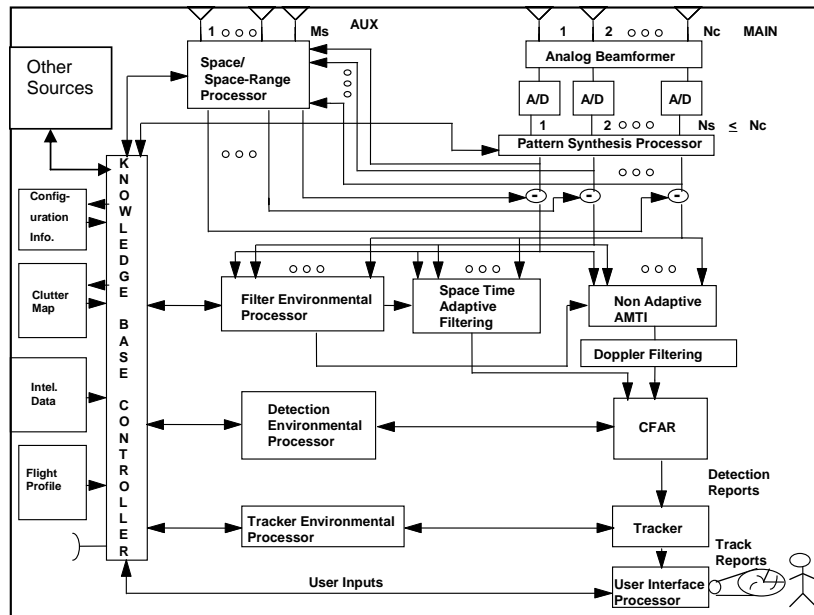

Figure J - 2. An AIRS Architecture

Space/Space Range Processor (SSRP), Pattern Synthesis Processor (PSP), Filter Environmental Processor (FEP) and KBC Interfaces

The KBC will provide geographical information e.g. it will periodically provide the direction the receiver is looking, clutter maps, the location of the emitter, locations of hot clutter jammers, locations of direct jammers or electromagnetic interference sources, and discretes. The KBC will also provide tasks to the SSRP, PSP and FEP. For example, sources of "interference" shall be reduced by a defined amount. Sources of interference will be prioritized. The SSRP, PSP, and FEP, will implement and control their own algorithms and processing. The processors will optimize the KBC's request given the number of available degrees of freedom and their physical operational constraints.

The KBC will provide control and operational requests based upon global optimization considerations and/or input directions from the user. For example, the user may want to execute multiple algorithms and compare their results or restrict portions of an algorithm from being executed. This may require parallel processing on the same set of data. This approach of executing parallel algorithms, as directed by the user, will allow AIRS to learn which algorithms perform better under identical conditions.

The results of the KBC's tasks will be reported to the KBC, as a joint or cooperative accomplishment of the three processors. The amount of interference cancellation obtained for each interference source will be reported by the FEP. The information will include the amount of dB attenuation per interference source, whitening, and gain loss. All three processors (SSRP, PSP, FEP) will report to the KBC, the algorithms used and their parameter values.

The three processors' general operating procedure is to use all of their available resources while attempting to exceed KBC tasks. If the resultant global performance measures are not met then the KBC can change the tasks to these processors during the next iteration. The KBC is looking ahead based on the aircraft's flight plan and is preplanning for future processing.

Detection Environmental Processor (DEP) and KBC Interface

The KBC provides the DEP filter output data, clutter map data and results from the tracker such as the degree of belief or weights/importance of previously detected targets. This information allows the DEP to choose its models for the next iteration of data. For instance, the algorithm may adjust its threshold if a high priority target is entering a different clutter background.

The KBC directs the DEP through tasks as discussed in the previous stage. The results of the KBC's tasks will be communicated back to the KBC. Probability of detection, probability of false alarm, algorithms used, and their parameter values will be reported to the KBC.

Tracker Environmental Processor (TEP) and KBC Interface

The KBC provides data to the TEP that are not contained in the detection data provided by DEP e.g. priority of targets/tracks. The KBC provides control information to the TEP similarly as discussed above based upon parallel processes, choices of algorithms and their parameters, and any definitive requests made by the user or other outside sources such as multistatic operations.

The TEP will report back to the KBC for each process, each track's probability, the probability of missed tracks or lost tracks, and additional performance measures associated with the algorithms used and their parameter values.

User Interface Processor (UIP) and the KBC Interface

The KBC provides data and receives control from the user via the UIP. Directed by the user the KBC will task the Process Manager and Data Manager (not shown in Figure J - 2) to pre-configure the computers and algorithms for each of the above processors for the next flight iteration or CPI. It will provide information related to intermediate results, performance measures, how AIRS arrived at its solutions, and assist the UIP in configuring the antenna and processors.

Configuration Information and KBC Interface

The exchange between the Configuration Information and the KBC contains for example data regarding the radar, the radar's location, antenna, and transmitter characteristics. Some of these data can be modified by the user and are pre-stored in the Data Manager and accessed via the UIP.

Clutter Map and KBC Interface

The Clutter Map is defined given the flight profile of the aircraft. This file contains those parameters required by the AIRS' algorithms obtainable from actual terrain files such as LULC, digital elevation model and DLG databases. These data are provided by the USGS. These data will be stored in an environmental data file and accessed via the Data Manager along with clutter map data computed on the fly during flight.

Intelligence Data and KBC Interface

Intelligence community data are provided to the AIRS. These data may contain the location of jammers, a jammer's parameters, target parameters and a target's kinematics. These data will be used by different AIRS' algorithms and knowledge sources.

Flight Profile and KBC Interface

Flight profile data are stored and maintained in a database via the Data Manager. These data contain parameters required by AIRS' algorithms.

Antenna and KBC Interface

This antenna represents the communications link to outside sources for gathering and providing information during flight.

AIRS STATE PROCESSING

AIRS is a dynamic system, i.e., it changes its processing dependent upon its goals and the environment. This section provides an overview of a hypothetical AIRS and its operation during changing conditions. AIRS' processing begins by loading its computers with pre-flight mission, intelligence, and terrain data. The process will go through four states; pre-flight, initial transient state, correlation/performance/assessment/learning state, and steady state. Steady state probably won't occur until the aircraft flies at least one to two race tracks over the same area. The initial transient state will take 20+ CPIs before tracks can be formed and AIRS starts identifying interrogation-friend-or foe related tracks. The intermediate state: to correlate discretes, objects, shadow regions, and jammers, evaluate performance measures and set thresholds, and deciding which objects require nulling, how much nulling, and when nulling should occur. Described below are the four different states and the functions of the KBC, its performance processor, and the three main radar intelligent system processors (filter, detector and tracker). We have partitioned the KBC into two processor functions: one to control the AIRS and one to monitor and report its performance throughout its different stages.

States 1-2 Pre-Flight - KB Performance Processor & Controller

Locate and load all potential discretes, clutter boundaries, shadow regions, jammers, obstacles and set system parameters.

State 3 Pre-Flight – Intel. Filter

Define initial settings and performance measure thresholds. These data represent flight in-variant antenna characteristics, e.g. number of antenna elements and their configuration, antenna tilt angle and pointing direction, and location of the antenna on the aircraft, initial radar parameters, e.g. prf, transmitter frequency, size of data cube, and bandwidth of signal, and performance thresholds for evaluating antenna beam distortion parameters.

State 4 Pre-flight – Intel. Detector

Define initial settings and thresholds for probability of false alarm (Pfa). These data represent data that are initialized but are not necessarily fixed, e.g. range resolution, Doppler resolution, top percentile for trim mean constant false alarm rate (TM-CFAR), and bottom percentile for TM-CFAR. Performance measure data are also set such as Pfa thresholds for normal, low and very low levels of interest.

State 5 Pre-flight – Intel. Tracker

This state has similar data requirements as the pre-flight KB processor States 1-2. All three processors have access to the same data. This state also sets the tracker processor performance measures and parameters, e.g. number of correct tracks, number of dropped or lost tracks, and kinematics of potential targets.

State 6 Initiate System - KB Performance Processor

The processor will monitor the AIRS queues for number of potential targets and registration of obstacles, discretes, clutter boundaries, shadow regions, and jammers.

State 7 Initiate System - KB Controller

The processor will initiate the antenna processing and monitor the system queues, auxiliary data correlations, feedback from the different processors, system errors, number of potential targets and registration of obstacles, discretes, clutter boundaries, shadow regions, and jammers.

State 8 Initiate System – Intel. Filter

Execute non-STAP algorithm, determine the secondary rings for each cell under test given the stored terrain features, run the NHD algorithm if necessary, compute beam performance, and compute antenna weights based upon hypothesized KBC nulling tasks. Note for this state we don't want to distort the antenna beam pattern but gather data so the KBC can determine if nulls should be placed in the direction of interferers and whether STAP is feasible.

State 9 Initiate System – Intel. Detector

The processor will implement thresholds as assigned, will default to the standard detection cell averaging algorithm, and use standard window sizes unless the cell of interest is at a clutter boundary.

State 10 Initiate System – Intel. Tracker

To initiate a track requires multiple CPIs. Correlations with objects and shadow regions are just beginning, performance measures are computed, (number of correct tracks, number of dropped tracks, and number of incorrect tracks) and tracks are being formed. Tracker reports tracks and potential correlations along with other entities.

State 11 Learning – KB Performance Processor

Correlate discretes, clutter boundaries, shadow regions, potential jammers, and obstacles, evolve rules, insert synthetic targets and measure performances. This processor will use the correlations obtained by the KB Controller [in state 12] for the first portion of its processing, i.e. until it has correlated or discounted all the discretes, clutter boundaries, road traffic, and shadow regions with a high degree of confidence. Once this task is completed the processor will insert synthetic targets of varying sizes and velocities to test the performance of the AIRS. During the second complete scan of an area the KB performance processor will be able to determine if the performance measures have improved. Based upon these results the performance processor may place targets in other locations and/or direct the controller where they should or should not use STAP.

State 12 Learning – DB Controller

Correlate discretes, clutter boundaries, shadow regions, potential jammers, obstacles and evolve rules. There are two levels of correlation required: 1) position of the above entities within a defined range ring and 2) the power level at the receiver given the distance to the entity. Note the definition of the range rings relative to the Earth contain different entities as the aircraft moves. In addition, as the aircraft moves different entities may require nulling, the AIRS may or may not want to place a null in their direction. Correlating entities by power may be done along with correlations with road traffic and shadowed regions using data from the Intel. Tracker.

State 13 Learning – Intel. Filter

Compute number of secondary rings, run NHD, compute beam performance measures, set nulls, determine when and where STAP is feasible and evolve rules. Rules as to when STAP should and should not be applied are required. During the first complete flight over the defined scene the AIRS could execute a standard non STAP algorithm. The KB performance processor should place targets in non-homogeneous areas e.g. near roads and clutter boundaries. The position and type of synthetic targets are not made known to the KBC. In the second complete scan the KBC should attempt to use STAP where ever it can.

A method for determining if there is a sufficient number of training range rings for STAP is required. A method is to correlate each range ring with the terrain map to identify where there are discontinuities, major roads, etc. and label each region or sector-range with a terrain type. A classification code range ring correlator algorithm will implement this method in collaboration with the intelligent filter processor. The major or minor classification codes used in the USGS database, e.g. urban, forest, water, etc. will be used. Once range rings are chosen they can be evaluated for their homogeneity by using NHD. With a combination of the pre-flight loaded database, the use of the radar returns and the NHD, the system can "learn" which areas are homogeneous and evolve its rules as to which filter algorithms to employ.

During this state the controller will assign a low, medium, and high performance threshold levels for beam performance. This information along with requests of where to place nulls in the beam pattern will be provided to the intelligent processor. After a number of CPIs the KBC will evaluate performance measures from all the processors. Based upon this evaluation the KBC may assign different performance threshold levels and null requests for the filter processor.

State 14 Learning – Intel. Detector

Compute detections, re-compute and adjust pfa thresholds and evolve rules. This state uses the correlation data provided by the KBC to recognize terrain boundary locations. For those test cells within homogeneous regions the standard detection cell averaging algorithm and window sizes will be used. For those test cells near boundaries the CFAR processors will choose reference cells, algorithms, and window sizes as developed under the ES-CFAR program [J-1]. The processor will perform detections, implement thresholds as assigned, re-compute and adjust Pfa thresholds, evolve rules to apply the standard cell averaging rules, determine when to apply different algorithms, and when to recommend changing the detection threshold.

State 15 Learning – Intel. Tracker

Correlate Federal Aviation Administration (FAA) data with tracks, compute performance measures e.g. number of tracks, number of dropped tracks, number of incorrect tracks and evolve rules. Discrete objects, shadow regions, roads, and FAA data will be obtained from the KB Controller and used to help correlate with existing targets and tracks. Correlations of dropped tracks and highways will be performed with the KBC. Performance measures (number of correct tracks, number of dropped tracks, number of incorrect tracks) and sorting of tracks will be computed. It will report back to the KBC all its tracks and any discrepancies with the data obtained from the KBC. Discrepancies will be settled by the KBC and the other processors. As corrections are made the AIRS will evolve its rules and learn.

State 16 Steady - KB Performance Processor

The performance processor will constantly measure the performance of all processors to determine whether AIRS is performing better. The processor will continually look for changes or requests submitted by the user or changes in data from outside sources. It will monitor performance by checking the beam pattern performance data, detection data, and track data. It will insert known RCS synthetic targets at locations where there are boundaries in terrain types and evaluate the detection capability of the system. By placing different targets at different locations the performance of the current rules can be computed. If performance is low then the rules being used by the KBC will be modified.

State 17 Steady - KB Controller

The KBC will access the same performance measures as presented in state 16. Based upon these performance values the KBC will asses its current rules and apply changes accordingly. The rules the KBC can change are based upon a processor's reported data and the user requests, such as change in the antenna's beam pattern and the aircraft's flight path.

State 18 Steady – Intel. Filter Processor

This processor will monitor its beam pattern performance. It will change its rules based upon the environment and the number of nearby jammers and discretes. For example, the processor should manage the number of degrees of freedom required to notch jammers and descretes and yet maintain enough degrees of freedom to perform STAP processing. It will measure its own performance and report it to the KBC for total sensor performance evaluation.

State 19 Steady – Intel. Detector Processor

During this state its processor measures performance based upon the number of detections and number of false alarms. It will increase or decrease the threshold level, change window sizes for CFAR algorithms, and change rules for choosing CFAR algorithms based upon previous flights over the same or similar clutter interfaces.

State 20 Steady - Intel. Tracker Processor

This state measures performance based upon number of correct tracks, missed tracks, and number of false tracks. Based upon these numbers and the terrain, the processor will adjust its rules and thresholds to increase its performance.

SUMMARY

Integrating KB techniques within an airborne radar's signal and data processing chain was presented along with a detail design of an airborne intelligent radar system. Advances in technologies being pursued by the W3C and DARPA are required in order to field the next generation intelligent sensor systems.

REFERENCES

[J-1]   W. Baldygo, M. Wicks, R. Brown, P. Antonik, G. Capraro, and L. Hennington, "Artificial intelligence applications to constant false alarm rate (CFAR) processing", Proceedings of the IEEE 1993 National Radar Conference, Boston, MA, April 1993.

[J-2]   R. Senn, "Knowledge Base Applications To Adaptive Space-Time Processing", AFRL-SN-TR-146, Final Technical Report, July 2001.

[J-3]   P. Antonik, H. Shuman, P. Li, W. Melvin, and M. Wicks, "Knowledge-Based Space-Time Adaptive Processing", Proceedings of the IEEE 1997 National Radar Conference, Syracuse, NY, May 1997.

[J-4]   Multi-Channel Airborne Radar Measurement (MCARM) Final Report, Volume 1 of 4, MCARM Flight Test, Contract F30602-92-C-0161, for Rome Laboratory/USAF, by Westinghouse Electronic Systems.

[J-5]   G. T. Capraro, C. T. Capraro, and D. D. Weiner, "Knowledge Based Map Space Time Adaptive Processing (KBMapSTAP)", Unpublished Final Report, March 2000.

[J-6]   C. T. Capraro, G. T. Capraro, D. D. Weiner, and M. Wicks, "Knowledge Based Map Space Time Adaptive Processing (KBMapSTAP)," Proceedings of the 2001 International Conference on Imaging Science, Systems, and Technology, June 2001, Las Vegas, Nevada.

[J-7]   A. Farina, H. Griffiths, G. Capraro, and M. Wicks, "Knowledge-Based Radar Signal & Data Processing", NATO RTO Lecture Series 233, November 2003, Unpublished Report

APPENDIX K
SENSORS AS ROBOTS

By: G. Capraro, Capraro Technologies, Inc.; M. Wicks, AFRL Sensors Directorate;
W. Szczepanski, Helios Remote Sensing Systems, Inc.

INTRODUCTION

The monolithic military adversary of the twentieth century is no longer the number one threat. Single function radar systems are necessary but not sufficient for combating terrorism. The desire to AF2T2EA4 by the US Air Force will require changes to how we modify, build, and deploy radar systems. Coherent signal level fusion of homogeneous sensors and data fusion of heterogeneous sensors are being studied in order to obtain sensor coverage consistent with AF2T2EA4. However, we must also integrate these radar systems with heterogeneous sensors (e.g. acoustic, IR, EO) located on the ground, in the air, in space, and underground. The radar systems of the future must be intelligent and integrated within sophisticated systems of heterogeneous sensors that operate on many hypotheses at the same time.

The USAF Research Laboratory is attacking these issues from a sensor and information perspective and has generated a way forward in their defining of layered sensing. From reference [K-1]:

> *"Layered Sensing provides military and homeland security decision makers at all levels with timely, actionable, trusted, and relevant information necessary for situational awareness to ensure their decisions achieve the desired military/humanitarian effects. Layered Sensing is characterized by the appropriate sensor or combination of sensors/platforms, infrastructure and exploitation capabilities to generate that situation awareness and directly support delivery of "tailored effects"."*

The asymmetric enemy of the twenty-first century is causing havoc throughout the world. Layered sensing will give us the necessary ability to anticipate and counter their actions before they occur in today's dynamic and ever changing environment. In order to accomplish this goal we must begin by employing a synergistic approach of queuing, triggering, and intelligently aggregating information sources throughout our C4ISR systems. Specifically we must use intelligence and reconnaissance systems to help queue sensors looking for "triggers" that may indicate an action to be taken by an enemy combatant i.e. to anticipate an action before it occurs. The intelligent use of radar surveillance sensors is ideal for helping in identifying "triggers", especially in non urban areas. Detections can be made and observables can be "tracked" with the use of monostatic and multistatic radar systems where dedicated tracks of specific targets can be maintained using heterogeneous sensors. The use of dedicated EO/IR sensors can also be employed for ISR purposes and to assist radar sensors in their persistent tracking of mounted or dismounted combatants within urban and mountainous terrain. The use of heterogeneous sensors dynamically deployed based upon triggers, target detection, tracking, and identification will allow for expedient global decision making and engagements. If the USAF is going to anticipate actions before they occur, generate situational awareness, and directly support delivery of effects - then intelligent aggregation of sensor data, information sources, and knowledge in real-time is required.

The C4ISR system of the future must be able for example, to meet the following test scenario implicit requirements. Generic C4ISR Test Scenario: C4ISR for a country and its borders; One of its bordering nations is a peer nation; The terrain near the border is very mountainous – enemy combatants are known to cross the boarders in vehicles, on foot, horse, donkey, etc. and sometimes disappear possibly into caves; There are multiple medium size cities south of the mountains with many roadways connecting them – many of these roads are periodically populated with explosives; Inside the cities there are enemy combatants living in buildings with the civilian population; Communications between combatants are via email, Web sites, cell phones, land line phones, RF radios, couriers, etc.; Combatants launch weapons from civilian populated areas, churches, schools, etc., and Combatants use civilian vehicles for transportation.

How can the C4ISR system of the future detect and identify threats and meet the implicit requirements of this scenario in a timely manner? We must, as a first step to full automation, implement the following ground breaking changes: place more compute intensive resources closer to the source of the data and information gathering – (e.g. assign tasks to sensors to look for "triggers" created from ISR sources), provide for the analysis of intelligence data automatically and without human involvement, move the human sensor operator from managing data - to managing actionable knowledge and sensor aggregation, and develop "triggers" and rules for automatic assignment and management of heterogeneous sensors to meet dynamic and abstract requirements, e.g. track a specific vehicle or dismount.

The following sections address each of these changes with examples and where appropriate, reference works that are representative of portions of what needs to be done. This portion of the report provides a brief overview of the efforts being performed under the Sensors as Robots program.

AIRBORNE GMTI/SAR SYSTEMS

Modern surveillance radar systems are capable of detecting, tracking, and imaging surface, fixed [K-2] and moving targets. With the use of precision PNT data and software algorithms these detections can be displayed on background map data as shown in **Figure K - 1**, created using simulated radar data. The objective of this figure is to illustrate the capability to associate target tracks with detections on known roadways as compared to boats operating in the bay. The figure shows through the use of USGS data, that the knowledge of the terrain can be used to indicate whether targets are in an urban, forest

Figure K - 1. Mapping The Threat

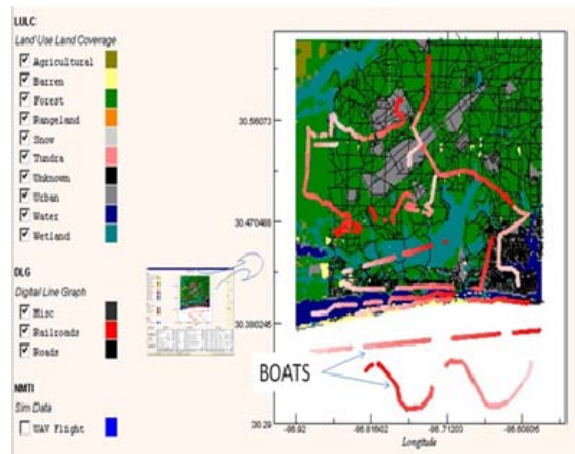or littoral zones, for example. By studying different geographic areas and hypothesizing different actions that a combatant may perform, triggers may be developed to indicate a possible anticipated action. For example, tracking vehicles on roads does not provide any significant additional information than what one would expect. However, if a vehicle leaves the road and or stops for any significant amount of time, then this may indicate a localized region worthy of additional analysis regarding activities at that location. KB algorithms can be written that integrate PNT data, USGS data, and tracking data that would alert an operator that a target has left the roadway and stopped. Once alerted that a trigger has been activated, the operator can pursue either redirecting the platform to obtain a radar image or use onboard IR/EO sensors to obtain thermal or optical signatures of the target. If IR/EO sensors are not available, the operator can request a nearby UAV with the required sensor to obtain images of the scene. These images can be processed in real-time via pattern recognition software and sent to an onboard analyst to determine the type of vehicle and whether there are humans near the road, or alternatively a compressed version of the image can be sent to a ground analyst for a similar quick assessment. Their gross findings can then be sent back to the platform along with messages to the command center. High resolution images can be saved for a ground based analyst to gather more details about the vehicle and humans if required for further study.

CYBER SURVEILLANCE

Imagine a Wi-Fi café within a city threatened by terrorism. A typical looking native arrives with his/her laptop computer and purchases a cup of coffee and accesses the freely available Wi-Fi. Intelligent software, monitoring the Internet server within the café, notices that someone is accessing web sites related to the purchasing of materials required for manufacturing a new kind of explosive, i.e. a trigger has been set. Within the immediate vicinity of the café there are cameras and sensors including software that monitors all activities both wired and Wi-Fi within the café. The café's server is being managed by software that can link the MAC address of each computer and has a record of web sites visited. A comparison is made of the visited web sites and the corresponding MAC address is determined. RF sensors using algorithms [K-3] can locate in which portion of the café the laptop with the suspect MAC address is located. By increasing the bit error rate to the MAC address, cameras detect which individual is linked to the MAC address since the user will attempt to move his computer closer to the wireless access point, and/or complain to the owner about the poor quality of Wi-Fi service. At this point, the system will notify the command center; they can view the images of the suspect person and apply techniques to automatically identify the individual. The command center will monitor the automated processes and can override or redirect actions based upon information obtained. Phone records, credit card transactions, news articles, etc. are simultaneously searched to obtain all possible information concerning this person. In parallel, imagery databases obtained from strategically placed cameras throughout the city are queried to determine through timeline analysis information pertaining to where and how the target arrived at the café, e.g. on foot or via a vehicle, if so its license plate number, etc. Also, a simulation with multiple hypotheses will compute when and what the individual may likely do next. Messages will be sent to multiple sensors (acoustic, IR, EO, RF) throughout the city to monitor his movements and continuously update predictions. Once the target is ready to leave the café the command center can engage the cameras near the café and begin tracking the target whether he is dismounted or not.

CLOSE IN SENSING

If the target from the café enters a vehicle then the command center will dispatch and alert sensors as to what to look for, i.e. an image of the person, an image of the vehicle, and if possible its license plate number. If we can't track the vehicle with fixed EO sensors because of a lack of sensors or inadequate lighting, one may want to use, for example, a UAV with a radar and/or an IR sensor. Consider **Figure K - 2** with three vehicles traveling down a two lane road.
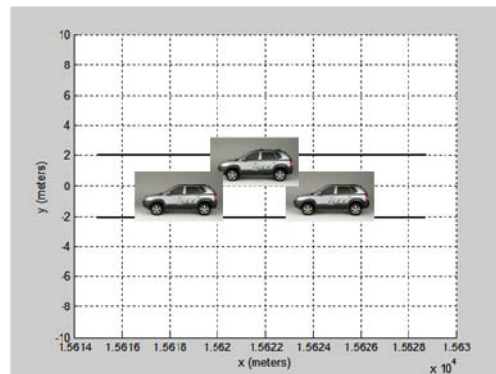

Figure K - 2. Scenario with Multiple Targets

If the receivers are placed as in shown in **Figure K - 3** where target (Tgt) represents the position of the three targets, then we will be able to clearly discriminate motion among them. This is illustrated in **Figure K - 4**, and presents a 3-D plot of normalized radar returns (assuming no noise and that all three targets have the same reflectivity). See reference [K-4] for a detailed discussion of these results.

This example uses only one transmitter and one waveform. See references [K-5]-[K-11] for additional results using waveform and geometric diversity and the
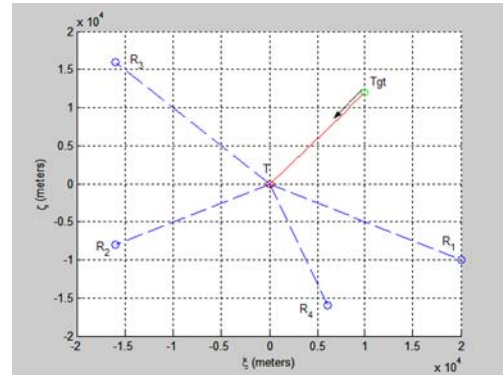

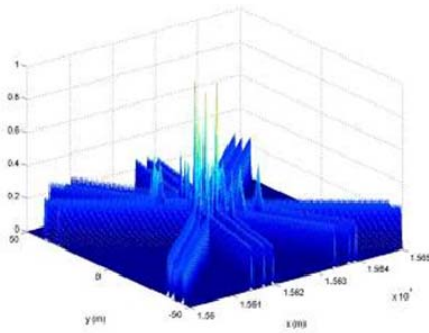**Figure K - 3. Geometric Diversity**

Figure K - 4. Multistatic Ambiguity Function For Three Targets

use of multiple receivers and transmitters. Additional work using transmitters of opportunity and waveforms of opportunity (e.g. FM, AM transmissions, cell phone transmissions, etc.) needs to be investigated to improve the multistatic ambiguity function and hence target detection and discrimination.

Consider the same scenario where our target of interest will merge with one or more targets with similar kinematics. It is assumed that the targets have been detected by a radar system, they are already in track, and that a preliminary classification [K-12] is available. Also assume that there is only one airborne platform with radar and imaging sensors. There can be a video camera, an IR camera, and/or a high resolution spotlight SAR onboard. The target image provided by one or more imaging sensors is then exploited to support the track operation in difficult situations, e.g. when similar targets travel close to each other. An example of such a scenario is described in **Figure K - 5**, in the case of two similar vehicles.

In **Figure K - 5**, the two vehicles have similar kinematic parameters. Let us assume that target A is under track by the radar. After its trajectory crosses that of target B, an ambiguous situation arises such that the target track could be lost, even momentarily. In a surveillance environment, this situation is undesirable. The suspect target must be continuously monitored. In this uncertain scenario the use of additional heterogeneous sensors provides an opportunity to collect more complementary information on the target and to use it in order to improve upon discrimination performance.
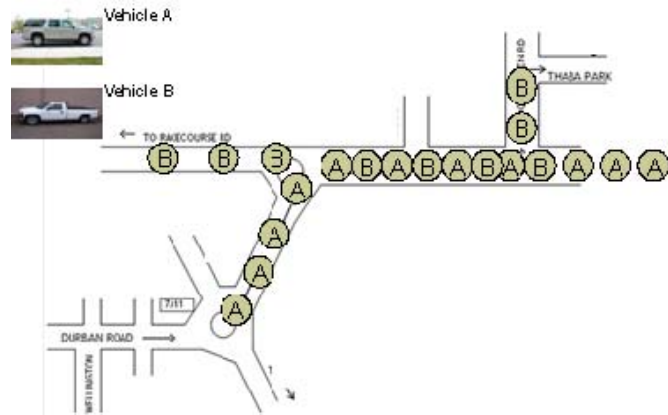

Figure K - 5. Two Similar Vehicles with Merging and Crossing Routes

Even though the solution described has some similarities with classical estimation or with model based classification techniques, it is actually quite different from the standard classification problem, since in those cases the target to be recognized or classified is usually compared with a set of available templates or with models stored in a database. In the case considered here, a template for the target does not exist. The template must be constructed concurrently with the tracking and before the discrimination tasks by exploiting one snapshot of target data (or more snapshots, when and where available) provided by an imaging sensor before the target track is lost or the uncertainty situation arises.

Scenarios were generated and simulations were performed using an EO sensor in conjunction with an airborne radar. The set of images used to test performance is represented by three classes of similar vehicles for seven different viewing angles, from 0° to 30° with a step of 5° between each image. Three classes of vehicles for view angles of 0° and 30° are shown in **Figure K - 6**, with infinite SNR.
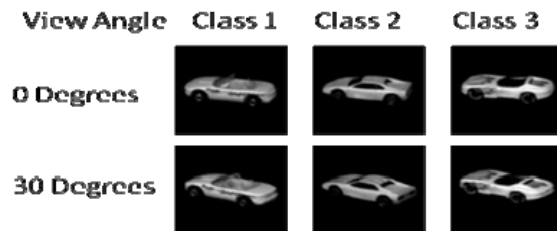

Figure K - 6. Images for Three Similar Vehicles

It is assumed that only one snapshot of the image is available to construct a fingerprint (FP) for each of the three classes. Each FP is constructed from the target image for the first view angle (0°) and it is represented by a single realization of the data affected by noise; the SNR is fixed and it is the same for the three FPs. Five values of SNR are considered for the FP: ∞ (clean FP), 20 dB, 10 dB, 0 dB, and -5 dB.

Consider the following three FPs created with a SNR of 20 dB at 0 degrees view angle for each of the three classes of vehicles shown in **Figure K - 7**. Each of the images in **Figure K - 6** is composed of 197 x 197 pixels with a grey scale depth of 256 bits. After removing the background pixels, i.e. the blackened area, a representation of the images is shown in **Figure K - 7** as a histogram of 15 bins.
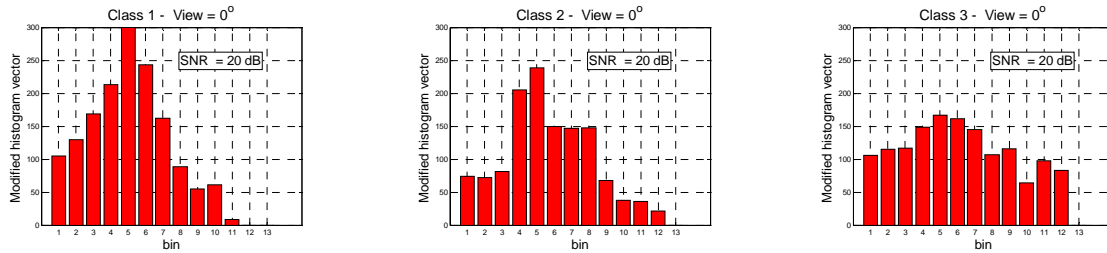

Figure K - 7. FP's Histograms at View Angle 0 Degrees and SNR = 20 dB for Three Similar Vehicles

If a second image of the vehicle is taken later during the tracking period when the view angle is not at 0 degrees or the SNR is not 20 dB, then the image's histogram will vary, thus increasing the difficulty to discriminate among targets. Consider the histograms in **Figure K - 8** where the view angle is 30 degrees and the SNR is 0 dB. It can be seen that, like the images in **Figure K - 6**, the histograms vary when viewed at different angles and at different SNRs.

In the surveillance scenario described, the analysis of the performance with respect to the view angles is useful in evaluating which angles allow us to better discriminate between the monitored targets and similar targets nearby. Two image matching algorithms were investigated, i.e. a chi-square, using the histogram approach, and a cross-correlation test performed on the images directly. The comparisons between the images under test and the FPs are performed by extracting some specific features from the target image and by performing an appropriate decision test. Preliminary results indicate that for best performance the view angle should be within fifteen degrees of the FP's view angle. This analysis can help develop similar rules for a KB system [K-13] to instruct the platform of sensors on how to adjust its trajectory and how to orient the imaging sensors involved in the surveillance operation. This use of heterogeneous sensors for persistent situational awareness requires further investigation and testing within realistic environments.
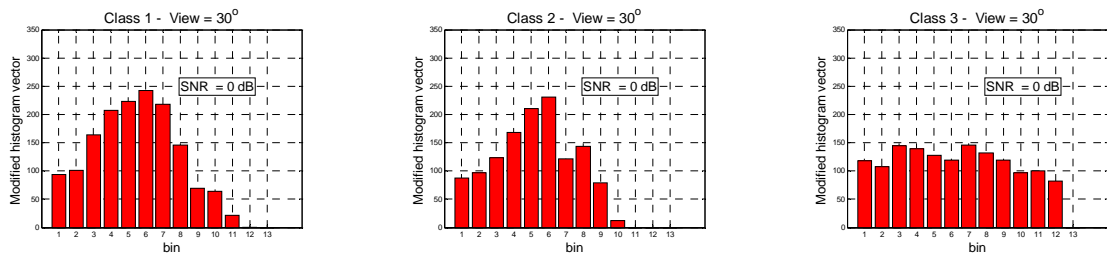

Figure K - 8. Histograms at View Angle 30 Degrees and SNR = 0 dB for Three Similar Vehicles

As an example for future study, the return from a tracking radar itself may contain enough information to discriminate between two or more similar targets/vehicles. Consider, in **Figure K - 9**, a simulated response from an airborne radar illuminating one of the vehicles shown above. Can similar algorithms developed for the EO sensor be used to quantize the resultant RF response of the target?
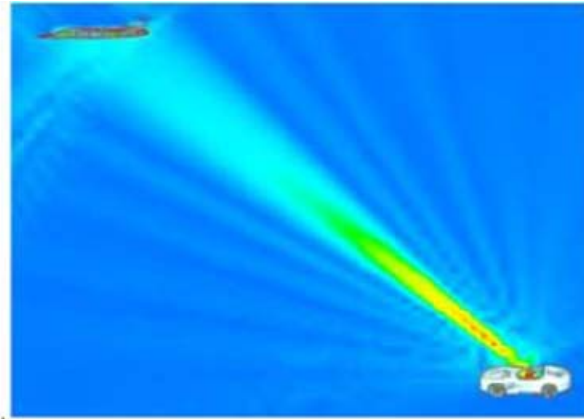

Figure K - 9. Simulated Radar Response

SUMMARY AND CONCLUSIONS

Appendix K of this report provided a brief overview and some highlighted results of the Sensors as Robots program. Geographically distributed radars and sensors, controlled by knowledge based systems and exercising waveform diversity offer technology that the USAF needs to implement to meet its AF2T2EA4 goal. A generic C4ISR scenario was presented along with three examples of how sensors can be dynamically engaged based upon "triggers" to detect, track and identify targets, and allow for expedient global decision making in order to direct future engagements. Numerous other examples can be envisioned but they must be dynamically implementable in real-time in order to engage and defeat the asymmetric threat. The key to the success of Sensors as Robots is that we must place sensors close in, with advanced computing closer to each node, automate low level functions, and develop triggers and rules for the automatic management of heterogeneous sensors.

REFERENCES

[K-1]   Bryant, M., Johnson, P., Kent, B.M., Novak, M., and Rogers, S., "Layered Sensing Its Definition, Attributes, and Guiding Principles for AFRL Strategic Technology Development", "http://www.wpafb.af.mil/shared/media/document/AFD-080820-005.pdf, 1 May 2008.

[K-2]   Wicks, M.C., and Zhang, Y, "Optimized Detection of Spatially Extended Fixed Objects In Clutter", 2009 IEEE Radar Conference, 4-8 May 2009.

[K-3]   Capraro, G.T., Bradaric, I., Wicks, M.C., and Ratazzi, E.P., "Intelligent Sensor – Wi-Fi", Proceedings of the 2007 International Conference on Artificial Intelligence, Las Vegas, Nevada, USA, June 25-28, 2007.

[K-4]   Bradaric, I, Capraro, G.T., and Wicks, M.C., "Sensor Placement for Improved Target Resolution in Distributed Radar Systems," IEEE Radar Conference, Rome, Italy, May 2008.

[K-5]   Weiner, D.D., Wicks, M.C., Capraro, G.T., "Waveform Diversity and Sensors as Robots in Advanced Military Systems," 1st International Waveform Diversity and Design Conference, Edinburgh, UK, November, 2004.

[K-6]   Capraro, G.T., Bradaric, I., Weiner, D.D., Day, R., Peretta, J. and Wicks, M.C., "Waveform Diversity in Multistatic Radar", International Waveform Diversity and Design Conference, Lihue, HI, January 2006.

[K-7]   Bradaric, I., Capraro, G.T., Weiner, D.D., Wicks, M.C., "Multistatic Radar Systems Signal Processing", IEEE Conference on Radar, Verona, NY, USA, April, 2006.

[K-8]   Bradaric, I., Capraro, G.T., and Zulch, P., "Signal Processing and Waveform Selection Strategies in Multistatic Radar Systems", International Waveform Diversity and Design Conference, Pisa, Italy, June 2007, invited paper.

[K-9]   Bradaric, I., Capraro, G.T., and Wicks, M.C., "Waveform Diversity for Different Multistatic Radar Configurations", Asilomar Conference on Signals, Systems, and Computers, November, 2007.

[K-10] Capraro, C.T., Bradaric, I., Capraro, G.T., and Lue, T.K., "Using Genetic Algorithms for Radar Waveform Selection", IEEE Radar Conference, Rome, Italy, May 2008.

[K-11] Bradaric, I., Capraro, G.T., Weiner, D.D., Wicks, M.C., "A Framework for the Analysis of Multistatic Radar Systems with Multiple Transmitters", International Conference on Electromagnetics in Advanced Applications, Torino, Italy, September, 2007.

[K-12] Giompapa, S., Farina, A., Gini, F., Graziano, A. Croci, R. and Di Stefano, R., "Study of the Classification Task Into an Integrated Multisensor System for Maritime Border Control", IEEE Radar Conference 2008, Rome, Italy, 26-30 May 2008.

[K-13] Knowledge-Based Systems for Adaptive Radar: Detection, Tracking, and Classification, IEEE Signal Processing Magazine, Volumer 23, Number 1, January 2006